Hybrid Imaging and Radionuclide Therapy of Musculoskeletal Diseases

24

Paola Anna Erba, Martina Sollini, Roberta Zanca, Roberto Boni, Lesley Flynt, Elena Lazzeri, Giuliano Mariani, and Torsten Kuwert

Contents

P. A. Erba · R. Zanca · G. Mariani
Regional Center of Nuclear Medicine, Department of Translational Research and Advanced Technologies in Medicine and Surgery, University of Pisa, Pisa, Italy

M. Sollini
Department of Biomedical Sciences, Humanitas University, Milan, Italy

R. Boni
Nuclear Medicine Service, "Papa Giovanni XXIII" Hospital, Bergamo, Italy

L. Flynt
Department of Nuclear Medicine, M.D. Anderson Cancer Center, Houston, TX, USA

E. Lazzeri
Regional Center of Nuclear Medicine, University Hospital of Pisa, Pisa, Italy

T. Kuwert (✉)
Clinic of Nuclear Medicine, Friedrich-Alexander-University of Erlangen-Nürnberg, Erlangen, Germany
e-mail: Torsten.Kuwert@uk-erlangen.de

D. Volterrani et al. (eds.), *Nuclear Medicine Textbook*, https://doi.org/10.1007/978-3-319-95564-3_24

Learning Objectives

- To understand the principles of bone physiology and metabolism.
- To understand bone remodeling and bone development.
- To learn the protocols used for bone scintigraphy, including SPECT/CT.
- To become acquainted with how a bone scintigram should be interpreted.
- To become familiar with quantitative skeletal SPECT/CT.
- To learn the principles of ^{18}F-fluoride PET and of potential new tracers of bone metabolism.
- To learn how bone scintigraphy can be used in the diagnostic workup of primary bone tumors.
- To learn how bone scintigraphy can be used to stage malignant disease.
- To understand how bone scintigraphy in conjunction with SPECT/CT can be used in the diagnostic workup of bone pain.
- To learn the scintigraphic appearance of benign bone disease such as metabolic bone disease, osteonecrosis, fractures, inflammation, and infection and how bone scintigraphy can be used in the diagnostic workup of these conditions.
- To understand the rationale of using bone-seeking radiopharmaceuticals labeled with radionuclides emitting electrically charged particles for treatment of painful bone metastases.
- To learn the principles and procedures of employing bone-seeking radiopharmaceuticals labeled with radionuclides emitting β^- or α^{++} particles for treating patients with metastatic bone disease.

24.1 Structure and Functions of the Skeletal System

Bone tissue is a specialized form of connective tissue, which allows deposition of calcium and phosphate in its extracellular matrix conferring remarkable hardness and strength. It fulfills three main functions:

- Support of the body and as a site for the insertion of skeletal muscles.
- Protection of major organs and bone marrow.
- Storage of calcium and phosphate, with a central role in maintaining calcium homeostasis in body fluids.

24.1.1 Bone Structure: Osteoblasts, Osteoclasts, and Hormonal Control

The cells involved in the bone formation process are called osteoblasts. Their differentiation from stromal progenitor cells (originally mesenchymal cells from the mesodermal germ line) is stimulated by factors such as parathyroid hormone (PTH), prostaglandin, and some growth factors. The main function of the osteoblasts that produce many molecules (e.g., TGF, IGFs, PDGF) is to synthesize the bone matrix—an organic backbone. After its synthesis, the bone matrix is mineralized and constantly regenerated as a result of the continuous bone remodeling process. The main constituent of the bone matrix is type I collagen, although minimal amounts of collagen type III, V, and FACIT are involved; non-collagen proteins account for about 10–15% of the bone matrix. The extracellular matrix, and especially type I collagen that guar-

antees elasticity and flexibility, determines bone structure. Growth of the mineral component (initially localized in specific sites of the collagen matrix, in the spaces between fibers) is facilitated by high levels of calcium and phosphorus.

Osteoclasts are plurinuclear giant cells responsible for initiating the bone remodeling process. They are produced by the bone marrow, and mature cells act under the effect of PTH and other local substances, such as tumor growth factor (TGF), tumor necrosis factor (TNF), interleukin-1 (IL-1), and interleukin-6 (IL-6). Vitamin D (1,25-dihydroxycholecalciferol) is a powerful stimulator of osteoclastic activity, promoting the differentiation of osteoclast precursors and inhibiting proliferation of T cells via interleukin-2 (IL-2); calcitonin (CT) inhibits the action of mature osteoclasts. Other local factors are involved in the control of bone remodeling, IL-1 being one of the most powerful stimuli for osteoclasts (although its effect is mediated, at least in part, by PGs). Another important cytokine involved in this complex process is IL-6, which is secreted by bone cells in response to PTH and vitamin D. Osteoprotegerin (OPG) acts as an antagonist on the bone remodeling process of osteoclasts. The sequence of the cellular events that accompany bone tissue loss is at the base of the bone remodeling processes that takes place both during aging and in some pathological conditions (e.g., osteoporosis, fractures, myeloma, metastasis).

Cortical bone and trabecular bone can be considered as two distinct entities, each characterized by specific modifications at each stage of bone remodeling, depending on the environment in which bone cells are.

24.1.2 Bone Remodeling

Bone remodeling is a continuous process of renewal of the skeleton that occurs throughout life, with the aim of preserving its mechanical integrity. This process involves continuous removal of bone tissue (bone reabsorption) followed by the synthesis of new bone matrix and subsequent mineralization (bone formation). The removal of the "old" bone by the osteoclasts implies the release of calcium and other components of the matrix into the serum. Bone remodeling involves two types of cells, osteoclasts and osteoblasts, the interaction of which is finely balanced; minimal alterations of this balance may result in loss of bone matrix or, rarely, increase in the bone mass.

The outer portion of the bone is a thick layer of calcified tissue, the cortical bone (i.e., compact bone), located in the diaphysis where the hematopoietic bone marrow is contained. Toward metaphyses and epiphyses, the cortical bone becomes thinner, and the medullary channel is occupied by trabecular structures thin and calcified that form the spongy bone (i.e., trabecular or cancellous bone). The space circumscribed by trabeculae contains hematopoietic elements in direct communication with those contained in the medullary cavity of the diaphysis. Despite their structural and functional differences, cortical bone and trabecular bone are composed of the same cellular elements and extracellular matrix. The main structural difference is quantitative: 80–90% of compact bone is calcified, while the calcified component accounts for only 15–25% in the trabecular bone. This difference in composition mirrors functional differences: cortical bone has purely protective and structural functions, while the main function of the trabecular bone is metabolic.

24.1.3 Bone Development and Changes with Age

The volume of cortical bone (mainly present in the long bones and the appendicular skeleton) is regulated by the formation of the periosteal bone and the remodeling of both Havers channels and endosteal bone. In females, the loss of cortical bone (which is the main factor predisposing to vertebral and femoral fractures) begins after 40 years and is accelerated 5–10 years after menopause. The loss of trabecular bone occurs only after menopause. Bone remodeling begins with the activation of the osteoclast precursors and is followed by the formation of "mature" osteoclasts that are usually grouped in small pits (the Howship lacunae) on bone surfaces; it ends with the apoptosis (programmed cell death) of osteoclasts. Osteoclasts' apoptosis causes some osteoblastic cell modifications (chemotaxis, proliferation, and differentiation) which promote bone mineralization that ends with discontinuation of osteoblast activity (usually with complete regeneration of the reabsorption lacunae).

Key Learning Points

- Bone remodeling is a continuous process of renewal of the skeleton.
- It involves bone reabsorption and new bone formation by the osteoclasts and osteoblasts, respectively.
- After the age of 40, loss of bone occurs, considerably accelerated in females post menopause.

24.2 Radiopharmaceuticals for the Evaluation of the Skeletal System

24.2.1 ^{99m}Tc-Diphosphonates

Bone uptake and retention of radiopharmaceuticals belonging to this family (see Chap. 2) is related to calcium content: soft tissues have a low calcium level (0.005%) and exhibit only weak uptake, while bones have a high calcium content

(14–24%) and exhibit high uptake. Other factors determining the degree of radiopharmaceutical uptake in bones include bone perfusion, the nature of calcium phosphate deposits, including size, hydration status, Ca/P ratio, and the osteoblastic/osteoclastic metabolic activity. Trabecular bone has a higher retention index than cortical bone. Therefore, the femur (with its thick cortical component) has a lower retention index than the ribs. Retention in metaphyseal bone (with 14.3% calcium content, rich vascularization, and high metabolic activity) is 0.77% dose/g at 3 h, higher than 0.49% dose/g in diaphyseal bone (which has 23.9% calcium content but is less vascularized). Uptake of bone-seeking radiopharmaceuticals is bound to adequate blood perfusion, so that avascular necrosis appears on the bone scan as a "cold" spot in the early stage (1–2 weeks). Only after the beginning of bone remodeling, the previously "cold" area shows radiopharmaceutical uptake. Increased blood flow results in high radiopharmaceutical uptake.

24.2.1.1 Protocols for ^{99m}Tc-Diphosphonate Scintigraphy

Current EANM guidelines provide an overview of the protocols used for radionuclide imaging of bone metabolism [1]. The average injected activity for bone scintigraphy in an adult person is 500 MBq (13 mCi), and the skeleton receives the highest radiation exposure. In children, the administered activity must be based on body weight according to the EANM/SNMMI Pediatric Dosage Harmonization Working Group [2, 3]; however, a minimum activity of 40 MBq is required to obtain images that can be interpreted correctly.

Images are usually acquired about 3 h after radiopharmaceutical injection, except for the three-phase bone scan typically performed in case of a clinical suspicion of infection or inflammation (e.g., osteomyelitis, prosthesis loosening, or infection). The three-phase bone scan requires dynamic acquisition of a rapid sequence of images of a specific region of interest, which yields a vascular (or blood flow) phase image, performed simultaneous to the i.v. injection of the radiopharmaceutical. This is followed by blood pool phase images acquired about 1–10 min after injection; finally, about 3 h later, a whole-body scan and planar (and possibly SPECT/CT) images of specific regions of interest are acquired.

In the interval between radiopharmaceutical injection and late image acquisition, the patient should be hydrated with at least 1.5 L of water to promote urinary excretion of the fraction of radiopharmaceutical not adsorbed to the skeleton, and to enhance scintigraphic contrast as well as the bone-to-soft-tissue ratio. Overall quality of the images can be affected by other factors, such as renal and/or heart failure, obesity, and advanced age.

Images are acquired with a single- or double-headed gamma camera equipped with low-energy high-resolution parallel-hole collimators (recommended). Alternatively, low-energy general-purpose collimators may be used [1]. A high-resolution pinhole collimator can be used to evaluate small anatomical details (e.g., the femoral head), particularly in children.

Total-body imaging (see example in Fig. 24.1): Acquisition of anterior and posterior views with a matrix of 256 × 1024 or 512 × 2048, zoom factor 1, scanning speed between 10 and 15 cm/min (adjusted to obtain more than 1.5 million

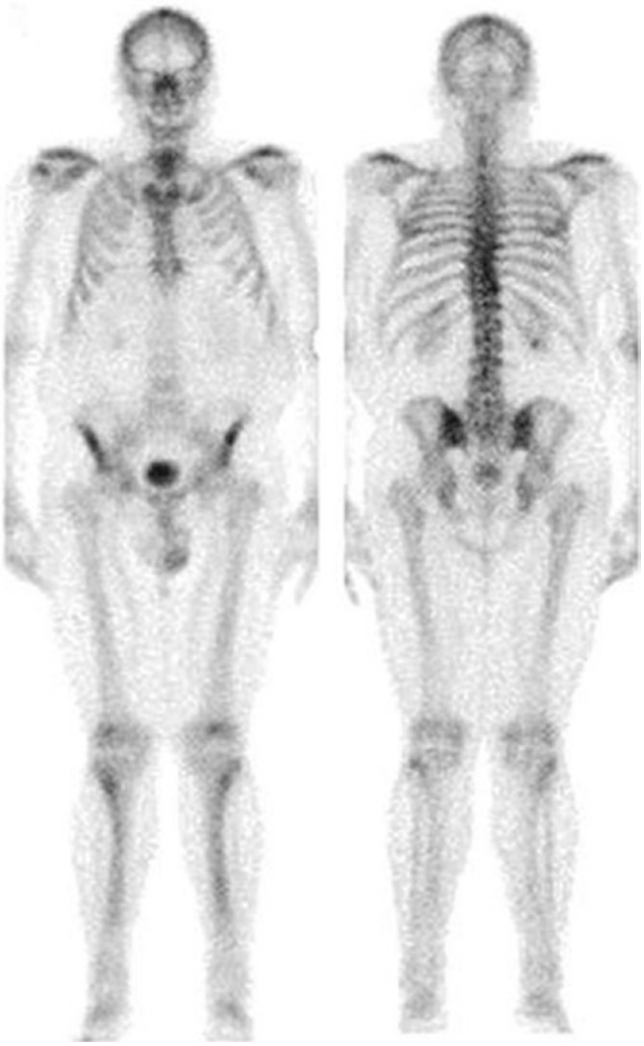

Fig. 24.1 Standard images acquired for planar whole-body skeletal scintigraphy about 3 h after the i.v. administration of ^{99m}Tc-HDP. The left panel depicts the anterior and posterior views obtained in the whole-body imaging mode (with arms along the body). Tracer distribution throughout the skeleton only shows diffuse mild inhomogeneities (e.g., in lower portion of thoracic spine), with mildly increased uptake corresponding to the anterior arc of the second left rib. Furthermore, there is apparent focally increased tracer uptake at the posterior tract of the last ribs, due to overlapping of these bone segments with the kidneys, site of physiologic excretion. Radioactivity accumulation in the urinary bladder is clearly recognized (*modified from: Volterrani D, Erba PA, Mariani G, Eds. Fondamenti di Medicina Nucleare – Tecniche e Applicazioni. Milan: Springer Italy; 2010*)

counts/image). If available, a body contour system should be used, as it automatically changes position of the gamma camera head to maintain a minimum distance between the collimator and the patient. Without automatic contouring, the distance between the head of the gamma camera and the patient should be maintained as close as possible. Total-body images can be obtained in two different modes (often both options are available with the same scanner):

- Sequential images: the head of the gamma camera collects an image, then it moves to the adjacent district, and the acquisition/processing system provides at the end a complete picture of the skeleton.
- Continuous images (preferred in adults).

When a total-body acquisition system is not available, multiple planar images may be acquired, paying attention to overlap each spot to the next one, in order not to miss any area that could be the site(s) of pathological findings.

Planar images of regions of interest (see example in Fig. 24.2): The anterior, posterior, oblique, or lateral views are generally acquired with a matrix of 128 × 128 or 256 × 256, zoom factor 1.33, and a predefined acquisition time (4–10 min) or predefined number of counts. When using a predefined number of counts, this should be determined based on the region of interest (Table 24.1) depending on the field of view (FOV) of the gamma camera: the larger the FOV, the greater the number of total counts required to yield similar count densities over equivalent regions of the skeleton [1].

Planar imaging may be integrated with images obtained using a pinhole collimator (50,000–100,000 total counts) to evaluate small structures or to better visualize some details (Fig. 24.3).

SPECT or SPECT/CT acquisition: The region of interest should be placed in the center of the FOV of the gamma camera. SPECT imaging should be performed as recommended

Table 24.1 Recommended number of counts per region of interest according to the EANM practice guidelines for bone scintigraphy

Region of interest	Predefined number of counts
Skull and large joints	250,000–400,000
Thoracoabdominal region	700,000–1,000,000
Distal joints	150,000–250,000

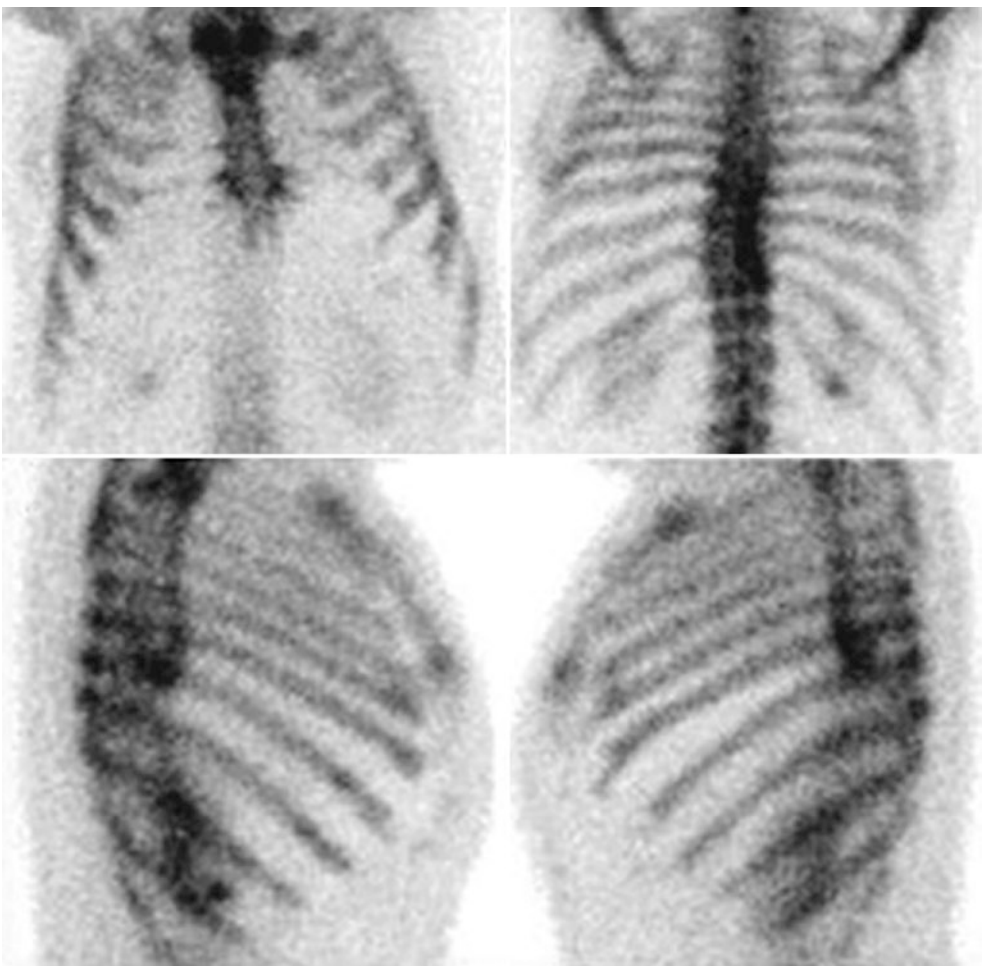

Fig. 24.2 Planar spot images obtained in the same patient as in Fig. 24.1. The top panel depicts the anterior and posterior views of the chest that are acquired with the arms raised in order to resolve in part overlapping of anatomic structures in the upper torso—particularly in the posterior view. Irregular tracer uptake in the cartilaginous tract of ribs adjacent to the sternum reflects partial calcification of the sterno-chondral tracts. The bottom panel depicts the right lateral and left lateral views of the chest. There is some scintigraphic visualization of the kidneys, projecting almost to overlap the spine (*modified from: Volterrani D, Erba PA, Mariani G, Eds. Fondamenti di Medicina Nucleare – Tecniche e Applicazioni. Milan: Springer Italy; 2010*)

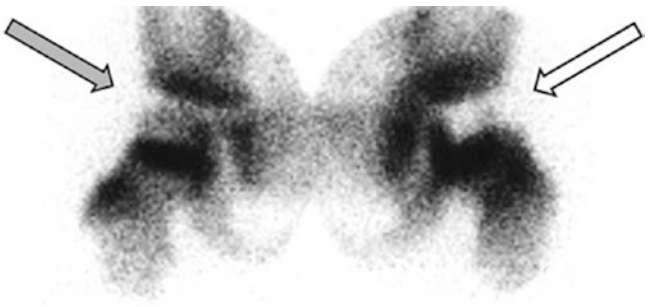

Fig. 24.3 High-resolution acquisitions using a pinhole collimator of the two hips obtained about 3 h after administration of ^{99m}Tc-HDP in a 16-year-old boy with recent avascular necrosis of the left femoral head. Acquisition with a pinhole collimator results in the production of a circle-shaped image; the two images acquired separately for each hip are positioned side-by-side. The right hip (indicated by gray arrow) shows a normal pattern of tracer distribution, where the growth plates are clearly visible (due to young age of the patient); in the left hip, there is a focal area of reduced tracer uptake, corresponding to the non-perfused bone. At later stages after onset of the event, bone remodeling in the left hip during healing will result in increased tracer uptake (*reproduced with permission from: Volterrani D, Erba PA, Mariani G, Eds. Fondamenti di Medicina Nucleare – Tecniche e Applicazioni. Milan: Springer Italy; 2010*)

by the gamma camera manufacturer [1]. In a typical acquisition protocol for a dual-headed gamma camera with the detector heads oriented in a 180°geometry using a *step-and-shot* modality, a total of 60 or 64 frames per detector head, each with a duration of 10–30 s, are acquired over 360° into a 128 × 128 matrix (pixel size 4.6 × 4.6 mm). The acquisition time should be increased to 30–40 s per angular view when imaging regions with low counts (e.g., the skull). An equivalent total number of counts should be acquired if continuous acquisition is used. Regarding the CT component of a SPECT/CT acquisition, particular attention should be paid to patient positioning, since the region of interest must be entirely included in the space delimited by the specific points on the imaging table.

Three-phase bone scan acquisition (see example in Fig. 24.4):

- Vascular or blood flow phase: dynamic acquisition (30–60 frames of 1–2 s) of the region of interest starts simultaneously with the i.v. injection of the radiopharmaceutical.
- Blood pool phase: planar images of the region of interest (3–5 min, matrix size 128 × 128 or 256 × 256, zoom factor 1.33) are acquired within 10 min of tracer injection, preferably at 5 min.
- Delayed phase: acquisition of the whole body in anterior and posterior views about 3 h after tracer administration.

Whole-body images may be implemented with additional planar images of the specific region of interest including anterior, posterior, oblique, and/or lateral views (matrix 128 × 128, zoom factor 1.33), with SPECT (preferably SPECT/CT) acquisitions, or with images acquired with a pinhole collimator.

24.2.1.2 Post-acquisition Processing for ^{99m}Tc-Diphosphonate Scintigraphy

No specific image processing is required for whole-body and planar images, except for setting the display contrast to visualize the low-count segments. Processing is more complex for dynamic three-phase scintigraphy (Fig. 24.4). The blood flow phase is processed by drawing two regions of interest (ROIs), respectively, over the suspected area and over a reference region—typically the contralateral, nonaffected segment. The corresponding activity/time curves so obtained show the regional blood flow, which increases in case of acute inflammation/infection. For the blood pool images, the degree of radiopharmaceutical accumulation in the area of interest (which is compared to the contralateral one) reflects the degree of capillary permeability, which is abnormally increased in case of inflammation/infection. In the delayed images, any area of increased tracer uptake resulting from bone remodeling is evaluated.

In case of SPECT and SPECT/CT acquisitions, parameters for image reconstruction may vary for different manufacturers.

Images are a crucial component of the examination; therefore, they should be provided to the patient and to the referring physician together with the final medical report.

Key Learning Points

- Bone uptake of ^{99m}Tc-diphosphonates depends on perfusion, bone calcium content, and the osteoblastic/osteoclastic metabolic activity.
- Whole-body images of bone metabolism are usually acquired about 3 h after radiopharmaceutical injection.
- In case of infection/inflammation, the delayed images are complemented by images of blood flow obtained directly after tracer injection and of blood pool acquired about 5 min later.
- Planar scans may be complemented by SPECT or SPECT/CT acquisitions.

24.2.1.3 Interpretation Criteria

The most important finding of a normal bone scan is its left-to-right symmetry. The bone segments more exposed to physical stress (e.g., sacroiliac region, vertebrae, major joints) undergo more active bone remodeling and can therefore appear as "hot" spots relative to the remainder of the skeleton

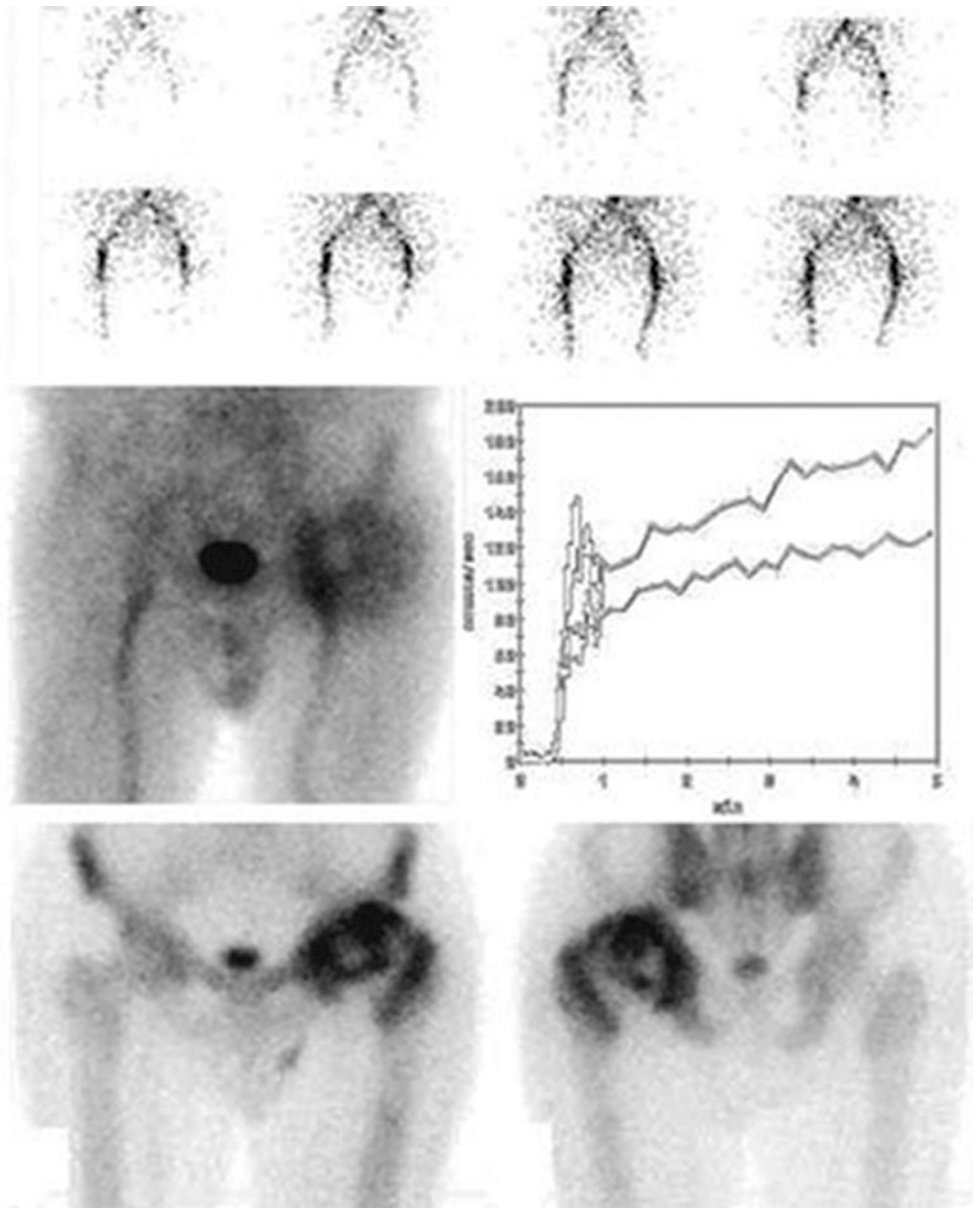

Fig. 24.4 Summary information derived from a three-phase bone scintigraphy performed in a patient with avascular necrosis of left femoral head evaluated in the subacute phase. The eight images in top panel are selected frames from the dynamic acquisition, showing the tracer still in the intravascular phase immediately upon its i.v. bolus injection; the aortoiliac bifurcation is clearly recognized. The activity/time curves in right middle panel correspond to two ROIs defined over the two femoral heads; the higher curve corresponds to the left femoral head, where blood perfusion is now enhanced versus the right femoral head—corresponding to the recovery phase. The left middle panel depicts static acquisition at 5 min post-injection—the so-called "blood pool" phase; there is obviously increased radioactivity accumulation at the left hip, corresponding to increased capillary permeability. The two images in lower panel depict the static anterior and posterior views acquired about 3 h post-injection; markedly enhanced bone remodeling in left hip, where the core of the femoral head still exhibits reduced metabolic activity and is surrounded by active bone remodeling (*modified from: Volterrani D, Erba PA, Mariani G, Eds. Fondamenti di Medicina Nucleare – Tecniche e Applicazioni. Milan: Springer Italy; 2010*)

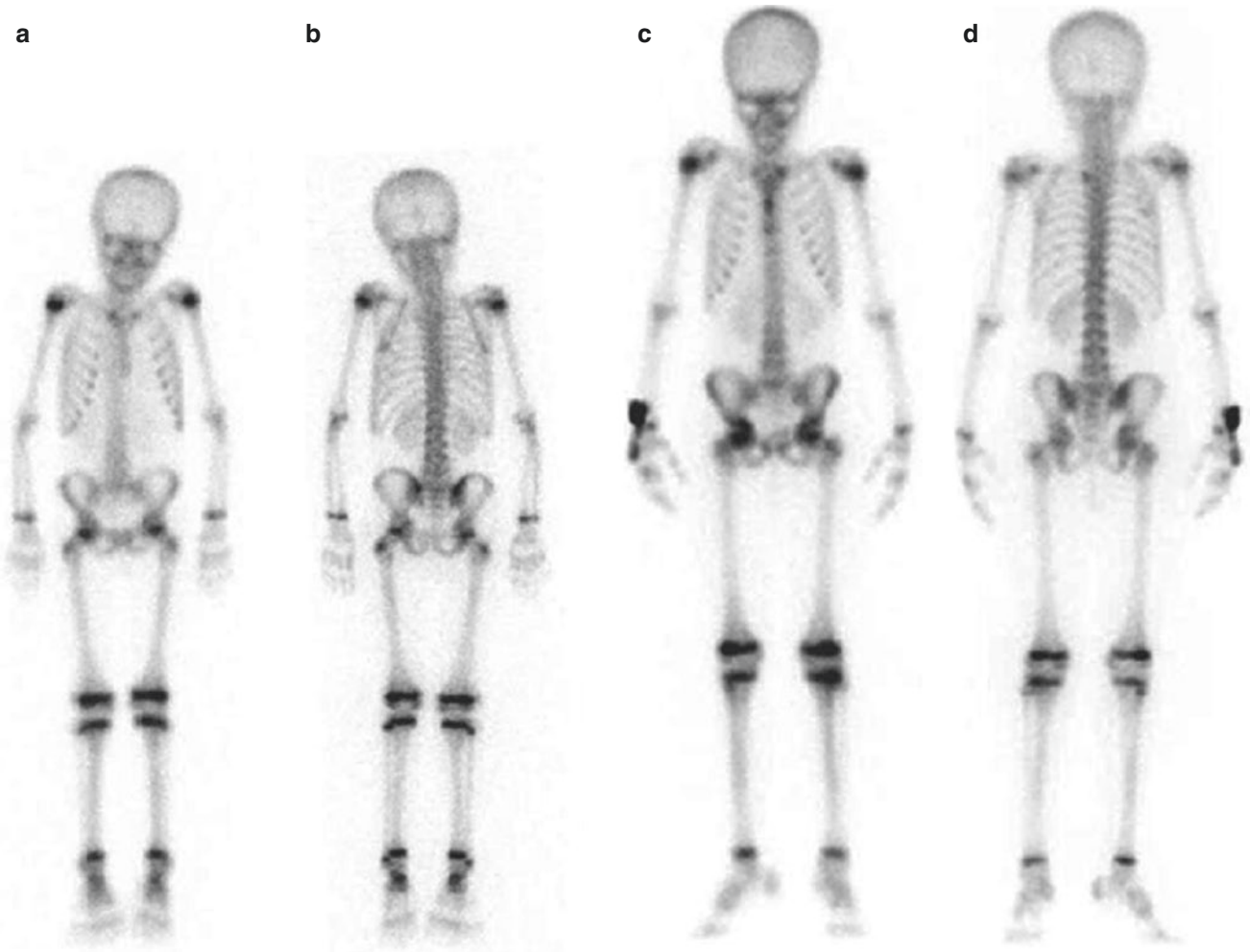

Fig. 24.5 Planar whole-body skeletal scans in children and adolescents. Anterior (**a**) and posterior (**b**) views obtained in a child in the 6–8-year age range. Anterior (**c**) and posterior (**d**) views obtained in a preadolescent child in the 10–12-year age range (radioactivity accumulation at the right wrist is due to some residual tracer remaining at the injection port)

(Fig. 24.1). Similarly, areas with active bone remodeling during growth in children and adolescents exhibit markedly increased uptake on the bone scan (Fig. 24.5). Particular attention should be paid to the evaluation of some districts:

- Skull: counts are relatively low. Cranial suture lines are visualized in approximately 1% of the adults. In the anterior view, orbital and facial bones are well visualized; some uptake may be present at maxilla and ethmoid, as result of chewing-induced stress. In childhood, the suture between the sphenoid and the occipital bone may be particularly evident.
- Neck: the cervical vertebrae can be distinguished only using high-resolution acquisitions; the spinous process of C7 is usually well visualized. In physiologic conditions, tracer uptake in the neck (in the absence of free ^{99m}Tc-pertechnetate) can be observed in the thyroid cartilage or the hyoid bone.
- Chest: the joint between the manubrium and body of the sternum may exhibit increased tracer uptake, as also the sternoclavicular joints. In elderly people it is common to observe some tracer uptake in the calcified rib cartilages. The ribs normally exhibit relatively low tracer uptake, although insertion of the erector spinae muscles can cause uptake inhomogeneity (physiological variant in about 7% of subjects). The scapulae are well visualized, with increased activity at the lower tip, where the mechanical stress associated with muscle insertion is greater.
- Spine: the upper thoracic vertebrae are not displayed individually, whereas the lower thoracic and lumbar vertebrae are well seen. The physiological lumbar lordosis often makes the lumbar vertebrae to seem relatively "hot" in the anterior view.
- Pelvis: tracer uptake is usually symmetric between the right and left sides; even if the patient is asked to void the bladder immediately before acquiring the scan, it is com-

mon to observe some residual accumulation of activity in the bladder, which may mask the pubic bone/symphysis and sacrum.
- Upper and lower limbs: there is relatively low activity. A relatively increased tracer uptake is typically seen in the periarticular regions; in children the presence of increased tracer uptake in the epiphysis of long bones (growth plate) is common as it reflects the physiologic process of bone growth (see Fig. 24.5).

Scintigraphic images depict the extent of bone remodeling, mostly with reference to the mineral component. In fact, the degree of tracer uptake is mainly related to increased osteoblastic activity. Osteolytic lesions (most often caused by bone metastases from various cancers) are almost invariably associated with an osteoblastic reaction, which (although insufficient to counterbalance osteolysis) is generally sufficient to induce increased tracer uptake on the bone scan. However, the uptake of bone-seeking radiopharmaceuticals is related to several physiological and pathological conditions in the absence of significant osteolysis: bone fracture (increased tracer uptake may last for years), osteoarthritis, Paget's disease of the bone, and so on. "Pure" osteolytic lesions without osteoblastic reaction (such as those frequently caused by myeloma and some metastases from renal cancers) are generally negative on the bone scan. Based on these considerations, an accurate medical history aimed at identifying prior traumas, fractures, surgical interventions, or other concomitant diseases should be obtained before performing and evaluating bone scintigraphy.

In certain clinical situations, the normal contrast between healthy and pathological tissues (as well as between the skeleton itself and soft tissues) is reduced as a consequence of an increased background activity due to altered distribution and/or excretion of the tracer, for example, in case of renal failure or obesity (Fig. 24.6). Altered biodistribution of the radiopharmaceutical can also result from an error during administration, as it occurs in case of partial tracer extravasation out of a vein; in this case a focal area of uptake is observed at the injection site, and it may be associated with visualization of one or more (axillary) lymph nodes on the same side. Such findings are generally well recognized as non-pathological; however, in case of nontypical sites of injection, such "hot" spot areas may be a potential source of misinterpretation of images. Although rarely happening, there is the possibility that the radiopharmaceutical is erroneously injected in an artery rather than in a vein; in this case, scintigraphy differs considerably from the normal pattern, resulting in intense tracer accumulation in the portion of the arm distal from the injection site, where bone/soft tissue contrast is remarkably low due to persisting high background activity (Fig. 24.7).

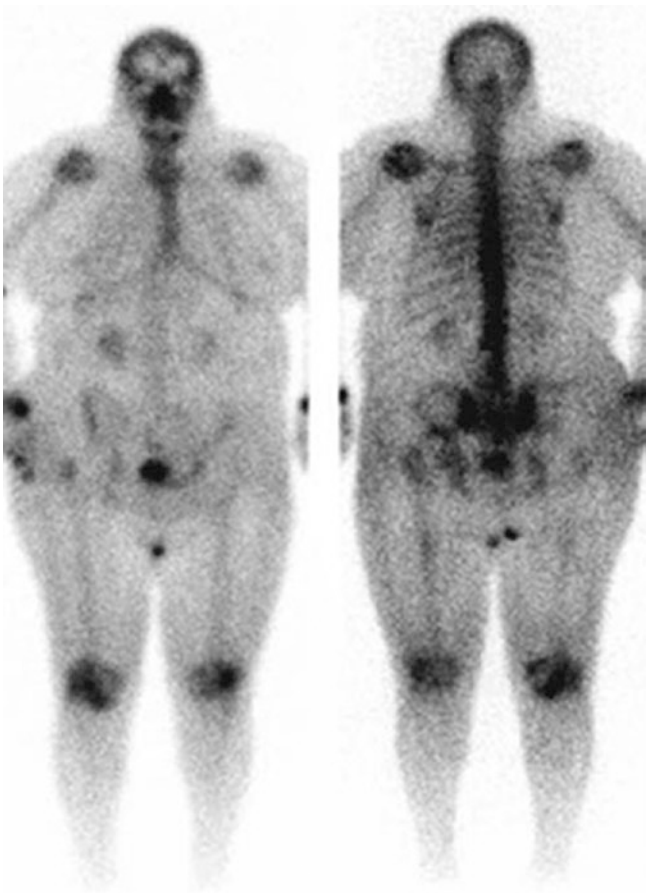

Fig. 24.6 Planar whole-body scan (anterior and posterior views) obtained in a morbidly obese woman about 3 h after i.v. administration of ^{99m}Tc-HDP. Scintigraphic visualization of the skeleton is markedly impaired both because of low bone-to-soft-tissue ratios and because of attenuation of γ-rays by the overabundant adipose tissue, particularly in the anterior view. Increased tracer uptake can be noticed at the knees, most likely due to degenerative osteoarticular disease caused by the increased workload on the joints associated with obesity (*reproduced with permission from: Volterrani D, Erba PA, Mariani G, Eds. Fondamenti di Medicina Nucleare – Tecniche e Applicazioni. Milan: Springer Italy; 2010*)

In three-phase bone scintigraphy, the activity/time curve of the pathological segment reaches a higher peak than the contralateral side when blood flow is increased, while the peak is lower in case of reduced perfusion. Increased radioactivity accumulation in the blood pool image is a consequence of increased capillary permeability (with possible local edema) associated with inflammation/infection, while increased tracer uptake observed in the delayed phase denotes an active process of bone remodeling. Three-phase bone scintigraphy is generally used to confirm lesion(s) characterized by hyper-vascularization and increased bone remodeling. A typical example is seen in acute osteomyelitis, where increased vascularization (accumulation in the blood flow phase) coexists with increased capillary permeability (accumulation in blood pool images) and with increased osteoblastic activity

(uptake in delayed images). The early phase of aseptic (avascular) necrosis of the femoral head is characterized by hypovascularization (hypoperfusion in the blood flow phase) visible as a "cold" area with an intense peripheral uptake in the delayed images, the latter reflecting repair and bone remodeling. A three-phase bone scintigraphy is the investigation of choice in patients with suspected prosthetic loosening with some probability of infection.

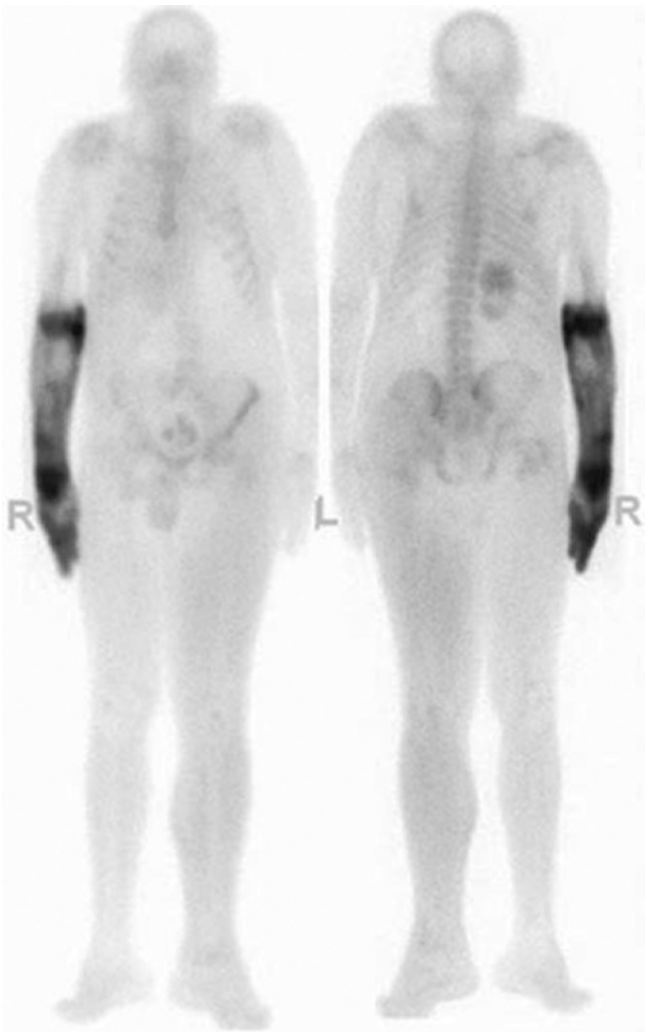

Fig. 24.7 Planar whole-body scan obtained about 3 h after administration of ^{99m}Tc-MDP in a patient previously submitted to left nephrectomy. The tracer had inadvertently been injected intra-arterially rather than intravenously, resulting in markedly enhanced radioactivity accumulation in the soft tissues distal to the point of intra-arterial injection, with a pattern resembling an "evening glove." As an incidental finding, the left lower limb (where lymphedema secondary to left nephrectomy and lymphadenectomy is present) is increased in size and exhibits enhanced radioactivity accumulation versus the right lower limb (*reproduced with permission from: Volterrani D, Erba PA, Mariani G, Eds. Fondamenti di Medicina Nucleare – Tecniche e Applicazioni. Milan: Springer Italy; 2010*)

In conclusion, the possible sources of error when interpreting a bone scan include focal soft tissue spot (e.g., intramuscular injections, hematoma, severe renal failure, hypercalcemia), partial tracer extravasation, attenuation artifacts caused by metal prostheses, motion artifacts, urinary contamination, superimposition of bladder activity, "pure" lytic lesions, renal failure, and homogenously increased bone activity (e.g., superscan) [1].

Table 24.2 summarizes the main clinical indications for bone scintigraphy with ^{99m}Tc-diphosphonates [1].

Table 24.2 Summary of indications for bone scintigraphy with ^{99m}Tc-diphosphonates according to the EANM guideline[a]

Oncology
• Solid tumors with high propensity for bone metastasis, including prostate, breast, lung, and renal cancers
• Malignant hematological disease (lymphomas) limited to bone
• Primary bone tumors and bone dysplasia, including osteosarcoma, osteoid osteoma, osteoblastoma, fibrous dysplasia, giant cell tumor
• Soft tissue sarcomas, including rhabdomyosarcoma
• Paraneoplastic syndromes, including hypertrophic pulmonary osteoarthropathy, algodystrophy, polymyalgia rheumatica, poly-dermatomyositis, and oncogenic osteomalacia
• Distribution of osteoblastic activity before radionuclide therapy with bone-seeking agents
Rheumatology
• Chronic inflammatory arthritis, including rheumatoid arthritis, spondyloarthropathies and related disorders (ankylosing spondylitis, psoriatic arthritis, Reiter's arthritis, SAPHO syndrome [synovitis, acne, pustulosis, hyperostosis, osteitis], chronic recurrent multifocal osteomyelitis), and sacroiliitis
• Osteoarthritis of the lumbar facet joints and hip, femorotibial and femoropatellar osteoarthritis, rhizarthrosis, tarsal osteoarthritis
• Enthesopathies, including plantar fasciitis, Achilles tendinitis, and bursitis
• (Avascular) Osteonecrosis, most frequently located at the femoral head, femoral condyle, and tibial plateau
• Osteonecrosis of the jaw
• Complex regional pain syndrome type I of the hand, hip, knee, and foot
• Tietze's syndrome (costochondritis)
• Polymyositis
• Paget's disease of bone
• Langerhans cell histiocytosis (LCH): single system LCH and multisystem LCH with bone involvement
• Non-Langerhans cell diseases, such as Erdheim-Chester disease, Schnitzler syndrome, and Rosaï-Dorfman disease
• Other rare osteoarticular diseases, including sarcoidosis with bone involvement, mastocytosis, Behçet's disease, and familial Mediterranean fever
Bone and joint infection
• Osteomyelitis (acute, subacute, or chronic, of bacterial, mycobacterial, or fungal origin)
• Septic arthritis
• Spondylodiscitis or spondylitis

Table 24.2 (continued)

• Septic loosening or mechanical complication of internal fixation (long bones or spine) or arthroplasty (hip, knee, ankle, or shoulder)
• Malignant (necrotizing) external otitis
Orthopedics, sports and traumas
• Periostitis, including shin splints and thigh splints
• Enthesopathies, including plantar fasciitis, Achilles tendinitis, and bursitis
• Spondylolisthesis (acute or subacute)
• Radiologically occult stress-related fractures (e.g., scaphoid, tarsals) or nonspecific symptoms
• Insufficiency fractures, including osteoporotic vertebral or occult fractures, sacral fractures, femoral head or neck fractures, tibial plateau fractures, and tarsal and metatarsal fractures
• Septic loosening, mechanical complication, and synovitis of internal fixation (long bones or spine) or prosthesis (hip, knee, ankle, or shoulder)
• Pseudoarthrosis (delayed union, nonunion)
• Periarticular heterotopic ossification
• Viability of bone graft
Metabolic bone disease
• Primary and secondary hyperparathyroidism
• Osteomalacia
• Renal osteodystrophy
• Rare skeletal manifestations of endocrine disorders, including hyperthyroidism and acromegaly
• Vitamin D deficiency
Pediatrics
• Osteochondritis of the hip (Legg-Calvé-Perthes disease)
• Transient synovitis of the hip
• Osteoid osteoma
• Battered child syndrome
• Mandibular condylar hyperplasia
• Bone infarction (sickle cell disease, thalassemia)
Exploration of unexplained symptoms
• Subacute or chronic musculoskeletal or bone pain with normal clinical examination and radiographs (arthralgia, monoarthritis, oligoarthritis, polyarthritis, localized or multifocal bone pain, backache)
• Further exploration of abnormal biochemical (e.g., phosphate or calcium metabolism) or radiological findings
• Fever of unknown origin: exclusion of osteomyelitis

[a]It should be noted that this basically is a compilation of the skeletal conditions that imply increased uptake of bone-seeking radiopharmaceuticals. Therefore, from the diagnostic point of view, virtually all such conditions should be considered when interpreting a positive bone scintigraphy, taking into account also the specific clinical scenario based on which the referring physician ordered the bone scan

24.2.2 Quantitative Bone SPECT/CT

To date SPECT/CT systems allow quantification of osseous radioactivity concentration in absolute units, such as kBq/mL with an acceptable degree of accuracy. About 3 h after i.v. injection of ^{99m}Tc-diphosphonates, vertebral radioactivity concentration is in the range of 50 kBq/mL, translating into standardized uptake values (SUV) of around 6 [4]. SUV correlates with CT density. In principle, using quantitative SPECT/CT, normal values of tracer uptake can be established for each skeletal region. These normal values might be used to diagnose diffuse abnormalities of tracer uptake in disseminated bone disease. Furthermore, quantitative SPECT/CT allows monitoring of the activity of osseous metastases in the course of treatment. Preliminary evidence indicates that this technology might also be useful to assess the floridity of skeletal lesions more accurately than visual evaluation of tracer uptake [5]. Future work will show how this new potential of bone scintigraphy can be used with benefit in clinical routine.

Key Learning Points

- The most important finding of a normal bone scan is its left-to-right symmetry.
- The intensity of tracer uptake is mainly related to increased osteoblastic activity, which is present also in most predominantly osteolytic metastases.
- Purely lytic metastases, e.g., from myeloma, may escape detection at bone scintigraphy.
- Increased radioactivity accumulation in the blood pool image is a consequence of increased capillary permeability associated with inflammation and/or infection.
- To date SPECT/CT cameras afford the determination of tissue radioactivity concentration expressed, e.g., as SUV values, which is around 6 in vertebral bone on the delayed images.

24.2.3 ^{18}F-Fluoride PET

^{18}F-Fluoride accumulates in bones with a mechanism similar to diphosphonates (see Chap. 3) and may therefore be used to acquire PET images of the skeleton. Upon i.v. injection, ^{18}F-fluoride diffuses quickly from the blood to reach the extracellular bone matrix. All ^{18}F-fluoride that reaches the bone (about 50% of injected activity, similar to ^{99m}Tc-diphosphonates) is adsorbed. The exchange of $^{18}F^-$ ions with the hydroxyl groups of hydroxyapatite crystals allows linking to the surface of the bone matrix, while its retention at bone remodeling sites depends on subsequent migration inside the crystalline bone matrix. Bone accumulation and blood clearance are fast (with bi-exponential kinetics and half-lives of 0.4 h and 2.6 h, respectively), so that 1 h after administration only 10% of the injected activity is still circulating. Therefore, a high bone/soft tissue ratio is reached within a short time, resulting in high-quality images as early as even <1 h after injection.

Fig. 24.8 Patterns of normal distribution of ^{18}F-fluoride visualized during PET, displayed as maximum intensity (MIP) attenuation-corrected images. The adult skeleton (left) is characterized by well-evident tracer uptake—relatively enhanced in the skull, ribs, spine, borders of the scapula, pelvis, and along the cortices of the long bones (the focal area of activity accumulation in the right foot corresponds to some extravasation of the tracer at the injection site in a subject with difficult venous access). The pattern of ^{18}F-fluoride distribution observed in the pediatric skeleton (as in the 14-year-old girl represented here) shows, in addition, linearly increased tracer uptake along the epiphyseal growth plates of the long bones, similar to a conventional ^{99m}Tc-MDP bone scan (*image of the normal adult scan kindly provided by Guofan Xu, MD, PhD, Department of Nuclear Medicine, M.D. Anderson Cancer Center, Houston, Texas, USA*)

Estimates of radiation burden to patients following administration of ^{18}F-fluoride or ^{99m}Tc-diphosphonates (2.11 MBq/kg and 7.4 MBq/kg, respectively) indicate that in adults there are no significant differences between the two radiopharmaceuticals (4 mSv and 3 mSv, respectively, for a 70 kg patient), whereas the effective dose is lower for ^{99m}Tc-diphosphonates (2 mSv) than for ^{18}F-fluoride (about 3.5 mSv) in children weighing <20 kg.

^{18}F-Fluoride PET imaging may be started 15–30 min after the injection, acquiring a number of bed positions sufficient to cover the region of interest according to the clinical indication; if the region of interest is limited (e.g., the spine), 2–3 bed positions may be sufficient, while whole-body images are required for all oncological indications [6] (see example in Fig. 24.8). The acquisition time should be 3–5 min per bed position, but it may be modified according to the scanner and the injected activity; the 3D acquisition mode is generally set as the standard operation mode in current PET scanners. In general, the parameters used for [^{18}F]FDG PET imaging can be used also for ^{18}F-fluoride PET, although sometimes it may be necessary to use some filters to correct for the high concentration of activity in very small segments. Artifacts may occur (most evident in sagittal and coronal sections) for the thoracic spine (lungs attenuate less than soft tissues) when no attenuation correction is applied. Attenuation correction produces images with better uniformity than without attenuation correction; the decision as to whether or not to correct the images for attenuation varies according to the segment to be explored. The residual bladder activity due to the urinary excretion of ^{18}F-fluoride may obscure the pelvis.

The overall time required for a ^{18}F-fluoride PET scan is much shorter than for conventional bone scintigraphy: 15–30 min waiting time after tracer injection (versus about 3 h for ^{99m}Tc-diphosphonates) and 15–30 min acquisition time (versus at least 40 min when SPECT images are acquired in addition to planar imaging). This faster acquisition time results in better patient's compliance, thus reducing artifacts due to patient's movements.

The clinical indications for ^{18}F-fluoride PET are the same as for conventional bone scintigraphy. Generally, ^{18}F-fluoride PET identifies more lesions than scintigraphy with ^{99m}Tc-diphosphonates (especially if planar imaging only is acquired), particularly in the axial skeleton, and reduces the number of doubtful/equivocal findings (see Fig. 24.9). Given the extremely high sensitivity of ^{18}F-fluoride PET in identifying skeletal areas with even mild changes in mineral metabolism, interpretation of the scans requires caution and close correlation with the CT counterpart of each focal area of increased tracer uptake.

Table 24.3 summarizes the main clinical indications for ^{18}F-fluoride PET/CT according to the SNM guideline released in 2010 [7].

24.2.3.1 ^{18}F-Fluoride PET Acquisition Protocol

Uptake of ^{18}F-NaF in the skeleton measures the amount of osteoblastic activity in actively mineralizing bone. This process consists of ^{18}F-fluoride being deposited on the hydroxyapatite surface of newly forming bone by exchanging fluoride with hydroxyl ions and creating fluorapatite. Standardized uptake values (SUVs) are calculated on the basis of the activity concentration (kBq/mL) normalized to injected activity (MBq) and body weight (kg) of the patient. SUV of a lesion or a structure is often expressed as a maximum value (SUV_{max}) or mean value (SUV_{mean}) [8, 9]. Alternatively, since the rate-limiting step of tracer uptake is regional blood flow,

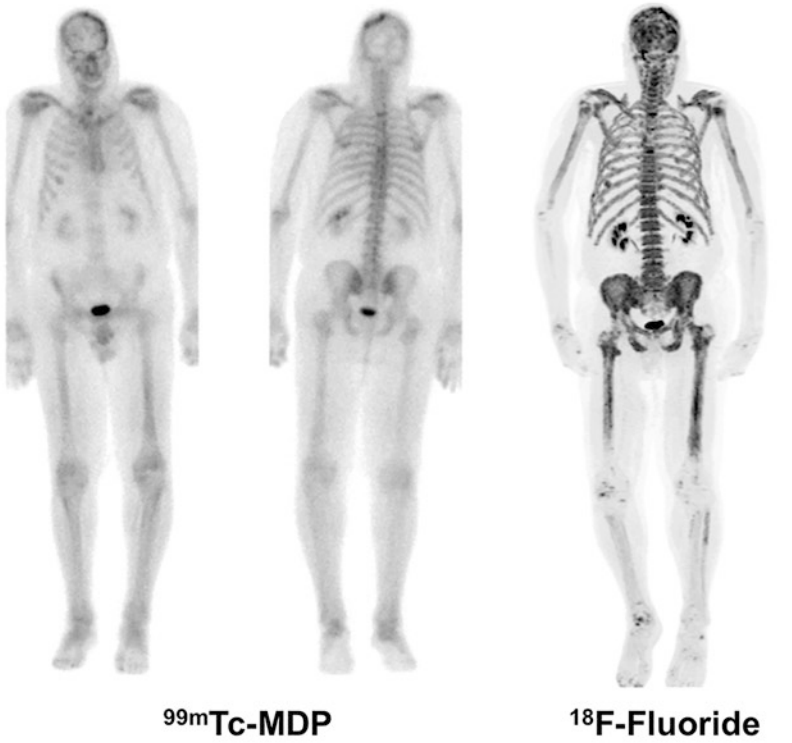

Fig. 24.9 Comparison of conventional ^{99m}Tc-MDP bone scintigraphy (anterior and posterior whole-body images on the left) and PET with ^{18}F-fluoride (MIP image on the right). Images refer to a 69-year-old man with a history of metastatic prostate cancer and rising serum PSA levels. The conventional bone scintigraphy revealed only irregularly increased tracer uptake in the left parietal bone, with equivocal findings in the thoracic spine. PET with ^{18}F-fluoride performed shortly after the ^{99m}Tc-MDP bone revealed multifocal bone metastases, well evident in the skull, in the thoracic spine, and in other skeletal segments

Table 24.3 Summary of indications for PET/CT with ^{18}F-fluoride according to the SNM guideline[a]

Primary indication
• Identification of skeletal metastases, including localization and determination of the extent of disease
Indications without sufficient information, but most likely appropriate
• Back pain and otherwise unexplained bone pain
• Child abuse
• Abnormal radiographic or laboratory findings
• Osteomyelitis
• Trauma
• Inflammatory and degenerative osteoarticular disease
• Avascular necrosis
• Osteonecrosis of the mandible
• Condylar hyperplasia
• Metabolic bone disease
• Paget's disease of bone
• Bone graft viability
• Complications of prosthetic joints
• Reflex sympathetic dystrophy
• Distribution of osteoblastic activity before radionuclide therapy with bone-seeking agent

[a]It should be noted that this guideline was issued in 2010. In the time elapsed since that date, a much more important body of evidence has been acquired on the clinical benefits of this imaging modality in a vast variety of clinical conditions

bone and plasma clearance measurements normalized to the ratio of uptake values to arterial tracer concentration are calculated as an index of new bone formation. The Hawkins method calculates plasma clearance (K_i) using a three-compartment model to analyze the bone time-activity curve and the arterial input function [10]. Patlak graphical analysis is a simplification of the Hawkins method, calculating plasma clearance as the slope of normalized bone uptake against normalized time [11].

Although plasma clearance measurements from dynamic PET can accurately trace bone formation rate, practical issues limit its potential for routine clinical use. Patients must endure a 60 min image acquisition and undergo arterial blood sampling. The 60 min dynamic scan is also costly to perform and can only examine one skeletal region at a time. Therefore, a whole-body assessment requires multiple scans over different sessions. Plasma clearance measurements scans are frequently used, however, because they include tracer availability when calculating relative uptake among competing skeletal sites.

Key Learning Points

- ^{18}F-Fluoride allows the visualization of bone metabolism in a manner similar as the ^{99m}Tc-diphosphonates.
- ^{18}F-Fluoride-PET offers higher signal-to-noise ratios and better spatial resolution than ^{99m}Tc-diphosphonate-SPECT.
- Waiting time after tracer injection is 15–30 min, much shorter for ^{18}F-fluoride PET than for ^{99m}Tc-diphosphonate SPECT.

24.2.4 Perspectives for Radiolabeled Diphosphonates

The availability of clinical ^{68}Ge/^{68}Ga generators (^{68}Ga $T_{1/2}$ = 67.7 min; high positron branching = 89%) provides new options to image bone metastatic disease with PET/CT. In fact, several compounds of biological interest can be labeled with ^{68}Ga as obtained from generators in the chemical state of ^{68}Ga(III). Since gallium is a metallic element, radiolabeling requires the use of a chelator in order to bind the radionuclide to the molecule of interest. The macrocyclic chelators most frequently used to this purpose are 1,4,7,10-tetraazacyclododecane-1,4,7,10-tetraacetic acid (DOTA) and 1,4,7-triazacyclononane-1,4,7-triacetic acid (NOTA) or their derivatives. The combination of novel bisphosphonates with macrocyclic chelators provides promising tracers for either diagnosis and/or therapy of bone metastatic disease, according to the current concept of *theragnostics*. In fact, the good target-to-background ratio, which all bisphosphonates have in common, is also advantageous for therapeutic applications due to reduced radiation dose for nontarget tissue. ^{68}Ga-NO2AP^{BP} is characterized by a very high uptake in bone metastases (30–60 min after injection), combined with fast blood clearance and very low uptake in soft tissue. This pattern of biodistribution (which is comparable to ^{18}F-fluoride) is superior to that of ^{99m}Tc-MDP [12].

The use of the DOTA-based radiopharmaceutical ^{177}Lu-BPAMD has proved valuable for therapeutic purposes, since the low-energy β^- emission of ^{177}Lu hardly reaches the bone marrow; accordingly, only low or no hematologic toxicity was observed in pilot clinical investigations. New ^{68}Ga- and ^{177}Lu-labeled bisphosphonates possessing improved pharmacological properties are being explored for possible clinical use [13].

Preliminary studies suggest a high therapeutic potential for zoledronic acid, the most potent bisphosphonate currently employed in patients with bone metastatic disease, upon conjugation with DOTA (DOTA^{ZOL}) for labeling with ^{177}Lu. A NODAGA-based zoledronic acid derivative (NODAGA^{ZOL}) has the advantage over the DOTA analog that purification is not required after labeling with ^{68}Ga. Both ^{68}Ga-NODAGA^{ZOL} and ^{68}Ga-DOTA^{ZOL} exhibit similarly high bone accumulation, low uptake in soft tissue, and fast renal clearance. Nevertheless, bone accumulation is greater for NODAGA^{ZOL} than for DOTA^{ZOL}. Considering the potential of ^{177}Lu-DOTA^{ZOL} for endoradiotherapy, ^{68}Ga-NODAGA^{ZOL} might become a theranostic agent for bone metastases.

Key Learning Point

- The development of ^{68}Ga-labeled PET tracers suitable for investigating bone metabolism is ongoing.

24.3 Clinical Applications

24.3.1 Primary Bone Tumors

Malignant primary tumors of the bone usually feature highly increased bone metabolism as well as increased tracer uptake in the first two phases of a three-phase bone scintigraphy. In malignant primary bone tumors, bone scintigraphy is usually not indicated to diagnose the primary but rather to define the extent of osseous spread. Detection of a primary bone tumor on a bone scan performed for bone pain is in most cases incidental. In malignant as well as in the benign bone tumors, planar radiography and MRI are usually performed before bone scintigraphy. However, in some cases X-ray and MRI cannot identify the exact nature of an osseous lesion. Bone scintigraphy is not very well suited for distinguishing malignant from benign bone lesions, as many of the benign tumors also have highly increased uptake of the ^{99m}Tc-diphosphonates. However, as a rule of thumb, the absence of an increase in bone metabolism usually points to a benign tumor.

[^{18}F]FDG PET/CT has recently emerged as an extremely valuable diagnostic tool in primary bone tumors. In an extensive meta-analysis, Bastiaannet et al. demonstrated that [^{18}F]FDG PET/CT has high sensitivity and specificity in discriminating between sarcomas and benign tumors, as well as low-grade from high-grade sarcomas based on the semiquantitative measurements of glucose consumption (SUV) [14]. Despite this favorable experience, the current American College of Radiology (ACR) appropriateness criteria guideline (https://acsearch.acr.org/docs/69421/Narrative/) does not recommend the use of PET/CT with [^{18}F]FDG the staging or characterization of primary bone tumors, in part likely because of the overlap in the range of SUVs between benign and malignant lesions. Instead, PET/CT with [^{18}F]FDG is currently included in the NCCN guidelines for primary and metastatic bone tumors [15], and it constitutes an extremely useful tool for many orthopedic oncologists, who are increasingly referring patients for [^{18}F]FDG PET/CT because of its high sensitivity (well over 80%) [16, 17] for the detection of bone metastases and recurrences.

24.3.1.1 Osteosarcoma

Osteosarcoma (OS) is the most common primary malignant bone tumor in children and adolescents and the second most common primary malignant bone tumor following multiple myeloma in all age groups [18]. OS is more common in males than in females and usually presents as a painful mass rising at the metaphyseal regions, the knee being the most common site. Histologically, osteosarcomas can be divided into a number of subtypes according to the degree of differentiation, location within the bone (intramedullary, surface/juxtacortical, extra-skeletal), and histological variants. Osteosarcoma may also occur as a secondary lesion in asso-

ciation with underlying benign conditions (secondary osteosarcoma). The most common subtype of OS is the conventional type (80%). Typical X-ray features include medullary and cortical bone destruction, wide zone of transition, permeative or moth-eaten appearance, and aggressive periosteal reaction (sunburst type, Codman triangle, lamellated-onion skin reaction, soft tissue mass with variable calcified and osteoid tumor matrix).

CT is generally used for staging or identification of predominantly lytic lesions in which small amounts of mineralized material may be undetected on both plain film and MRI. In particular, chest CT is the most appropriate exam for the screening of pulmonary metastases from osteosarcoma.

A joint-to-joint MRI is the most accurate imaging investigation for local staging, particularly in evaluating for intraosseous tumor extension, soft tissue involvement, or skip metastases. Assessment of the growth plate is essential as up to 75–88% of metaphyseal tumors do cross the growth plate into the epiphysis. On MRI imaging, the non-mineralized soft tissue component shows intermediate T1w and high T2w signal intensity, while the mineralized/ossified components show low T1 and T2 signal intensity. Scattered regions of hemorrhage with variable signal or of necrosis are also frequent. Evaluation for enhancement of the solid tumor component is essential for guiding biopsy.

For some decades scintigraphy with ^{99m}Tc-diphosphonates has constituted one of the mainstays in the characterization and management of patients with osteosarcoma. The tumor lesions are characterized by avid uptake of the bone-seeking agent, both at the primary site (Fig. 24.10) and at possible metastatic sites within the skeleton (Fig. 24.11) and/or in soft tissues (e.g., pulmonary or liver metastases). In patients who are candidates for limb amputation (which is employed with declining frequency in case of osteosarcoma, because of effective neoadjuvant therapies reducing the need for such aggressive treatments) or to other forms of less invasive surgery, bone scintigraphy can serve as a guide to select the most appropriate level of bone resection—based on identification of the segment of bone showing increased tracer uptake, therefore involved by the disease.

Although [^{18}F]FDG PET/CT in osteosarcoma is not yet considered appropriate by ACR criteria, multiple studies have demonstrated that PET/CT can provide useful information regarding the primary site, staging, and follow-up [19, 20]. Besides assessment of locoregional extent, [^{18}F]FDG PET/CT has proven to be of value in estimating the biological aggressiveness of the tumor, as high-grade sarcomas are characterized by intense [^{18}F]FDG avidity. Furthermore, the tumor is often metabolically nonhomogeneous, and PET/CT may increase the diagnostic yield of biopsy by directing the needle to the area of most intense metabolism. Using a tumor-to-background [^{18}F]FDG uptake ratio cutoff level of 3.0 for malignant bone lesions [21], the sensitivity, specificity, and accuracy of [^{18}F]FDG PET in identifying malignant OS were 93%, 66.7%, and 81.7%, respectively. Furthermore, [^{18}F]FDG PET/CT is more accurate for preoperative staging of sarcomas than conventional imaging [22, 23]. [^{18}F]FDG PET/CT also plays a role in assessing response to treatment and has high prognostic significance [24]. Considering that the amount of necrosis induced by neoadjuvant chemotherapy is a significant prognostic factor for survival, a post-therapeutic SUV_{max} <2.5 predicts tumor necrosis in osteosarcoma [25]. After neoadjuvant chemotherapy, SUV_{max} <2 correlates with good histologic

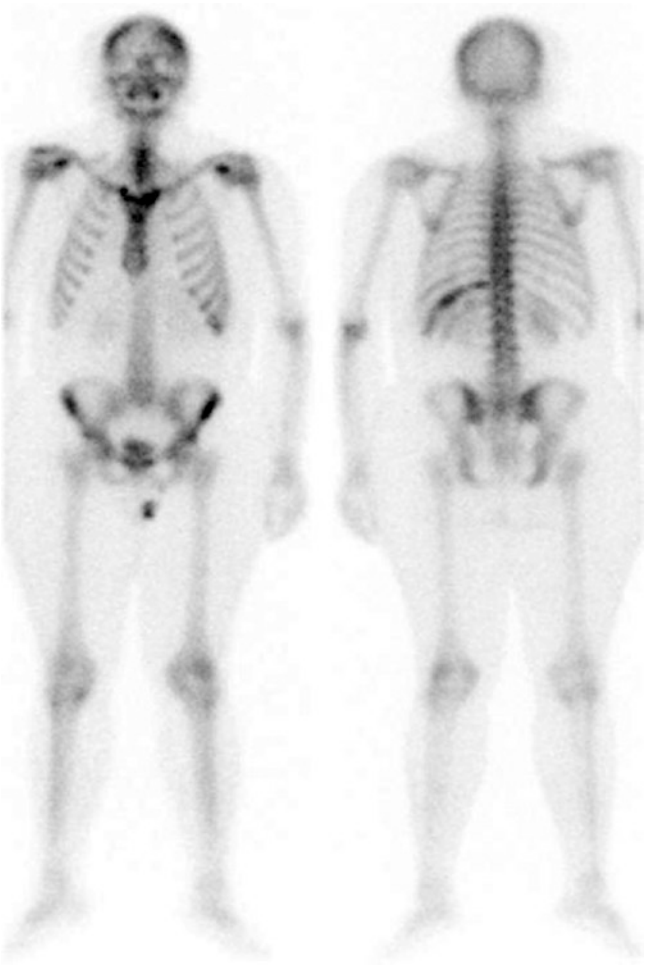

Fig. 24.10 Planar whole-body scintigraphy with ^{99m}Tc-HDP in a patient with newly diagnosed osteosarcoma confined to the left 11th rib, better imaged in the posterior view. The scintigraphic pattern per se does not have distinctive features allowing a differential diagnosis versus other bone diseases (*reproduced with permission from: Volterrani D, Erba PA, Mariani G, Eds. Fondamenti di Medicina Nucleare – Tecniche e Applicazioni. Milan: Springer Italy; 2010*)

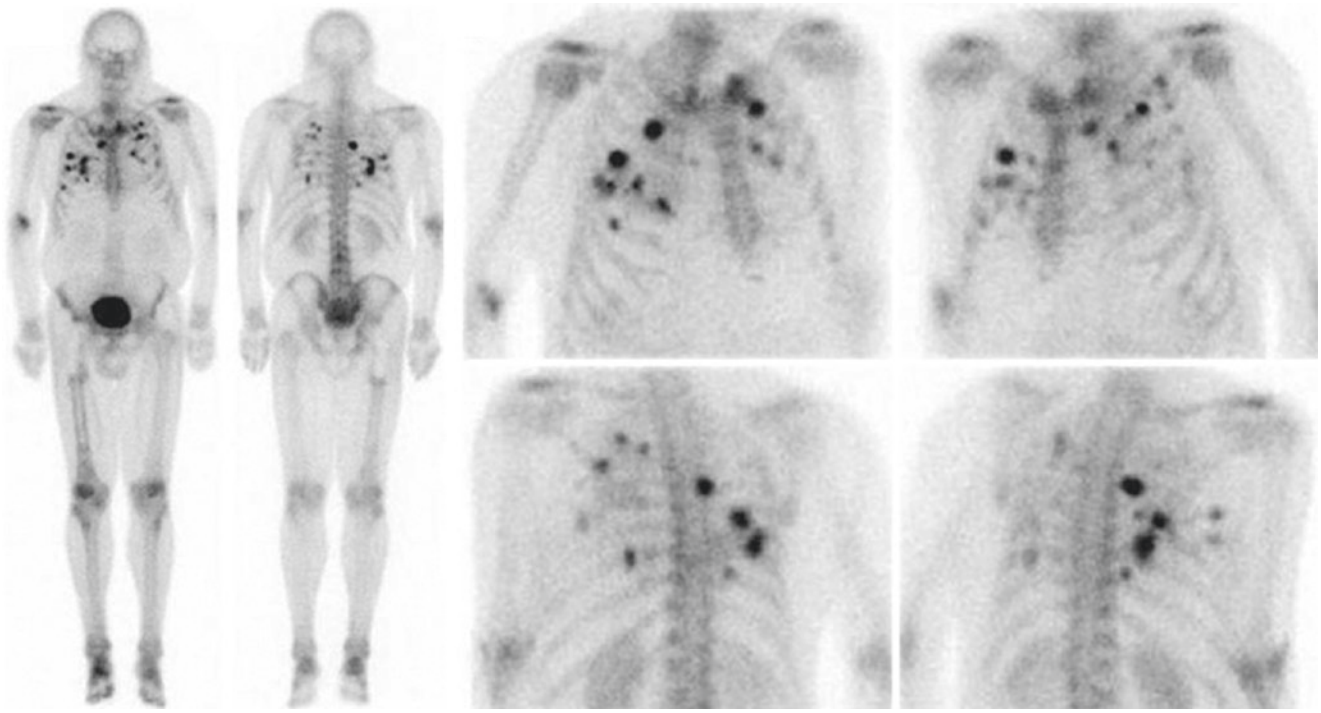

Fig. 24.11 Planar whole-body (**a**) and spot acquisitions (**b**) on the chest (orthogonal and oblique views) in a patient who had been previously treated for an osteosarcoma of the right femoral head, now the site of a prosthetic hip implant. There is no sign of active disease at the treated primary site, whereas multiple metastatic sites at the ribcage are clearly depicted as foci with markedly increased tracer uptake (*reproduced with permission from: Eary JF. Diagnostic applications of nuclear medicine: sarcomas. In: Strauss HW, Mariani G, Volterrani D, Larson SM, Eds. Nuclear Oncology – From Pathophysiology to Clinical Applications. New York, NY: Springer; 2017:1047–1064*)

response, while SUV_{max} >5 is associated with poor histologic response [26].

Concerning PET/CT with ^{18}F-fluoride, this investigation is useful for distinguishing postoperative changes from tumor recurrence after surgery, based on the fact that, unlike [^{18}F]FDG, ^{18}F-fluoride does not localize in areas of inflammation but only in newly mineralized bone.

24.3.1.2 Osteoid Osteoma and Osteoblastoma

Osteoid osteoma (OO) and osteoblastoma (OB) usually affect adolescents and young adults [27]. OO is commonly diagnosed in the cortex of the long bones (50% within the femur or tibia) as an intracortical nidus associated with a variable amount of mineralization, accompanied by cortical thickening and reactive sclerosis in a long bone shaft [28, 29].

OB is more common in the posterior element of the spine, especially in the cervical spine [30]. The differential diagnosis between OO and OB has traditionally been based on a size criterion (1.5 cm nidus); however, more recently OO and OB have been recognized to constitute two different pathologies rather than the differential expression of a single tumor [31]. In fact, OB has a greater potential for growth, with destruction of bone tissue or even malignant transformation, and recurs more often than OO. X-rays are usually the first imaging study obtained. CT or MRI is used for further characterization. CT can demonstrate the sclerotic lesion and the nidus, while MRI can better define intramedullary and soft tissue changes.

Bone scintigraphy with ^{99m}Tc-diphosphonates shows intense osteoblastic activity in the tumor region—without however any specific pattern allowing clear definition of the underlying disease. Although there is no specific role for [^{18}F]FDG PET/CT in the characterization of OO or OB, [^{18}F]FDG PET/CT can be used to assess response to local treatment [32], e.g., radioablation; efficacy of treatment translates into a significant decrease in [^{18}F]FDG uptake [33]. Tumor recurrence and/or persistence can be detected by focally increased radiotracer activity.

24.3.1.3 Ewing Sarcoma

Ewing sarcoma (ES) is the second most common malignant tumor in children and young adults. The first imaging modality in the evaluation of suspected Ewing sarcoma is the plain film, which usually demonstrates a lesion in the diaphysis of a long bone, most commonly the femur. Local staging is then performed with MRI, while CT is used for identifying distant metastases, particularly in the lung. The most important prognostic factors in the staging of ES are size of the lesion and distant metastases.

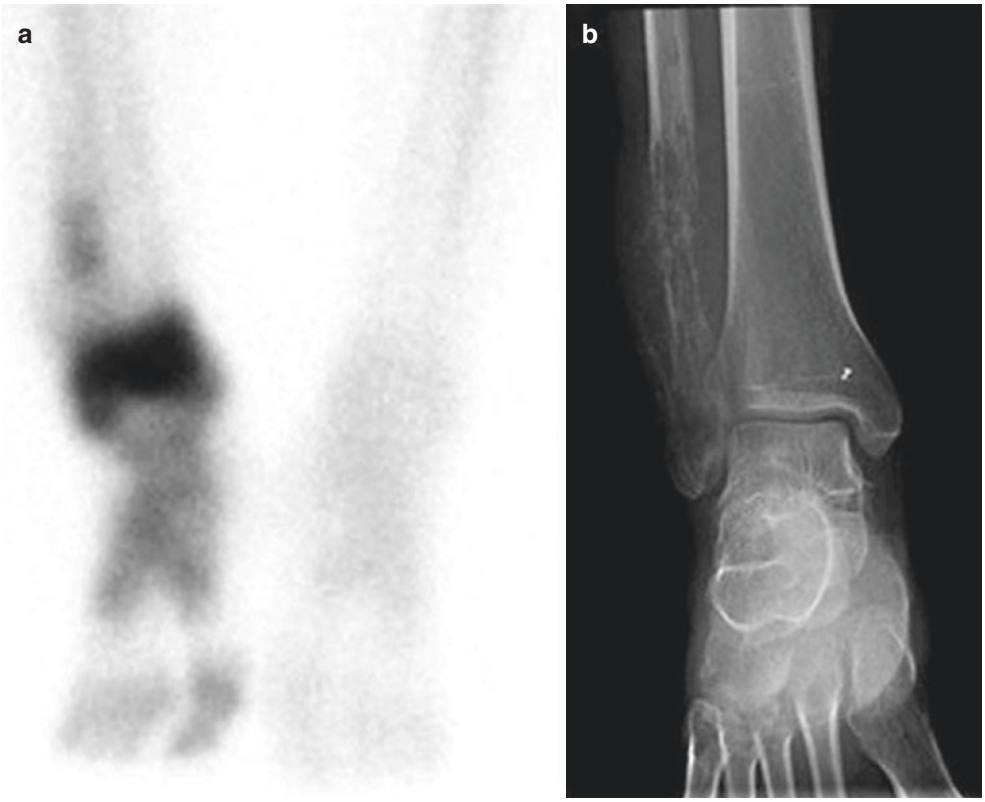

Fig. 24.12 Spot image of bone scintigraphy with ^{99m}Tc-MDP in a patient with Ewing sarcoma of the right ankle, showing markedly increased tracer uptake at the tumor site (**a**). Plain X-ray (**b**) shows fibular involvement with extension to surrounding soft tissue (*reproduced with permission from: Eary JF. Diagnostic applications of nuclear medicine: sarcomas. In: Strauss HW, Mariani G, Volterrani D, Larson SM, Eds. Nuclear Oncology – From Pathophysiology to Clinical Applications. New York, NY: Springer; 2017:1047–1064*)

Similarly as in patients with osteosarcoma, bone scintigraphy with ^{99m}Tc-diphosphonates has traditionally been employed as a valuable aid for clinical management of patients with Ewing sarcoma. Also in this case, the scintigraphic pattern shows nonspecific increased uptake of the bone-seeking agent both at the primary site (Fig. 24.12) and at metastatic sites.

[^{18}F]FDG PET/CT has been shown to be superior to MRI for skip lesions, especially in the active pediatric bone marrow [34], and in the detection of metastatic lymph nodes, but inferior to chest CT in the evaluation of pulmonary metastases [35]. However, with the most recent equipment where PET is combined with high-performing CT components, this is most likely no more the case.

Regarding the value of [^{18}F]FDG PET/CT for prognosis and for monitoring response to treatment in ES patients [36, 37], elevated pretreatment SUV correlates with high-grade tumors, and SUV_{max} >5.8 correlates with poor prognosis [38, 39]; furthermore, post-neoadjuvant treatment SUVs <2.5 correlate with good histological response (90% necrosis) and longer survival [40].

24.3.1.4 Cartilaginous Bone Tumors

Chondromas are benign tumors composed of mature hyaline cartilage. They generally have limited growth potential and are not locally aggressive. These tumors are called enchondromas when they occur in the medullary canal of the bone. Enchondroma has the same incidence in males as in females (with highest incidence in the 20–30-year age range), and most of the cases arise in bones of the hand; it usually manifests with a melting sore at pressure.

A rare form of chondroma is periosteal or juxtacortical chondromas. They occur on the surface of the bone, affecting equally males and females between the ages of 30 and 40 years. They can arise in the diaphysis of long bones of the limbs or in the phalanges, where they manifest with a painless, slow-growing swelling.

Chondromas can also arise from the synovial sheaths of tendons or in the soft tissues adjacent to the tendons in the hand and feet of adults; in such cases, they are referred to as soft tissue or synovial chondromas.

Therapy consists in surgical removal of tumor tissue by scraping. Radiotherapy is not useful because this is one of the least radiation-sensitive tumors. Figure 24.13 shows an example of bone scintigraphy in a patient with cervical chondroma, characterized by intense uptake.

The diagnosis of cartilaginous tumors is based on clinical examination and imaging findings. There is a wide spectrum of cartilaginous tumors, ranging from benign tumors without metastatic potential (such as enchondroma and osteochondroma) to high-grade malignant tumors (such as chondrosarcoma with aggressive behavior and early metastases). Multimodality radiologic assessment is mandatory to define the pattern of the lesion. X-ray is generally the front-line diagnostic imaging modality used. However, plain X-ray is often

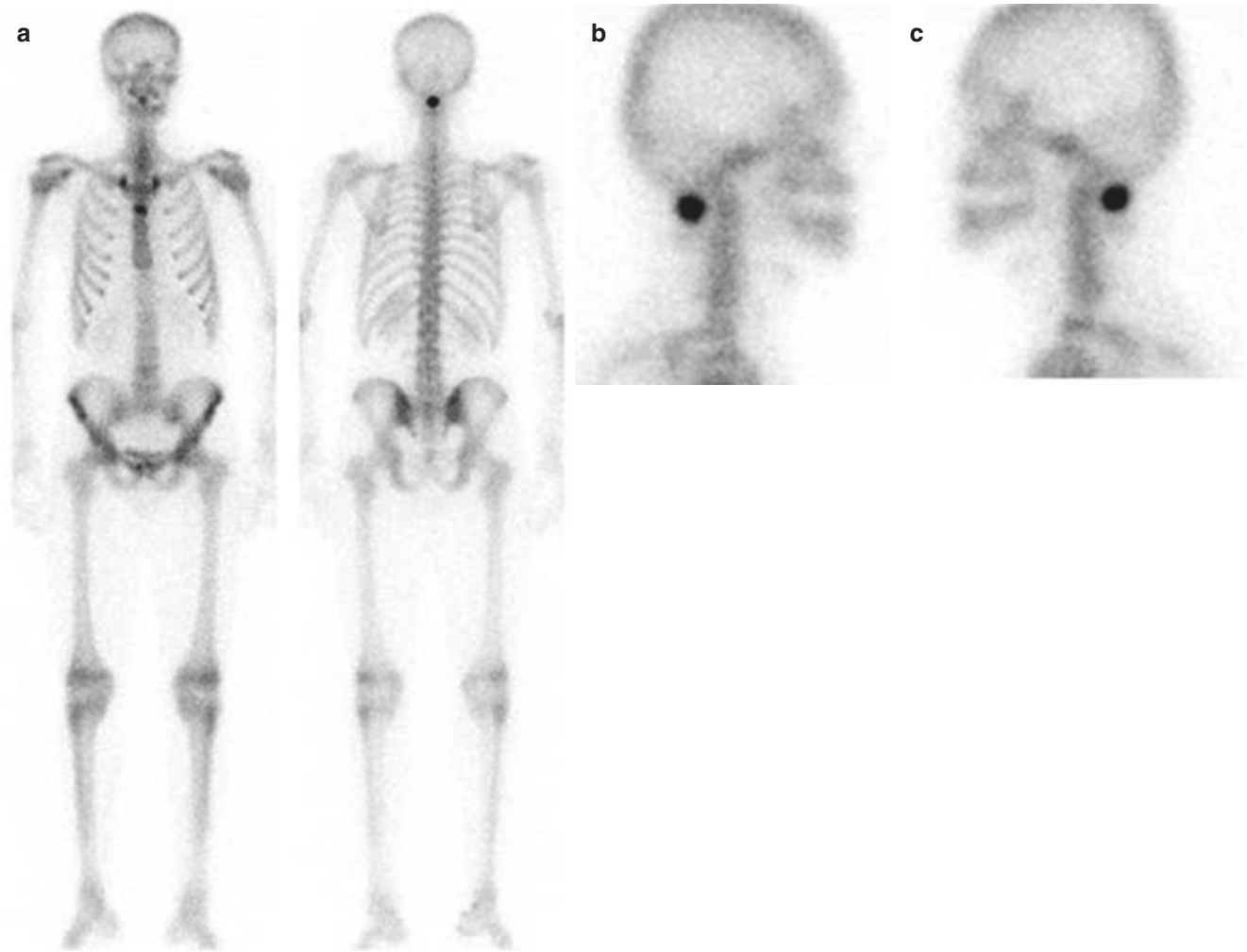

Fig. 24.13 Bone scintigraphy with ^{99m}Tc-HDP obtained in a patient with chondroma of the cervical spine. Both in the planar whole-body scan (**a**) and in the planar spot acquisitions obtained at about 3 h post-injection in the right lateral view (**b**) and in the left lateral view (**c**), the chondroma exhibits markedly enhanced tracer uptake. As an incidental finding, mildly increased tracer uptake can be noticed at the costoclavicular joints and between the upper third and the middle third of the sternum—a non-infrequent occurrence that is normally devoid of any clinical relevance (*reproduced with permission from: Volterrani D, Erba PA, Mariani G, Eds. Fondamenti di Medicina Nucleare – Tecniche e Applicazioni. Milan: Springer Italy; 2010*)

not capable to fully characterize the lesion, and further evaluation with cross-sectional imaging is warranted. CT images can better assess the cartilaginous matrix (arc-and-ring or stippled morphology) and the endosteal scalloping, which might be useful to distinguish enchondroma from a low-grade chondrosarcoma. Both MRI and CT are accurate in distinguishing osteochondroma from chondrosarcoma by measuring the thickness of the cap, which is usually >2 cm in malignant lesions.

Bone scintigraphy can contribute to the differentiation of benign from malignant lesions, as malignant lesions are characterized by markedly increased ^{99m}Tc-diphosphonate uptake. Similarly, high [^{18}F]FDG uptake might help in the differential diagnosis between benign and malignant lesions: benign lesions have low SUVs, benign lesions with atypical histological features have slightly higher values, and malignant lesions have markedly higher SUVs than benign lesions [41]. An SUV_{max} >2 has been suggested as the threshold for malignant nature [42].

24.3.2 Fibrous Bone Dysplasia

Fibrous bone dysplasia is a non-hereditary congenital benign skeletal disorder in which the bone is replaced with a fibrous-like tissue with early osteogenesis; its prevalence is not easily defined, as the illness is often asymptomatic. Bone lesions are generally monostotic but in about 10–15% of cases are polyostotic, especially when associated with genetic syndromes such as the McCune-Albright's or Mazabraud's syndromes. The polyostotic form is often unilateral or monomelic. Fibrous bone dysplasia presents in children or young adults as a painless osseous abnormality affecting the ribs (28%), femurs (23%), or neurocranium

(20%). However, in the polyostotic form, it is more likely that lesions are associated with pain and frail bone, with possible fractures. In some patients (or in some bone sites), lesions are hypertrophic and can cause neurological complications. The diagnosis is based on radiological and scintigraphic imaging, in which hyperactivity of the bone-seeking radiopharmaceutical is observed, both in bone lesions and in the complicating fractures. The amount of woven bone and fibrous tissue determines the X-ray and CT appearance, which can be sclerotic, cystic, or mixed cystic-sclerotic [43, 44]. Given its variable appearance, MRI is usually less useful for the diagnosis.

Bone scintigraphy demonstrates areas of reduced uptake alternating with areas of increased uptake, reflecting the complex structure of the lesion. In general, the fibrous or cystic elements concentrate little or no radiopharmaceutical, while bones or calcified areas exhibit increased tracer uptake. The tracer accumulates markedly in pathological fractures and moderately on the periphery, indicating the expansive nature of the disease with stimulation of the sclerotic edge. Tracer uptake begins to intensify when injuries are replaced by bone tissue.

[^{18}F]FDG PET/CT is useful to assess the extent of polyostotic disease; the bone abnormalities seen as ground-glass, mixed sclerotic, and lytic expansive lesions correspond to increased uptake on the PET scan [45]. [^{18}F]FDG PET/CT has been used to assess rare syndromes associated with fibrous bone dysplasia [46]. In those cases, the scan is also a valuable tool to detect other abnormalities associated with the specific syndrome, such as intramuscular myxomas in Mazabraud's syndrome. Furthermore, [^{18}F]FDG PET/CT can detect malignant degeneration [47] which can occur in 1–4% of cases, such as transformation into osteosarcoma, fibrosarcoma, and malignant fibrous histiocytoma, especially in the polyostotic form [48]. In case of progressively increasing [^{18}F]FDG uptake, malignant degeneration should be suspected, and a biopsy should be performed under PET/CT guidance.

Fibrous dysplasia and other fibrous lesions such as non-ossifying fibroma and fibrous cortical defect (see below) can be misdiagnosed as metastatic cancer in the staging of other primary tumors, as all of these diseases have enhanced [^{18}F]FDG uptake. Fibrous dysplasia is a potential pitfall also with ^{18}F-fluoride PET/CT, due to the high tracer uptake. In this case, CT imaging should be carefully reviewed to reduce the false positive rate and thus avoid unnecessary biopsies.

24.3.2.1 Giant Cell Tumor

The giant cell tumor (GCT) accounts for about 5% of all primary osseous tumors, 80% of cases occurring between the second and the fifth decades [49]. GCT arises following fusion of the growth plate and extends from the bone's metaphysis to the epiphysis; the most common site is the knee, involved in more than half of the cases. GCTs are generally benign tumors but may transform into sarcomas, although they rarely metastasize; therefore, they are often considered as quasi-malignant lesions.

The typical appearance of GCT on X-ray is an expansile lesion without bone matrix at the metaphysis/epiphysis of a long bone; this finding suggests further assessment with CT and MRI. CT better evaluates the absence of mineralization, the narrow transition zone, and the cortical thinning with possible periosteal reaction, while MRI shows a typical whorled appearance on T2-weighted sequences and better detects the presence soft tissue extent.

GCTs are extremely [^{18}F]FDG-avid, with SUVs overlapping those of malignant bone tumors [50]. Uptake is often more prominent at the periphery with a central photopenic region (doughnut sign). The high vascularity of the tumor leads to a generalized regional hyperemia, which can translate into diffuse increase in radiotracer uptake [51]. In the rare case of multicentric giant cell tumors, the role of [^{18}F]FDG PET/CT is to detect occult lesions [52]. Although rarely, GCT can metastasize or transform into malignant sarcomas; in this case, PET/CT is useful for detecting metastasis. In the primary malignancy, PET/CT can detect foci of more prominent uptake, which might be suitable for biopsy.

24.3.2.2 Cortical Fibrous Defects and Non-ossifying Fibroma

This is an asymptomatic condition characteristic of young boys, generally detected incidentally during an imaging test. It is typically represented by a single cortical lesion of long bones, which in most cases regresses spontaneously. Sometime the lesion persists and evolves in non-ossifying fibrous bone marrow. Bone scintigraphy might be normal; when positive, it shows an area of slightly increased radiopharmaceutical uptake characterized by a ringlike pattern surrounding a photopenic lesion. In case of calcification or ossification, uniform and intense uptake is present. Acquisition with a pinhole collimator and SPECT (or preferably SPECT/CT) might be useful.

Key Learning Points

- Malignant primary bone tumors usually exhibit increased uptake in every phase of a three-phase bone scintigraphy.
- This is also the case of most benign primary bone tumors.
- In malignant primary bone tumors, bone scintigraphy is usually not indicated to diagnose or characterize the primary lesion but rather to define the extent of osseous diffusion.
- This is also true of [^{18}F]FDG PET/CT, although in some conditions such as sarcomas, uptake of [^{18}F]FDG has been shown to correlate with tumor aggressiveness.

24.3.2.3 Myositis Ossificans

This rare benign condition most commonly presents as a localized, self-limiting lesion secondary to contusion trauma. Scintigraphy can be useful, especially to confirm the uniqueness of the lesion and for the differential diagnosis with both nonmalignant (nodular fasciitis, juxtacortical osteoma, osteochondroma, chondroma) and malignant lesions (osteogenic sarcoma). Figure 24.14 shows a typical example of bone scintigraphy in a patient with myositis ossificans.

Key Learning Point

- Myositis ossificans is characterized by high uptake of ^{99m}Tc-diphosphonates.

24.3.3 Metastatic Bone Tumors

Bone metastases occur frequently in patients with breast, prostate, lung, and renal carcinomas; the frequency of osseous involvement in postmortem examinations of patients with these tumors ranges between 30% and 70%. Bone metastases reduce survival significantly, between 6 and 48 months depending on tumor type.

As for other diagnostic tests, some knowledge on the pretest probabilities of a given condition is also relevant when bone scintigraphy is used for staging malignant disease [53, 54]. The pretest probabilities of bone metastases depend on tumor stage and other risk factors. In breast cancer stages I and II, it is between 0.8% and 2.6%, rising to 16.8–40.5% in stages III and IV. Risk factors for skeletal metastasis in prostate cancer patients are a serum PSA

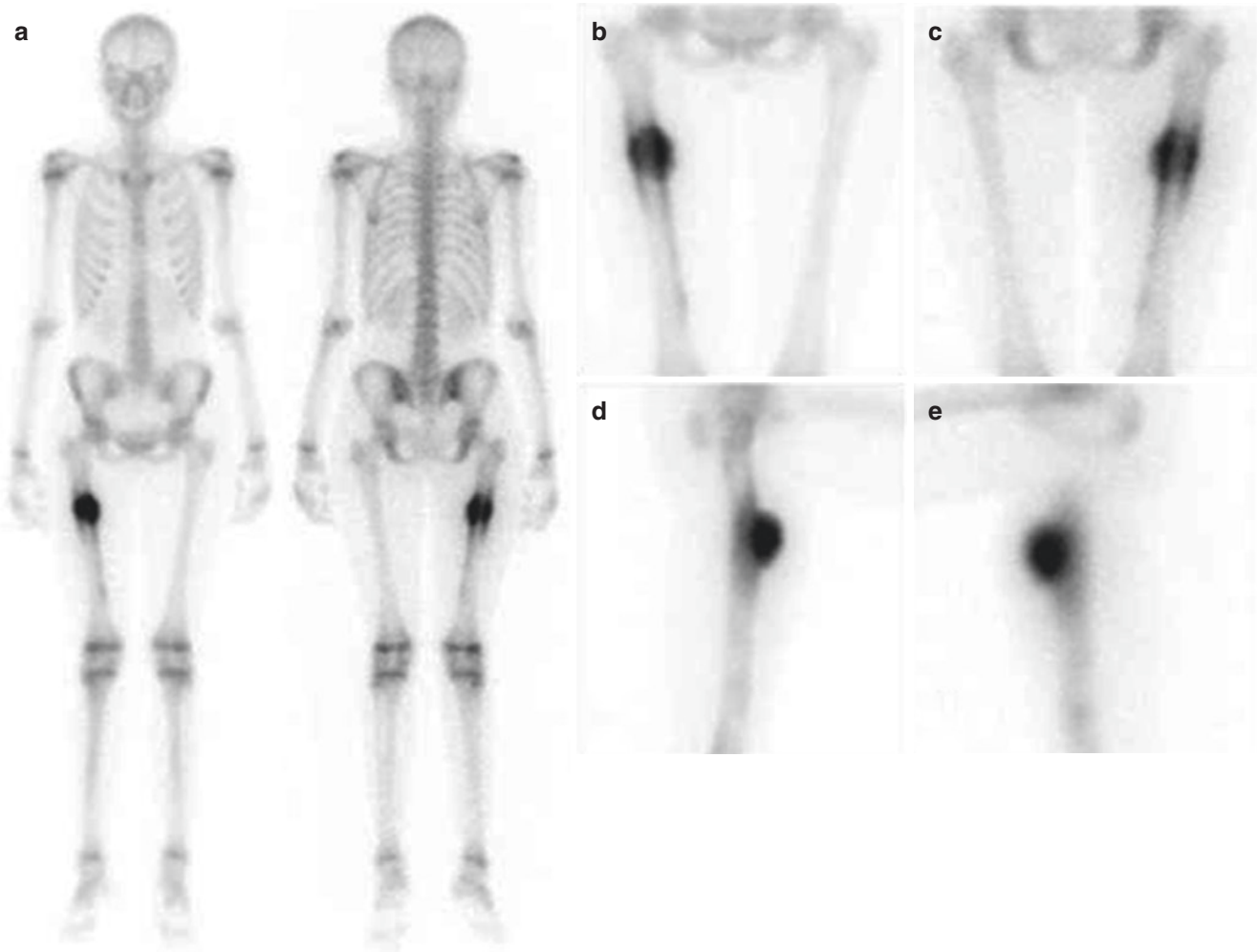

Fig. 24.14 Planar whole-body scintigraphy obtained about 3 h after administration of ^{99m}Tc-HDP in a young adult patient who had suffered contusion trauma of the right thigh muscles several months earlier. Besides the still metabolically active growth plates at the knees and ankles, the whole-body images (**a**) show an area of focally increased tracer uptake that appears to extend beyond the bone at the upper third of the right femur. The planar spot images acquired in the anterior and posterior views (**b** and **c**) and especially in the lateral views of the right thigh (**d** and **e**) better demonstrate that increased uptake is not associated with bone but rather involves the soft tissues adjacent to bone (*reproduced with permission from: Volterrani D, Erba PA, Mariani G, Eds. Fondamenti di Medicina Nucleare – Tecniche e Applicazioni. Milan: Springer Italy; 2010*)

level >10 ng/mL and a Gleason score ≥8; above these two thresholds, the pretest probability of osseous involvement in prostate cancer rises to 16.2%. Tumor patients experiencing bone pain also have a higher risk of harboring bone metastases than those who are asymptomatic.

Purely lytic metastases may escape detection by bone scintigraphy. Therefore, patients with renal cancer, myeloma, or lymphomas are usually not examined by bone scintigraphy. This limitation does not apply to breast or prostate cancer because these tumors cause predominant osteoblastic bone lesions. However, the broader availability of positron-emitting radiopharmaceuticals such as ^{18}F-fluoride, choline (labeled with either ^{11}C or ^{18}F), the synthetic amino acid *anti*-1-amino-3-^{18}F-fluorocyclobutane-1-carboxylic acid (^{18}F-FACBC, also known as ^{18}F-fluciclovine), and ^{68}Ga ligands that target the prostate specific membrane antigen (PSMA) are reducing the need for bone scintigraphy in prostate cancer patients, due to their higher diagnostic accuracy compared to conventional bone scintigraphy and to the possibility of detecting both skeletal and extra-skeletal metastatic disease with a single imaging procedure.

A similar scenario is developing also for patients with bronchial carcinoma, in whom conventional bone scintigraphy is being replaced with [^{18}F]FDG PET/CT, which is useful not only for staging but also for assessing response to treatment.

Since bone metastases develop by hematogenous spread, they are usually found in the parts of the skeleton that harbor the well-perfused red bone marrow. Therefore, hot spots on the bone scan caused by metastases are usually not joint-related. Multifocal involvement is usually more frequent than solitary bone metastases (Fig. 24.15). In disseminated metastatic disease, diffusely increased bone metabolism may be visualized by bone scintigraphy, raising the need for differential diagnosis between the so-called superscan due to disseminated metastatic disease (Fig. 24.16) and metabolic bone disease (due to, e.g., severe hyperparathyroidism). The markedly increased avidity of the skeleton for ^{99m}Tc-diphosphonates or for ^{18}F-fluoride occurring in patients with the superscan reduces radioactivity accumulation in soft tissues as well as excretion through the nephro-urinary tract.

Published evidence on the diagnostic accuracy of bone scintigraphy for staging cancer patients is of low quality, in particular because of the lack of a reliable gold standard [53, 54]. Published sensitivities range between 85% and 96%, higher in prostate than in breast cancer. Sensitivity is limited by suboptimal spatial resolution of the planar and/or SPECT gamma cameras—currently between 8 and 10 mm. Very small bone lesions may, therefore, escape detection by bone scintigraphy. However, detectability depends not only on size but also on the uptake ratio between lesion and background. In case of very high lesion uptake (as observed in, e.g., the osteoblastic metastases of prostate carcinoma), also lesions smaller than 1 cm may be detected by bone scintigraphy; whereas, metastatic lesions with low uptake (as observed in, e.g., the predominantly lytic metastases of breast cancer) may not be detected, even if larger than 1 cm.

Osseous metastatic spread begins with tumor cells infiltrating the bone marrow. Bone scintigraphy can detect metastases only when the neoplastic cells invading the bone marrow activate involvement of the mineralized component of bone, thus initiating a reactive increase in bone metabolism. Since MRI and radionuclide imaging with tumor-seeking radiopharmaceuticals (as typically occurring with PET) enable direct visualization of the neoplastic foci, they usually become positive for metastatic disease earlier than bone scintigraphy and are thus more sensitive than the conventional bone scan.

It is also known that, in face of a relatively high sensitivity, the specificity of bone scintigraphy for bone metastases is quite low, due in particular to the fact that numerous benign conditions also lead to focal increases of bone metabolism. Among these, degenerative changes of the skeleton (including osteochondrosis of the spine due to degeneration of the intervertebral disk and facet's osteoarthritis) raise in elderly patients the most frequent differential diagnosis. Nonetheless, these conditions have a typical appearance on CT; therefore, the specificity of bone scintigraphy in staging malignant disease is markedly improved by hybrid SPECT/CT imaging (Figs. 24.17–24.19).

Further benign differential diagnoses of a hot spot such as vertebral fractures (Fig. 24.20) or benign bone tumors are also amenable to CT characterization. Since the advent of SPECT/CT, a considerable amount of evidence has been published analyzing its utility for staging compared to planar or stand-alone SPECT imaging. It has thus been established that more than 90% of the foci of abnormal uptake considered indeterminate on stand-alone radionuclide imaging can be elucidated by SPECT/CT [55] (Figs. 24.21 and 24.22). Hybrid imaging has, thus, turned bone scintigraphy from a sensitive but nonspecific imaging procedure to a highly accurate diagnostic tool for staging the skeleton in malignant disease [55].

On the other hand, bone scintigraphy with ^{99m}Tc-diphosphonates can also be used to monitor the efficacy of therapy in patients with skeletal metastatic disease. Nevertheless, caution should be taken in the interpretation of the images so obtained (especially if no hybrid SPECT/CT imaging is employed), since abnormally increased tracer uptake may persist at the sites of metastasis up to several months after start of favourable response to treatment. This limitation is less stringent when using PET with ^{18}F-fluoride, where changes in the pattern of tracer distribution reflect more readily the pathophysiologic changes occurring during therapy – either in the case of progression despite treatment or in the case of favourable response to treatment (see Fig. 24.23)

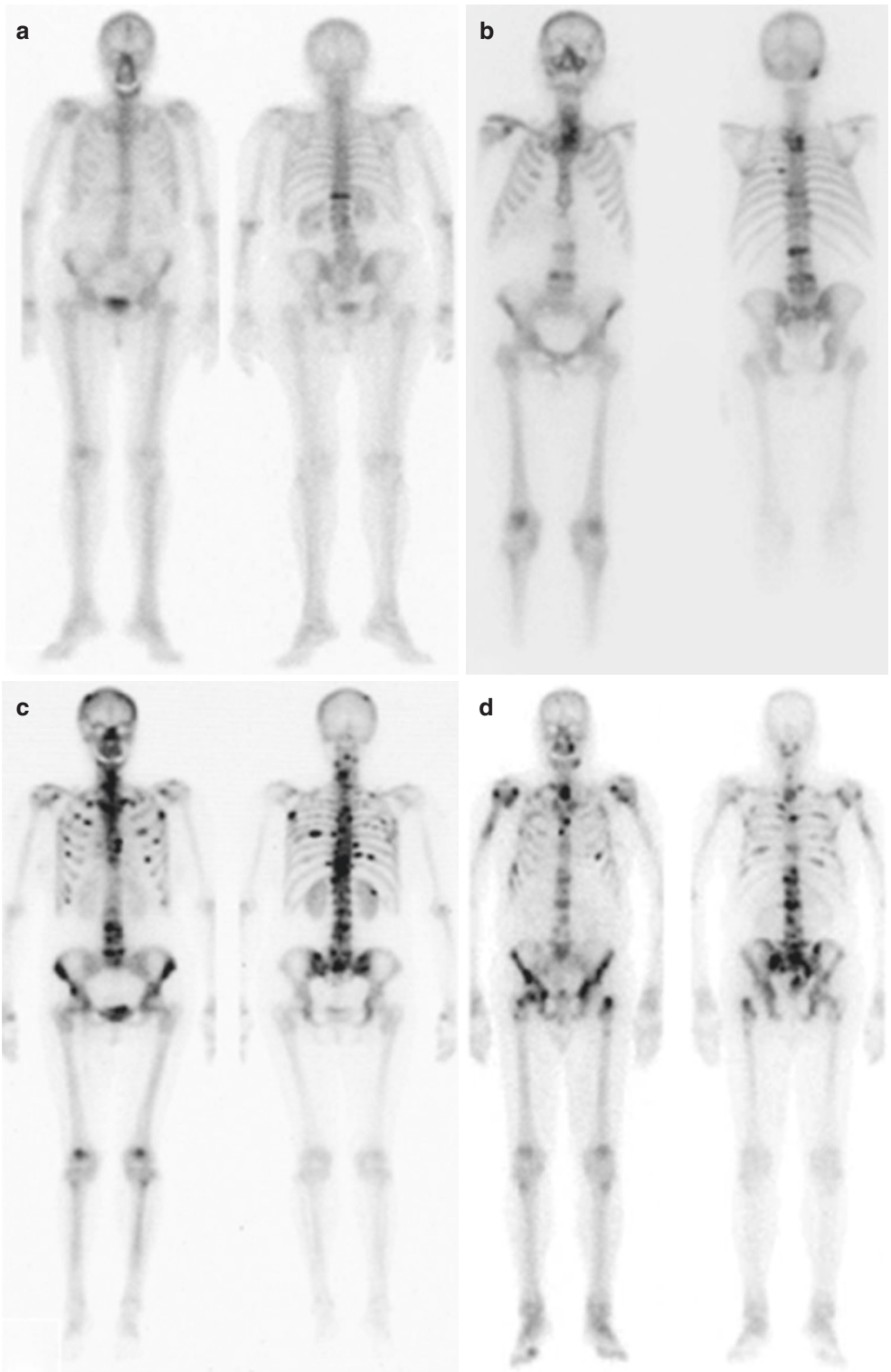

Fig. 24.15 Examples of planar whole-body scans obtained with ^{99m}Tc-diphosphonates in different patients with cancer. The cases are presented here with increasing severity of metastatic bone disease, including single lesion in a vertebral body in the lower thoracic spine (**a**); multiple lesions in the spine, ribs, and skull (**b**); and disseminated lesions throughout the skeleton (**c** and **d**) (*reproduced with permission from: Volterrani D, Erba PA, Mariani G, Eds. Fondamenti di Medicina Nucleare – Tecniche e Applicazioni. Milan: Springer Italy; 2010*)

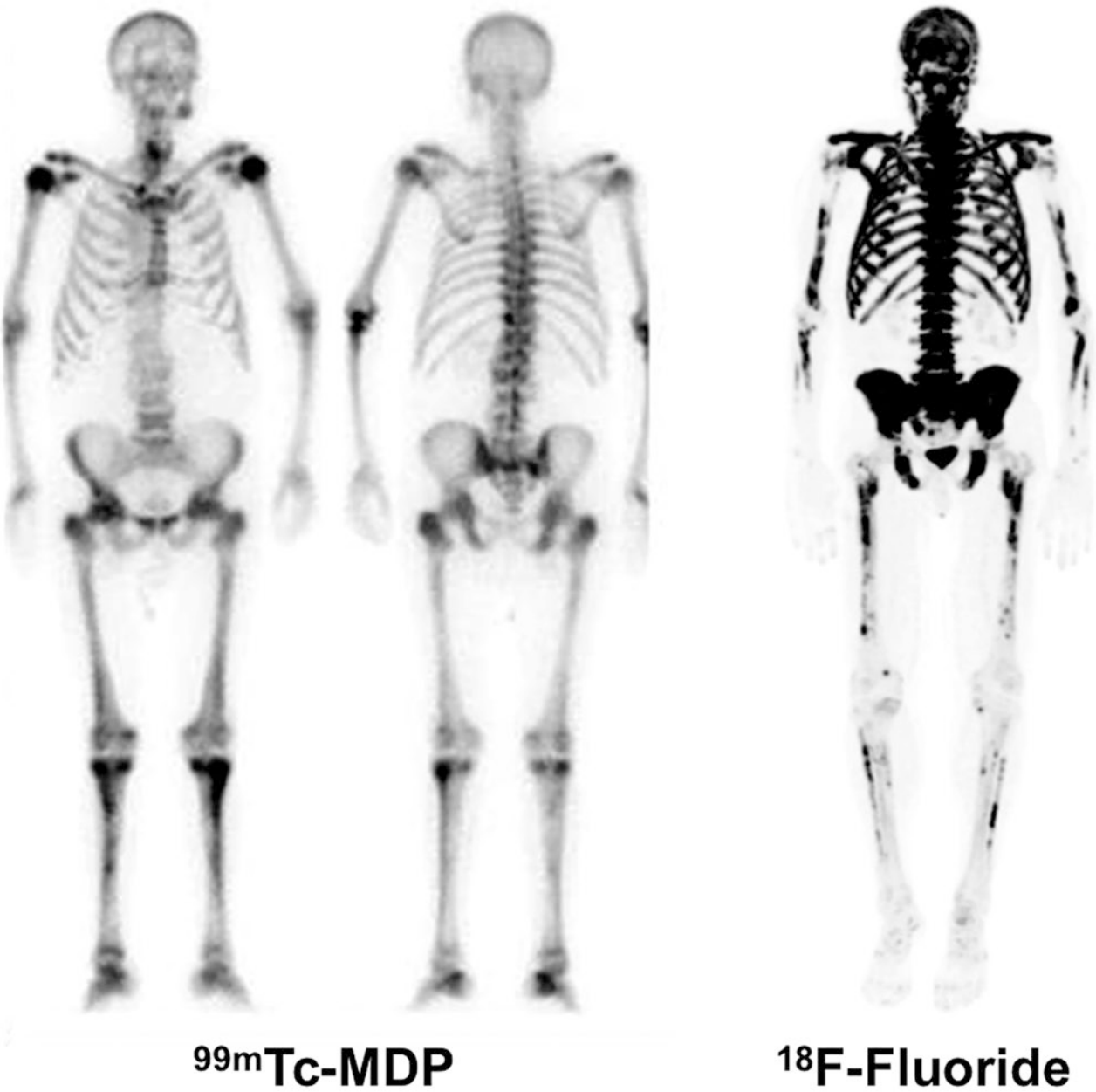

Fig. 24.16 Examples of "superscans" in patients with advanced metastatic prostate cancer as visualized in two different patients by conventional ^{99m}Tc-MDP bone scintigraphy (left) and by PET with ^{18}F-fluoride (right). Due to markedly increased avidity of bones for the bone seeking agents, in both cases there is very little radioactivity remaining in the soft tissues and very little excretion through the urinary tract (*superscan ^{99m}Tc-MDP image modified from: Volterrani D, Erba PA, Mariani G, Eds. Fondamenti di Medicina Nucleare - Tecniche e Applicazioni. Milan: Springer Italy; 2010. Superscan ^{18}F-fluoride image kindly provided by Guofan Xu, MD, PhD, Department of Nuclear Medicine, M.D. Anderson Cancer Center, Houston, Texas, USA*)

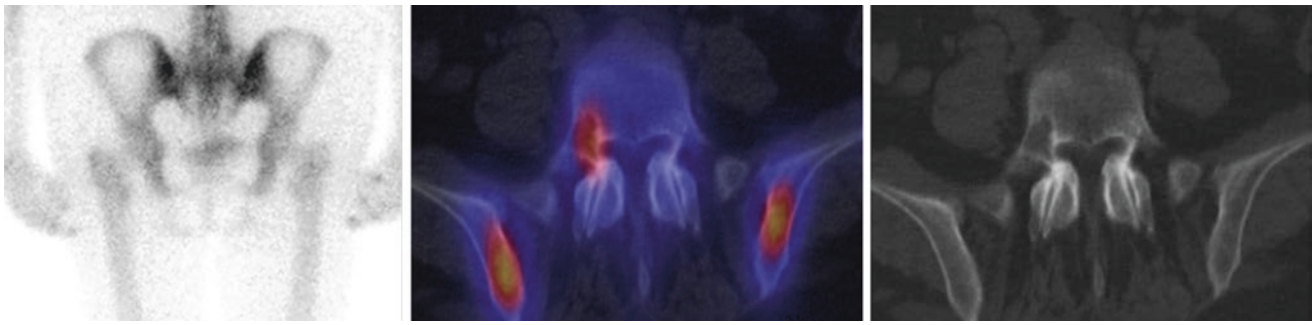

Fig. 24.17 Bone scintigraphy in a 55-year-old patient with breast carcinoma. On the dorsal planar view (left panel), a discrete focus of uptake projects to the lateral aspects of the fifth lumbar vertebral body. Images of SPECT/CT fusion (center panel) and low-dose CT (right panel) show that this corresponds to an area of osteolysis, possibly caused by metastasis

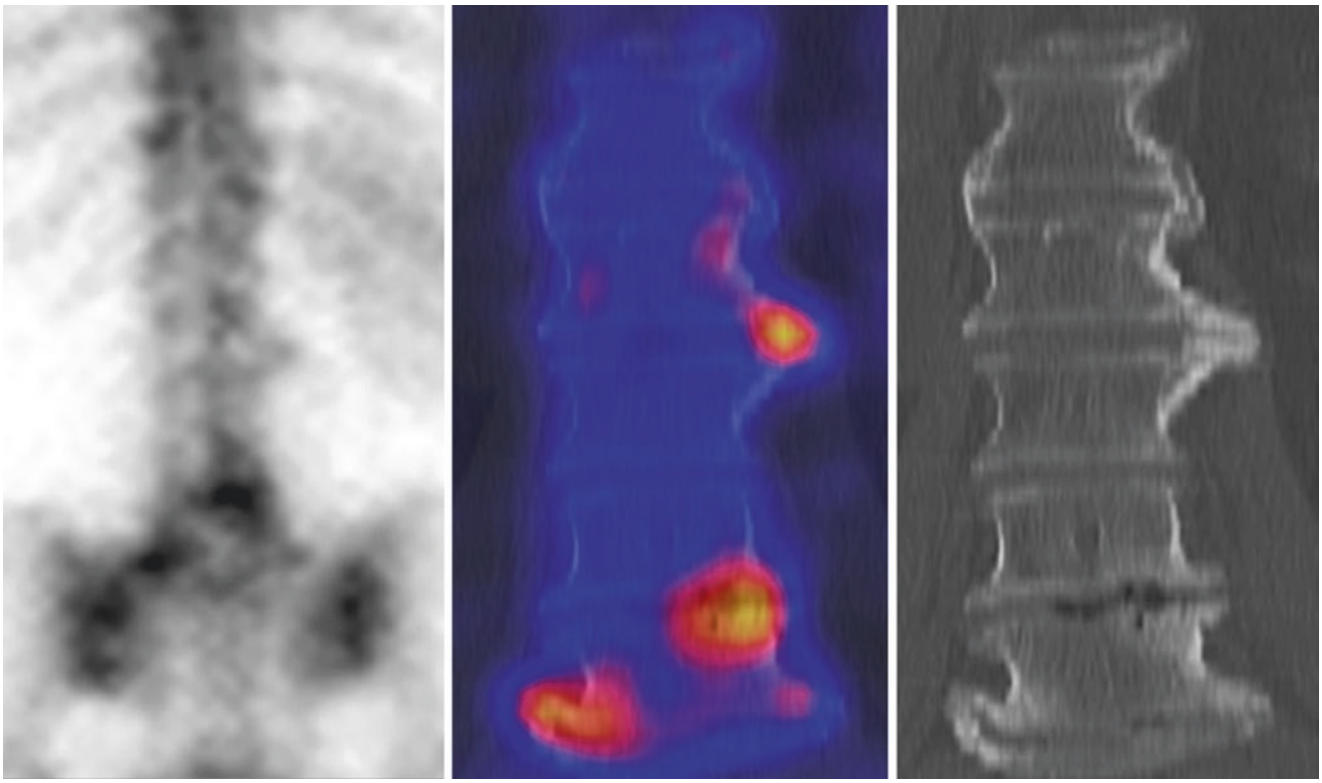

Fig. 24.18 Bone scintigraphy in a 72-year-old patient with breast carcinoma. Dorsal planar view (left panel) features two hot spots in the lower spine. The images of SPECT/CT fusion (center panel) and low-dose CT (right panel) disclose them as degenerative: osteochondroses between L5 and S1 as well as between L4 and L5 showing disk space narrowing, vacuum phenomena ("gas in disk"), and osteophytes

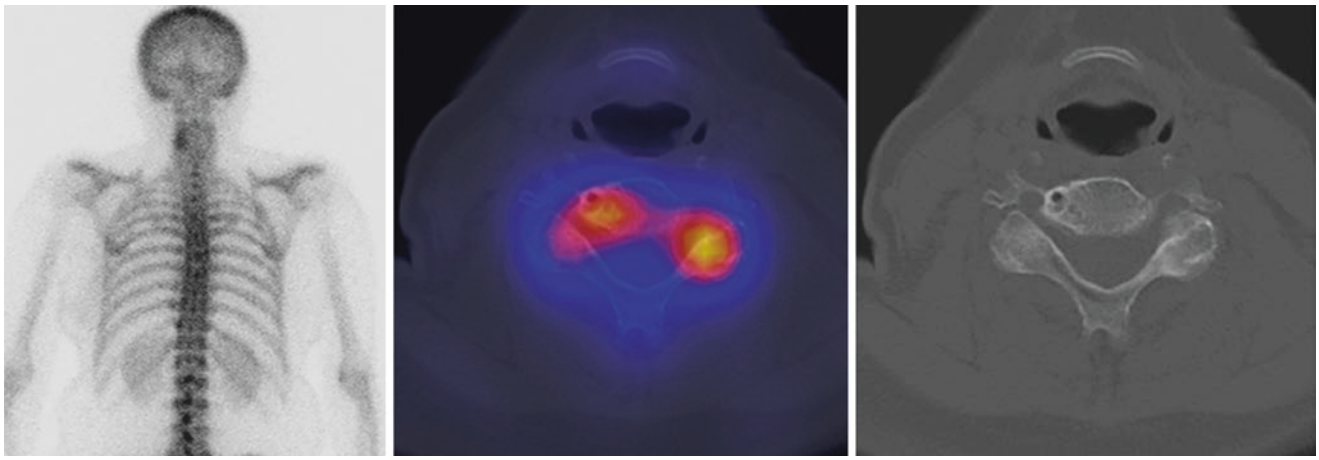

Fig. 24.19 Bone scintigraphy in a 71-year-old patient referred for staging of breast carcinoma. Dorsal planar view (left panel) shows focus of moderately increased uptake in the left-lateral aspects of the cervical spine. Hybrid fused SPECT/CT image (center panel) and CT image (right panel) disclose left-sided facet's osteoarthritis and right-sided uncovertebral arthropathy, the latter featuring a geode

Key Learning Points

- Bone scintigraphy is useful for staging breast and prostate cancer, in particular in those patients with a high risk for osseous metastases.
- Purely lytic metastases (such as those occurring in, e.g., renal cancer or myeloma) may escape detection by bone scintigraphy.
- Bone scintigraphy can detect metastases only when the neoplastic cells invading the bone marrow cause a reactive increase in bone metabolism.
- The sensitivity of bone scintigraphy to detect osseous metastases may thus be lower than that of MRI, which visualizes the integrity of bone marrow, or lower than that of imaging with tumor-seeking agents (e.g., PET/CT), which visualize the tumor cells directly.
- The specificity of bone scintigraphy to detect osseous metastases is greatly increased when SPECT/CT is used.

24.4 Benign Bone Disease

24.4.1 Workup of Bone Pain

Pain affecting the skeleton is very frequent. Its differential diagnosis is vast and can be roughly subdivided into extraosseous and osseous conditions. Bone scintigraphy can be used to detect osseous pain generators with rather high sensitivity, although specificity is reduced by its inability to morphologically characterize foci of increased tracer uptake. Many studies have shown that this limitation may be overcome by SPECT/CT hybrid imaging. Whereas the focal increase of uptake in a joint of the extremities is quite often accompanied by pain, this is not necessarily true for the spine. Therefore, the specificity of bone scintigraphy to detect the correlate of skeletal pain is in the case of spinal degenerative disease also limited.

When reading bone scans of patients affected by osseous pain, identifying major differential diagnoses is helpful to the referring physician. These categories are malignant and benign bone tumors, inflammation, trauma, degenerative disease, vascular disorders, and some miscellaneous conditions eluding this categorization. The pretest probabilities of these categories vary largely with clinical presentation. Therefore, before injecting the radiopharmaceutical, a detailed medical history with regard to the occurrence and nature of the pain as well as to that of possible trauma is highly relevant. Furthermore, concomitant laboratory findings such as the serum level of the C-reactive protein (CRP) or leukocyte counts should be available as well as the results and—ideally—also the image datasets from previous radiological examinations.

24.4.1.1 Degeneration

Degenerative conditions are one of the most frequent causes of bone pain. Joint degeneration is caused by degeneration of the joint cartilage, which is ultimately destroyed in this process. In the case of spinal degeneration, a progressive damage to the intervertebral disk occurs, which loses its elasticity and height. On CT and radiographic imaging, cartilaginous degeneration presents as thinning of the joint spaces; furthermore, calcifications as well as gas deposits can be seen. The latter is referred to as the so-called vacuum phenomenon. As a consequence of progressive destruction of these cartilaginous struc-

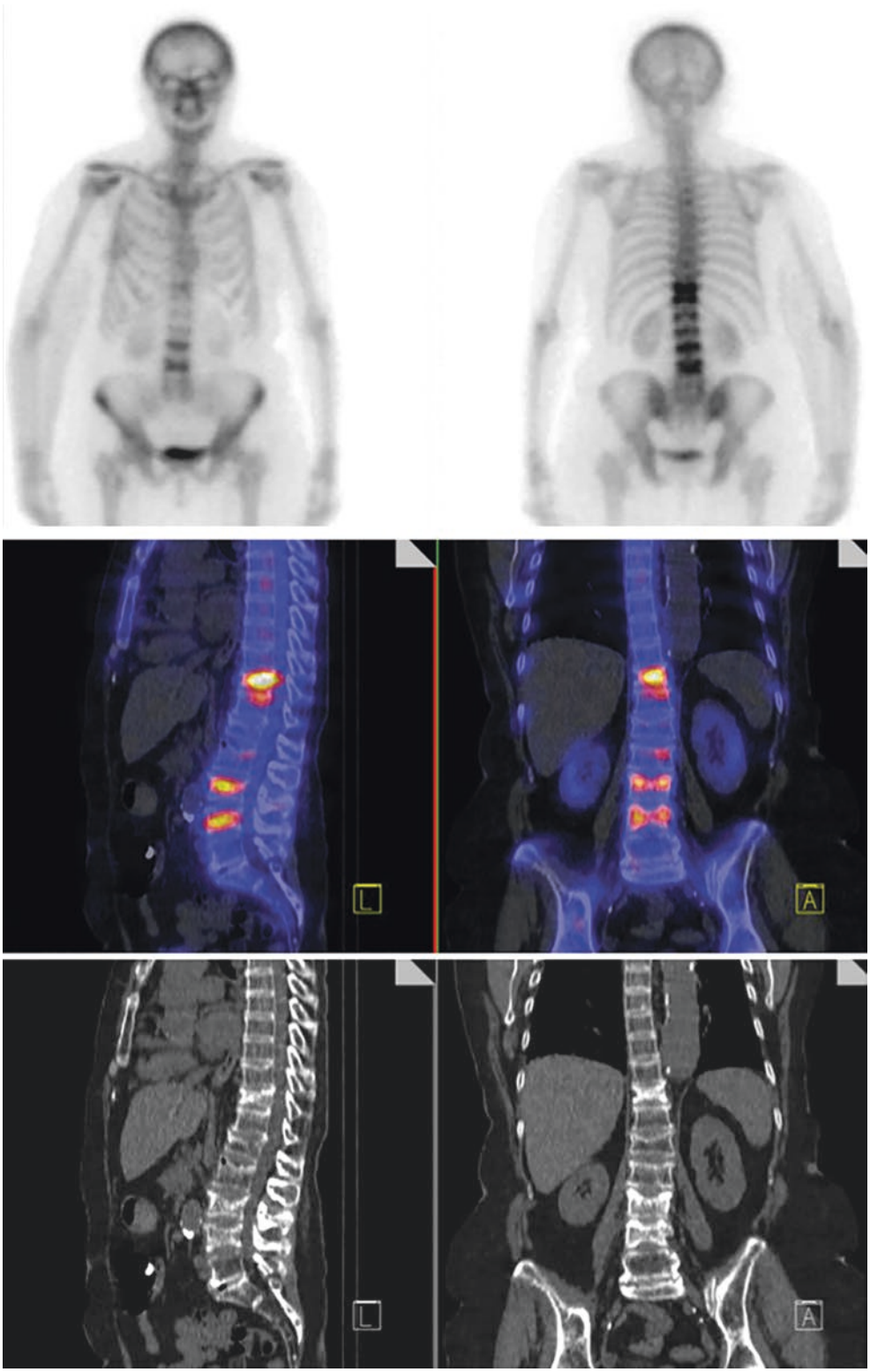

Fig. 24.20 Bone scintigraphy obtained in a patient with breast carcinoma. Planar views (upper panel) depict increased tracer uptake in at least four vertebral bodies. This is due to recent vertebral compression fractures, as demonstrated by SPECT/CT fusion images (middle panel) and low-dose CT images (bottom panel)

tures, the mechanical stress on the joint-forming bones increases, leading to subchondral bone edema and—subsequently—to subchondral sclerosis. Further sequelae are the so-called osteophytes or—in the case of the spine—spondylophytes, which are an indirect sign of joint instability. Degeneration may lead to inflammatory processes, causing pain. This so-called active osteoarthritis is accompanied by an increase in bone metabolism as well as an increase of uptake in the earlier phases of three-phase bone scintigraphy.

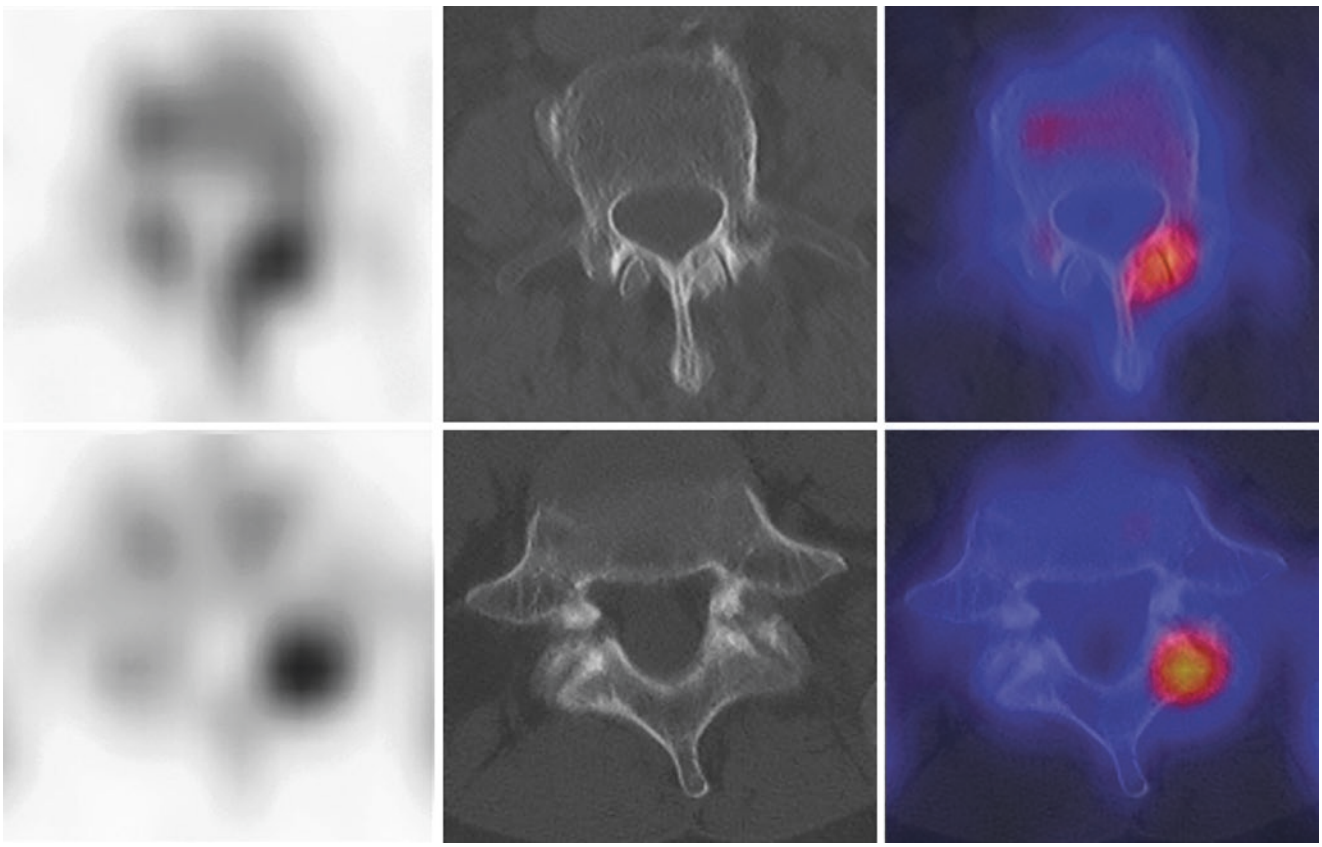

Fig. 24.21 Upper and lower rows represent transaxial SPECT (left panel), CT (center panel), and SPECT/CT fusion images (right panel) in two different patients with breast carcinoma referred for staging by bone scintigraphy. On the SPECT scans, increased tracer uptake projecting to the facet's joint of a vertebral body is seen in both patients. In the upper row, findings are due to facet's arthropathy with increased tracer uptake projecting to both sides of the joint with associated signs of osteoarthropathy such as joint space narrowing, subchondral sclerosis, and an osteophyte. In the lower row, signs of osteoarthropathy are absent, and the hot spot is found on one side of the joint only. Furthermore, bone is hypodense compared to contralateral, indicating a small osteolytic metastasis (*reproduced with permission from: Mariani G, Bruselli L, Kuwert T, Kim EE, Flotats A, Israel O, et al. A review on the clinical uses of SPECT/CT. Eur J Nucl Med Mol Imaging. 2010;37:1959–1985*)

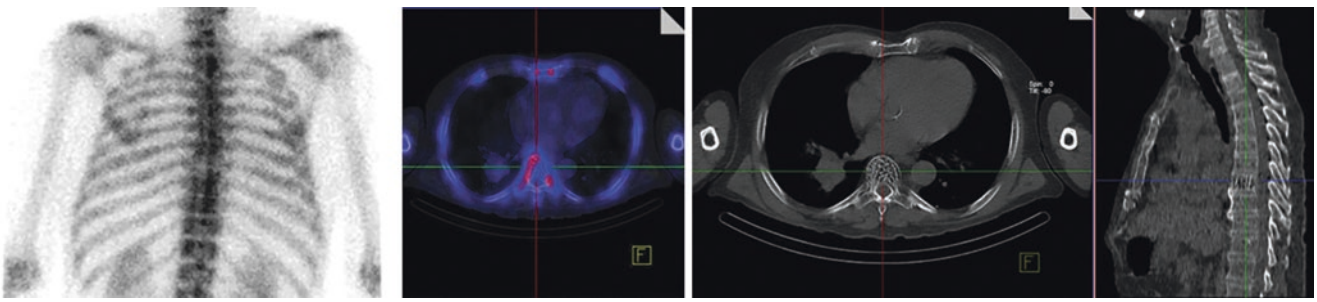

Fig. 24.22 Bone scintigraphy in a patient with bronchial carcinoma. Dorsal planar view (left panel) shows a cold spot in the 8th thoracic vertebra. Hybrid fused SPECT/CT image (second panel from left) and corresponding CT image (rightmost two panels) demonstrate findings typical of a hemangioma, with so-called salt-and-pepper appearance of the vertebra on the transaxial CT image—also containing fat

SPECT/CT helps in localizing foci of increased uptake and at the same time increases the diagnostic specificity considerably, as the hallmarks of osteoarthritis are readily visualized by the CT component of the scan. The degree of morphological alterations correlates only weakly with the floridity of the lesion, which in the case of the peripheral joints correlates well with increases in bone metabolism. In the case of the spine, the relationship between an increase in bone metabolism and pain generation is less direct. However, spinal regions with normal bone metabolism can

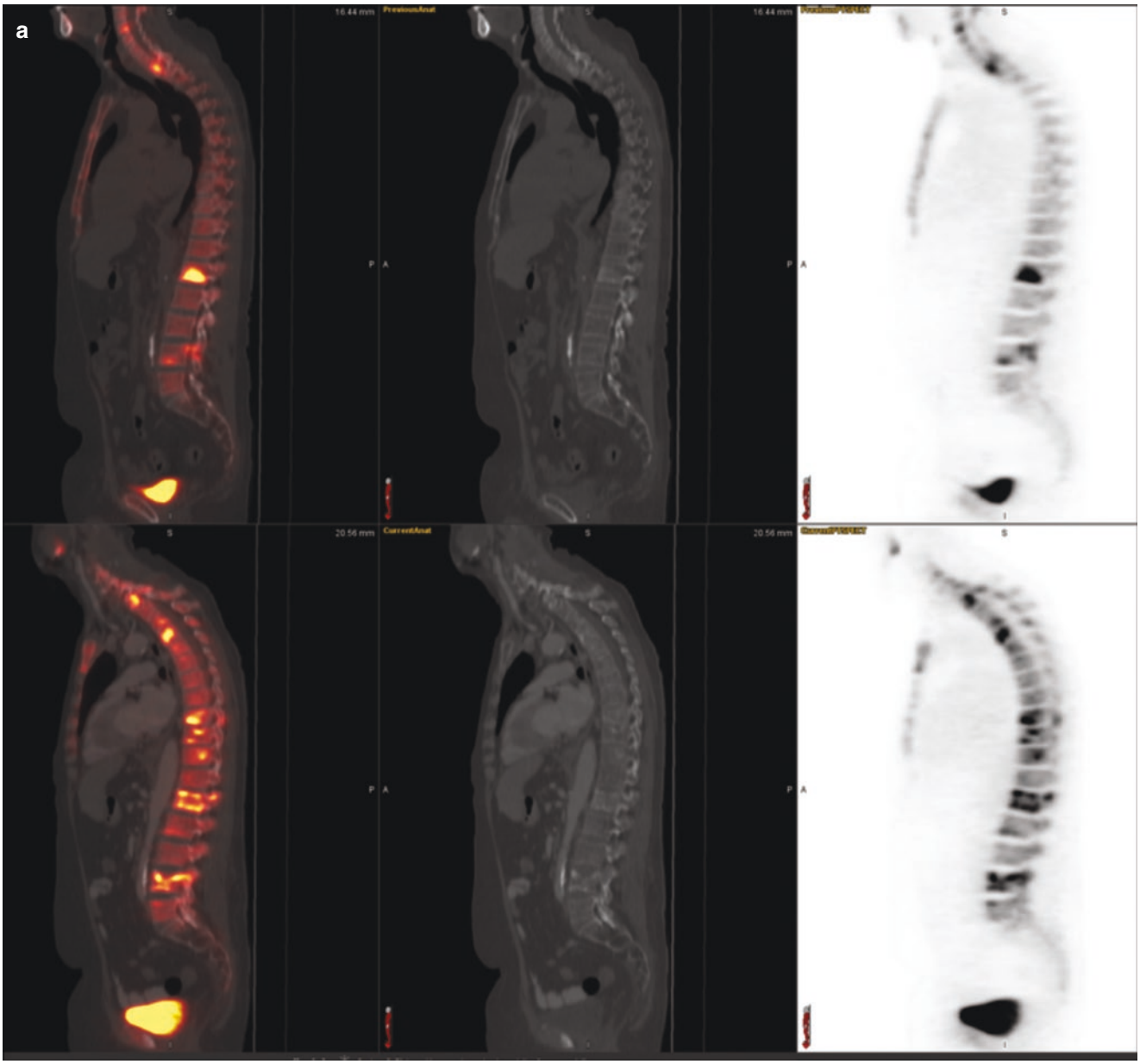

Fig. 24.23 Different patterns of response to androgen-deprivation therapy in two different patients with skeletal metastases from prostate cancer, as visualized by PET/CT with ^{18}F-fluoride. (**a**) The baseline, pre-therapy PET/CT scan obtained from this 65-year-old man (top row) reveals metastatic lesions within the vertebral bodies of C3, T2, L1, and L4 (fusion PET/CT image in left panel, CT image in center panel, PET image in right panel). Six months after initiation of androgen-deprivation therapy (bottom row), the PET/CT scan demonstrates progression of osseous metastatic disease, now involving multiple thoracic vertebral bodies. (**b**) The baseline, pre-therapy PET scan obtained from this 72-year-old man demonstrates diffuse skeletal metastatic disease involving the skull, spine, upper limbs, ribs, pelvis, and lower limbs (left panel). Considerable improvement is observed in the scan obtained 3 months after initiating androgen-deprivation therapy (center panel), with further improvement at 6 months (right panel)

Fig. 24.23 (continued)

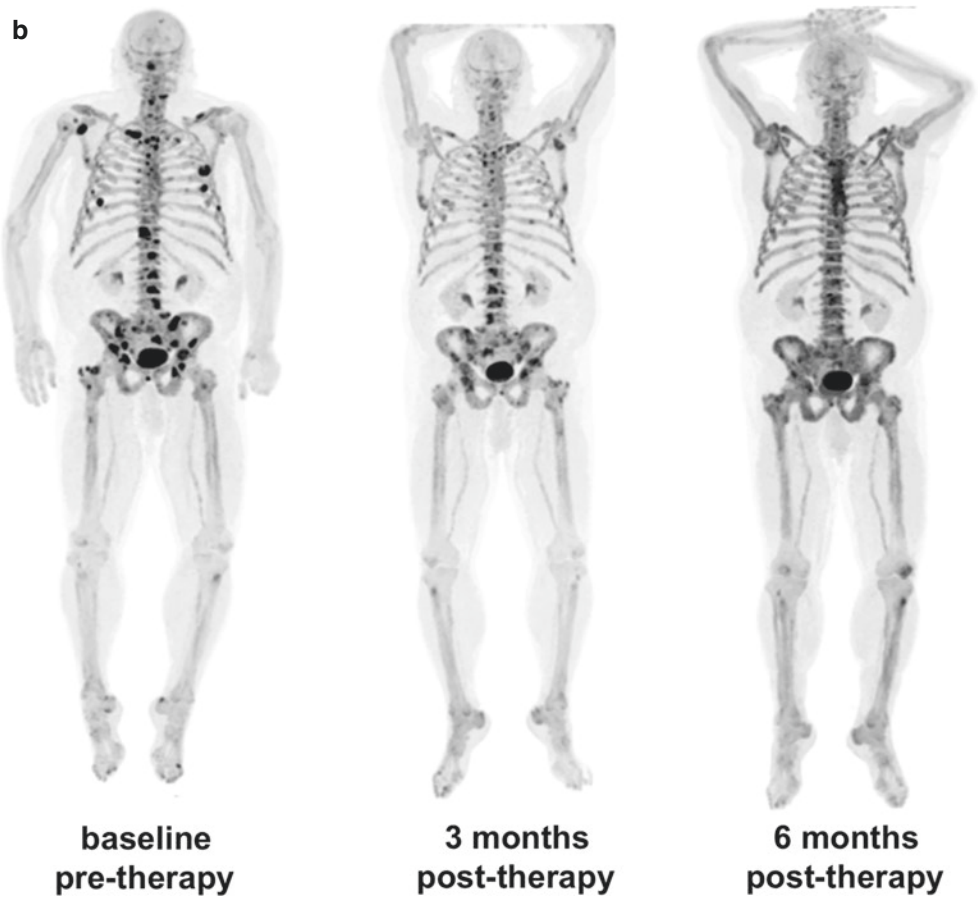

be ruled out as generators of bone pain. Considerable evidence has been published showing that SPECT/CT can guide minimal-invasive treatment of joint disease.

Key Learning Points

- When reading bone scans of patients with skeletal pain, listing of the possible differential diagnoses into major categories might be helpful.
- These categories are malignant and benign bone tumors, inflammation, trauma, degenerative disease, vascular disorders, and some miscellaneous conditions.
- Joint degeneration is one of the most frequent causes of bone pain and is caused by degeneration of the joint cartilage.
- Joint degeneration is accompanied by an increase in bone metabolism, when active.
- SPECT/CT helps in localizing foci of increased uptake and at the same time increases the diagnostic specificity considerably, as the hallmarks of osteoarthritis are readily visualized by the CT component of the scan.

24.5 Metabolic Bone Diseases

The term metabolic bone disease includes a group of alterations that involve the skeleton in full, characterized by an increase in bone turnover. The corresponding scintigraphic pattern is characterized by a diffuse increased uptake of the radiopharmaceutical. There are, in addition, features of focally increased uptake, such as the one involving long bones typical of hypertrophic pulmonary osteopathy (Fig. 24.24).

24.5.1 Osteoporosis

Osteoporosis is a metabolic skeletal disorder characterized by decreased bone density and quality, reducing bone strength and predisposing the patient to fractures even for minor traumas. There are two types of osteoporosis: postmenopausal osteoporosis and senile osteoporosis. Given the availability of effective treatments, early diagnosis of osteoporosis is crucial to slow down its evolution and thus reduce the risk of complications. Dual X-ray absorptiometry (DEXA) has completely replaced earlier techniques based on a sealed radionuclide

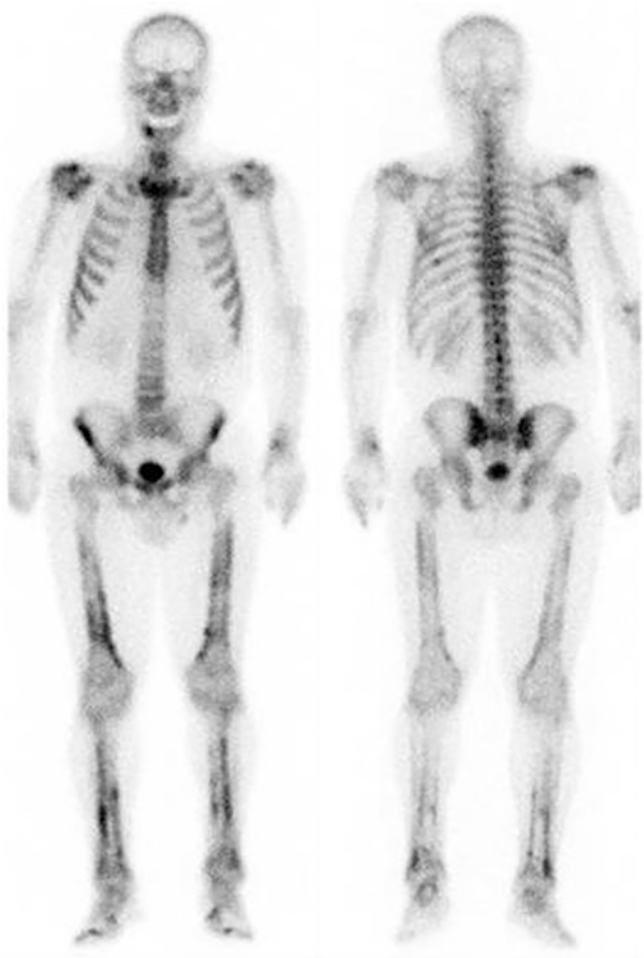

Fig. 24.24 Planar whole-body scan obtained about 3 h after administration of ^{99m}Tc-HDP in a patient with hypertrophic pulmonary osteopathy. Increased tracer uptake with a typical "railway" pattern is clearly recognized at the femurs and tibias (*reproduced with permission from: Volterrani D, Erba PA, Mariani G, Eds. Fondamenti di Medicina Nucleare – Tecniche e Applicazioni. Milan: Springer Italy; 2010*)

source emitting γ-rays either with a single energy peak (e.g., ^{125}I and/or ^{241}Am) or with two different energy peaks (such as ^{153}Gd). Therefore, nuclear medicine does not have a role in screening patients for osteoporosis.

Regarding instead the most common radionuclide bone imaging modality, i.e., bone scintigraphy with ^{99m}Tc-diphosphonates, there are several nonspecific findings that might suggest the diagnosis of osteoporosis, such as reduced bone-to-soft-tissue uptake ratio, decreased resolution of vertebral body endplates, and relatively increased skull uptake of the radiopharmaceutical (Fig. 24.25). However, the value of nuclear medicine imaging in patients with osteoporosis is predominantly in the assessment of complications, such as pathological fractures. This is particularly important with regard to vertebral fractures, since bone scintigraphy can exclude the coexistence of other skeletal diseases that may cause fractures. Bone scintigraphy is also of great help for the diagnosis of regional osteoporosis syndromes and algodystrophy. Nevertheless, scintigraphy does not allow one to diagnose reduced bone mass.

In patients with multiple vertebral fractures, bone scintigraphy may also disclose reduced height of the spine and chest cage closer to the pelvis. Detection of unknown vertebral or rib fractures is also possible, raising the suspicion of osteoporosis. Vertebral crush is visible at scintigraphy as an intense linear uptake of the tracer, corresponding to the site of fracture. Abnormal uptake at the site of fractures can be detected in 80% of cases within 24 h and in 95% of cases within 72 h. This high uptake decreases progressively over a period of time ranging from 6 to 18 months but extending even up to 3 years depending on fracture site and patient age, with a time trend that can help determine the age of the fracture.

In case of back pain, bone scintigraphy can help determine whether pain is attributable to vertebral fracture (Fig. 24.26); a normal scan excludes a recent fracture and directs the clinician toward other diagnostic options.

Bone scintigraphy can also reveal other causes of back pain, such as tumor metastasis, Paget's disease, and infection (Fig. 24.27). SPECT and SPECT/TC have increased the diagnostic value of bone scintigraphy, especially for the lumbar region, based on better scintigraphic contrast and the possibility to localize the area of hyperactivity more accurately.

SPECT images show that joint lesions are more common in patients with multiple vertebral fractures. Since most often the area of increased uptake occurs at the level of L4-L5 and L5-S1, it can be assumed that hyperactivity of the articulated joints in these areas is due to the simultaneous presence of osteoarthritis and to the stress due to the collapse of a vertebral body above or below those levels. Patients with vertebral crush can present other fractures that bone scintigraphy can detect at an early stage, when traditional radiological imaging is still negative or nonconclusive. Unknown fractures of the pelvis detected only by bone scintigraphy can mimic pain caused by vertebral crush. Similarly, unknown fractures of the femoral neck, scapula, radium and chest cage can be detected by bone scintigraphy.

The use of [^{18}F]FDG PET/CT can help distinguish a pathological vertebral fracture caused by tumor metastasis from an osteoporotic fracture. The latter tends to have no pathologically increased [^{18}F]FDG uptake, while high [^{18}F]FDG uptake is characteristic for malignant and inflammatory processes [56].

Nuclear medicine imaging might be of value also in the assessment of side effects from osteoporotic therapies. For example, bone scan can be used to assess possible fractures related to bisphosphonate therapy [57]. Long-standing bisphosphonate therapy changes the bone architecture, weakening the bone and resulting in an increased risk of low-energy atypical subtrochanteric and proximal diaphyseal femoral fractures. These fractures are often subtle and missed on initial radiography [58]; however, because of the risk of a delayed diagnosis of displaced complete fracture, early

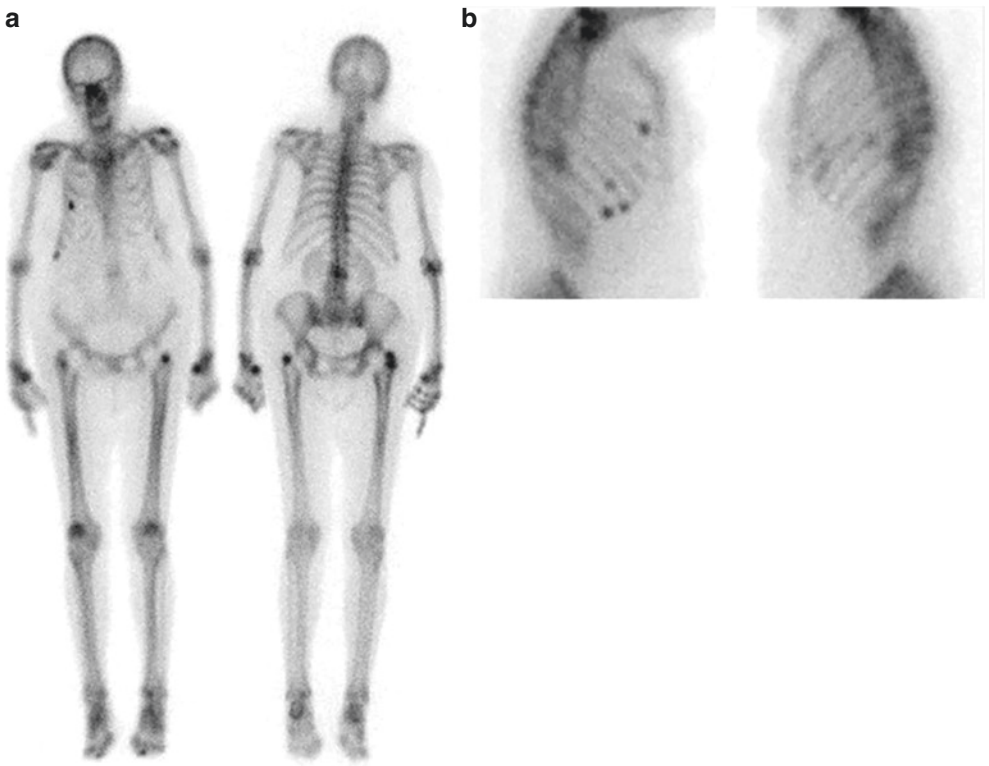

Fig. 24.25 Planar bone scintigraphy obtained about 3 h after administration of ^{99m}Tc-HDP in a patient with osteoporosis previously submitted to bilateral hip joint prosthetic implants. The whole-body anterior and posterior views (**a**) show diffuse inhomogeneities in tracer distribution throughout the skeleton, with multiple areas of focally increased uptake in the ribcage, better shown in the lateral views (**b**), corresponding to prior fractures cause by minor traumas—as typically observed in patients with osteoporosis. Increased tracer uptake is observed also at both hips, reflecting ongoing bone post-implantation remodeling (*reproduced with permission from: Volterrani D, Erba PA, Mariani G, Eds. Fondamenti di Medicina Nucleare – Tecniche e Applicazioni. Milan: Springer Italy; 2010*)

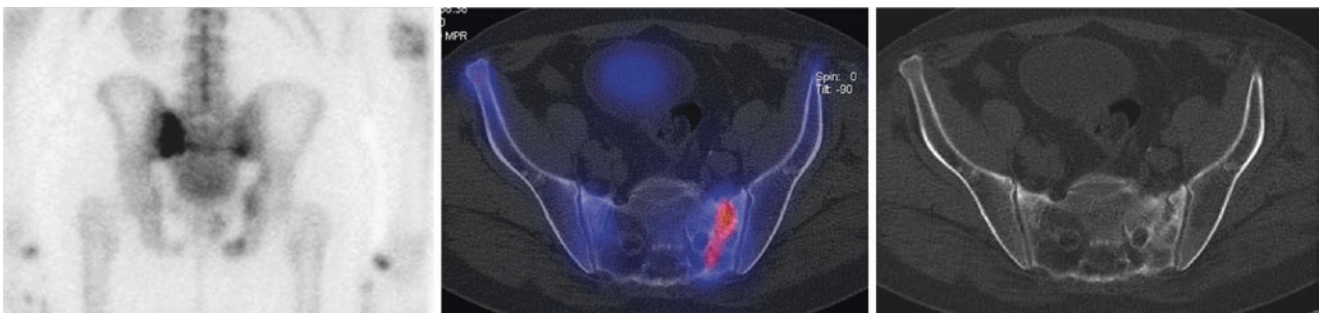

Fig. 24.26 Bone scintigraphy performed in an elderly patient with long-standing pelvic pain. Dorsal planar view (left panel) shows zones with markedly increased tracer uptake in/near both iliosacral joints, connected by a thin line of increased tracer accumulation, the so-called Honda sign; in the right os ischiaticum, a further hot spot can be detected. On hybrid fused SPECT/CT imaging (center panel) and CT imaging (right panel), increased uptake corresponds to a fracture cleft in the os sacrum. The findings are due to a sacral insufficiency fracture

assessment for such fractures using a highly sensitive technique, such as scintigraphy, is recommended.

The kinetics ^{18}F-NaF uptake in bone and the plasma clearance of this tracer in patients with osteoporosis have been investigated. As reviewed by Raynor et al., measurements of plasma clearance to assess response to new treatments for osteoporosis [59] have validated the use of ^{18}F-fluoride PET imaging as a noninvasive method of imaging and evaluating the efficacy of therapeutic interventions for osteoporosis. While there does not yet seem to be a consensus on whether to use static or dynamic PET, it is suggested that a single static PET acquisition may be able to closely approximate the 1-h dynamic PET values of regional blood clearance, while completing a scan in only 5 min [8, 60, 61].

A recent study compared the measurements obtained by static PET to those obtained by dynamic PET, reporting a cor-

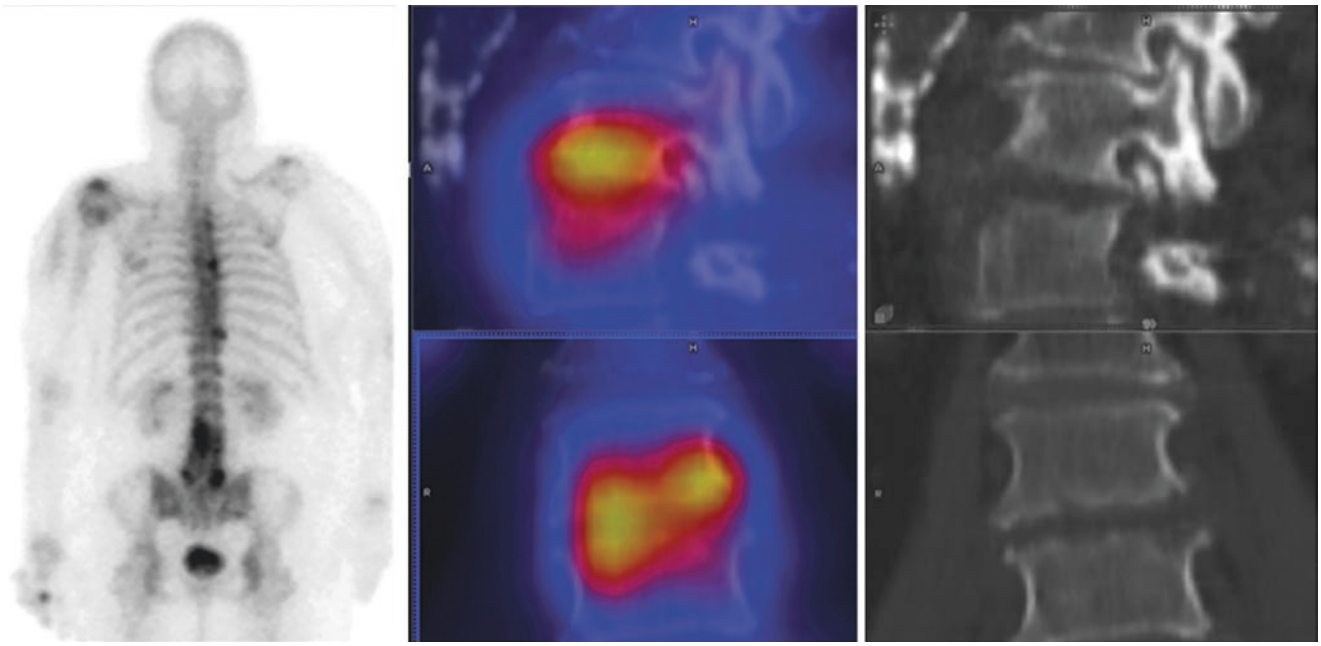

Fig. 24.27 Bone scintigraphy performed in a 67-year-old woman with considerable, long-standing back pain. Dorsal view of planar scan (left panel) shows markedly enhanced tracer uptake in the lower lumbar spine extending over at least two segments. Hybrid images (center panel) as well as low-dose CT (right panel) disclose this to be due to spondylodiscitis with contour defects of endplates and normal width of disk space. Other signs of osteochondrosis are also missing

relation coefficient between estimated K_i values and calculated K_i values 30–60 min after injection even >0.99. The potential of static scans to replace dynamic scans would eliminate the need for arterial blood sampling, as well as greatly reduce the duration of the imaging session. Bone turnover in the femoral neck—the site of most traumatic osteoporotic fractures—has also been investigated as marker for osteoporosis. The femoral neck region was defined using anatomical landmarks from CT scans, and quantification of ^{18}F-fluoride uptake in the entire neck was found to reflect global bone turnover. The metabolically active volume, maximum SUV, mean SUV, and total calcium metabolism were calculated. A correlation coefficient of −0.43 was found between age and global values, indicating a decline in global activity with aging [59]. These preliminary data demonstrate the potential role of global bone turnover in the femoral neck for early detection of osteoporosis but also the need for larger-scale studies to evaluate the clinical utility of this approach.

24.5.2 Osteomalacia

Osteomalacia and rickets are disorders characterized by abnormal mineralization of the skeleton resulting from defects in the phosphate, calcium, and/or vitamin D metabolism. Rickets is a childhood disease (most frequent in developing countries), whereas osteomalacia occurs in adults. The clinical scenario of skeletal deformities in rickets includes bowed legs, skull bossing, pectus carinatum, hyphoscoliosis, and costochondral swelling. Osteomalacia may present with a mild and subtle clinical picture without the visible bone deformities seen in the pediatric population. Bone scans in patients with osteomalacia can be normal, especially in early stages. The typical scintigraphic pattern in later stages of this condition is characterized by intense uptake of ^{99m}Tc-diphosphonates at the metaphysis and long bone ossification centers (so-called chicken bone). Figure 24.28 shows two typical examples.

Osteomalacia shares with hyperparathyroidism some metabolic features that on bone scintigraphy appear as increased bone-to-soft tissue uptake ratio, increased uptake in long bones and skull, beading of the costochondral junctions, and the "tie sternum" appearance [62, 63]. "Metabolic" fractures have also been described associated with osteomalacia and often misinterpreted as metastasis.

Oncogenic osteomalacia is a rare form of osteomalacia but deserves a special note for its clinical significance. This condition is also known as tumor-induced osteomalacia and is usually associated with mesenchymal tumors. This paraneoplastic syndrome is caused by the secretion of a substance that interferes with the normal metabolism of calcium and phosphate. If there is suspicion of tumor-induced osteomalacia, a whole-body scan such as [^{18}F]FDG PET/CT is recommended to locate the primary cancer. [^{18}F]FDG [64, 65] and the somatostatin receptor imaging agents

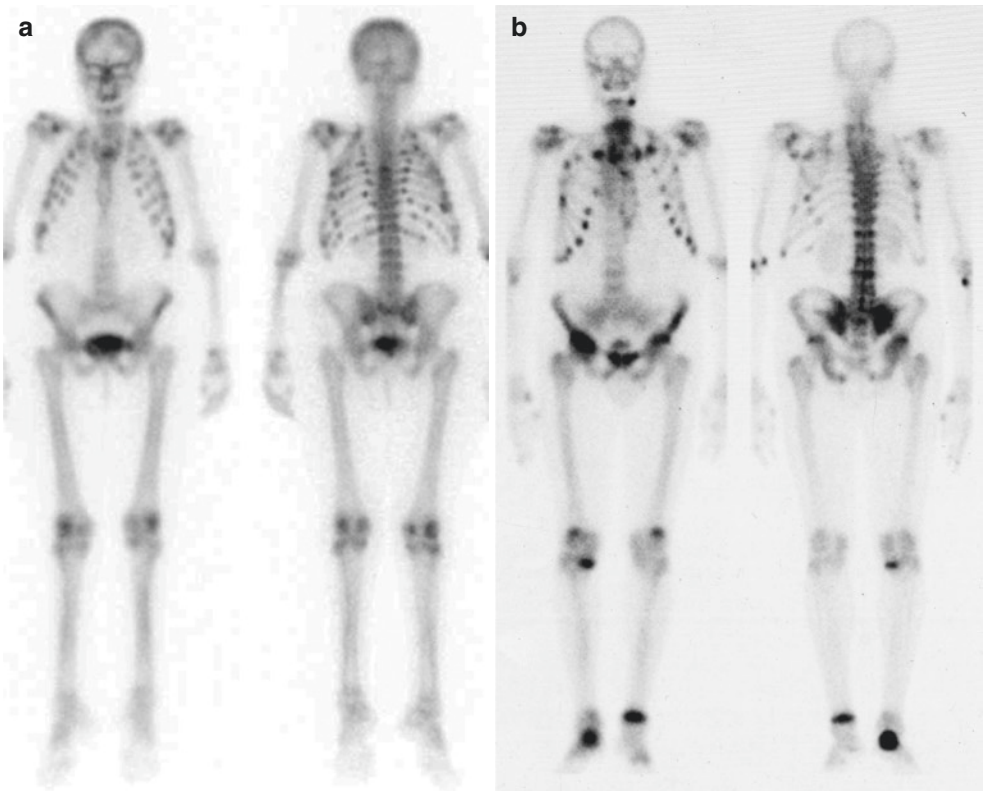

Fig. 24.28 Planar whole-body scans (anterior and posterior views) obtained in two different patients with osteomalacia about 3 h after administration of ^{99m}Tc-HDP. Both patients exhibit diffusely increased tracer uptake at multiple sites especially in the ribs for patient shown in panel (**a**), in whom the "chicken bone" pattern is visible particularly in the posterior view of the femora and tibiae. The predominant scintigraphic pattern for the patient shown in panel (**b**) is instead characterized by multiple foci of markedly increased tracer uptake involving also pelvic bones and the lower limbs (*reproduced with permission from: Volterrani D, Erba PA, Mariani G, Eds. Fondamenti di Medicina Nucleare – Tecniche e Applicazioni. Milan: Springer Italy; 2010*)

such as ^{68}Ga-DOTA-TATE [66, 67], ^{68}Ga-DOTA-NOC [68], and ^{68}Ga-DOTA-TOC have each been reported to detect the primary tumor in these cases. ^{18}F-DOPA might be also an option.

24.5.3 Primary and Secondary Hyperparathyroidism

Hyperparathyroidism is characterized by an excess of parathyroid hormone in the blood that results in weakening of the bones through loss of calcium. Depending on the etiology, hyperparathyroidism can be primary, secondary, or tertiary. Primary hyperparathyroidism is due to parathyroid adenoma in 80% of cases, parathyroid gland hyperplasia in 15–20%, and rarely cancer (<0.5%). Secondary hyperparathyroidism is usually related to vitamin D deficiency, chronic kidney disease, or other causes of low blood calcium levels resulting in hyperstimulation of the parathyroid glands. Tertiary hyperparathyroidism is characterized by autonomous parathyroid function following resolution of the initial cause of parathyroid stimulation. ^{99m}Tc-sestamibi scans play a key role in the preoperative localization of parathyroid adenoma(s) (see Chap. 28 of this book).

The typical bone scan pattern of hyperparathyroidism is represented by generalized increased radiopharmaceutical uptake in bones of the skull, jaw, sternum, and shoulder (Fig. 24.29). With high-resolution scintigraphy (e.g., using the pinhole collimator for acquiring spot views at selected sites), the characteristic sign of the linearly increased uptake in the subperiosteal bone, for example, at the level of the phalanxes, might be detected. Other signs associated with hyperparathyroidism are the "rosary beads sign" (increased uptake at the costochondral junctions) and the "tie sign" (prominent uptake in the sternum).

Hyperparathyroidism has also been described associated with brown tumors, soft tissue calcifications, fractures, and subchondral bone resorption. Brown tumors are also known as osteitis fibrosa cystica or osteoclastomas and result from replacement of the normal bone marrow with hemorrhage and granulation tissue. These tumors can be visualized with whole-body ^{99m}Tc-sestamibi scintigraphy, although [^{18}F]FDG

Fig. 24.29 Composite planar bone scintigraphy obtained about 3 h after administration of ^{99m}Tc-MDP in a patient with hyperparathyroidism secondary to renal failure. Markedly increased tracer uptake virtually in the whole head, including the calvarium, maxillary bones, and mandible. This scintigraphic pattern of the head is rather typical and resembles the appearance of a grenadier soldier (*reproduced with permission from: Volterrani D, Erba PA, Mariani G, Eds. Fondamenti di Medicina Nucleare – Tecniche e Applicazioni. Milan: Springer Italy; 2010*)

PET/CT has been reported as a more sensitive technique [69]. Soft tissue calcifications, also known as metastatic calcifications, have been described in the soft tissue of both upper and lower extremities [70], lungs [71], thyroid, and stomach [72]. Improvement of these features has been reported following resection of the hyperfunctioning parathyroid tissue [72].

24.5.4 Renal Osteodystrophy

The most typical scintigraphic pattern of renal osteodystrophy (a condition characterized by complex metabolic derangements including, among others, secondary hyperparathyroidism) is represented by homogeneously increased uptake of ^{99m}Tc-diphosphonates in the whole skeleton but particularly in the bones of the skull and jaw (see Fig. 24.29). The images acquired 24 post-administration are characterized by very high bone-to-soft-tissue tissue ratios; pulmonary, gastric, or renal calcifications may also be visualized.

24.5.5 Hypertrophic Osteoarthropathy

Hypertrophic osteoarthropathy can be idiopathic or secondary to malignancy. This condition is characterized by periosteal reaction, more prominent in the long bones. In the bone scan, linearly increased uptake in parallel lines along the cortex of the diaphysis of the radii, tibias, and femurs can be detected [73]. Secondary forms, for example, due to lung cancer, often resolve following treatment of the underlying cause.

Key Learning Points

- The term metabolic bone disease includes a group of alterations that involve the skeleton in full, characterized by an increase in bone turnover.
- The corresponding scintigraphic pattern is characterized by a diffusely increased uptake of the radiopharmaceutical.

24.6 Trauma and Fractures

On bone scintigraphy, fractures are characterized by increased uptake of ^{99m}Tc-diphosphonates along the fracture lines. In the acute stage, uptake may also be seen in the first and second phase of a three-phase bone scan. The time elapsed between the trauma and positivity of the fracture in a bone scan may vary, though. For instance, fractures in the extremities usually become positive within the first 24 h after trauma, but fractures of the spine, pelvis, or femoral neck may become positive only after several days. This also depends on patients' age and on the concomitant occurrence of osteoporosis. In elderly patients, even hip fractures may not become sites of increased uptake for several days after the traumatic event.

Patients with trauma are usually referred for planar X-rays and/or high-resolution CT. In rare cases, these modalities might not allow a diagnosis of a fracture, and bone scintigraphy might be helpful. This applies in particular to fractures in osteoporotic bone, in which the fracture lines may be detected only with some difficulty, for instance, in case of sacral insufficiency fractures. Sacral insufficiency fractures are scintigraphically characterized by linear uptake lines next to the iliosacral joints connected by a horizontal line of increased uptake so that an "H" is formed, the so-called Honda sign (see Fig. 24.26). They are usually accompanied by fractures of the pubis and/or ischium. In osteoporotic vertebral fractures, bone scintigraphy with SPECT/CT not only provides the diagnosis but can also assess their age and floridity. This feature has some therapeutic relevance, since only patients with younger fractures benefit from vertebral osteoplasty.

In athletes presenting with pain of the lower extremities, bone scintigraphy can distinguish between insertion tendinopathies (such as the so-called shin splints) and stress fractures. Again, SPECT/CT helps considerably in differentiating between increased uptake caused by fractures and that caused by other conditions, in particular in anatomically complex regions such as in the hands or feet. On CT imaging, fracture lines can in many cases be seen or also contour disruptions of the bone involved.

24.6.1 Occult Fractures or Trauma

While standard radiography is the primary imaging technique in case of suspected fracture, bone scintigraphy is useful to reveal occult fractures and to exclude a pathological cause when the radiological examination is still negative. The areas most frequently affected by occult fractures are the carpal bones, proximal femora, ankle, foot, and spine. Sensitivity of bone scintigraphy in disclosing occult fractures (though varying according to the site involved and patient age) is >95%, with a negative predictive value close to 99%.

The three-phase bone scintigraphy becomes abnormal shortly after the fracture; 95% of fractures in patients aged <65 years may be visualized at scintigraphy within 24 h and 100% within 72 h, while in patients aged >65 years the bone scan becomes positive within 72 h. Bone scintigraphy can also be used to estimate the age of the fracture in terms of time elapsed since the acute event.

The pattern of three-phase bone scintigraphy can be classified into three types: acute, subacute, and healing. In the acute phase (1–4 weeks), hyperemia and hematoma formation around the fracture site cause increased blood flow (in the vascular phase of the three-phase scan) and increased activity in the blood pool image. In the subacute phase (6–12 weeks), with the formation of bone callus and a relative decrease of regional blood flow, increased tracer uptake is noticed in particular around the fracture fissure (Fig. 24.30). In the final healing phase, the bone callus is reabsorbed and replaced by normal bone tissue, thus gradually reducing the intensity of tracer uptake. In uncomplicated fractures scintigraphy normalizes over 1 or 2 years; if increased uptake persists, suspicion of infection or lack of union of the bone fracture should be considered.

24.6.2 Stress Fractures

The proper definition and pathophysiology of the stress fracture currently encompass two processes with a similar end result. The *fatigue fracture* is the result of an abnormal load upon normal bone, while the *insufficiency fracture* is the result of normal loading upon abnormal bone (osteopenic bone). The fatigue fracture is the result of an abnormal repetitive load upon normal bone and occurs during an abrupt increase in frequency, duration, or intensity of activity when bone resorption (osteoclasts) is greater than bone replacement (osteoblasts).

This type of stress fracture commonly occurs in the young active individual, such as the athlete or military recruit. Contributing risk factors, which are not mutually exclusive of one another, can be divided into two broad categories: extrinsic (training regimen, footwear, training surface, and type of sport) and intrinsic factors (gender, age, race, and overall fitness level, as well as skeletal, muscle, joint, and biomechanical factors). Females have a higher incidence of fatigue fractures compared with males, in part as a consequence of the "female athlete triad": eating disorders, amenorrhea, and osteoporosis. Through a complex interplay of nutritional deficiency, hypothalamic and estrogen abnormalities, as well as delayed menarche, reduced bone mineral

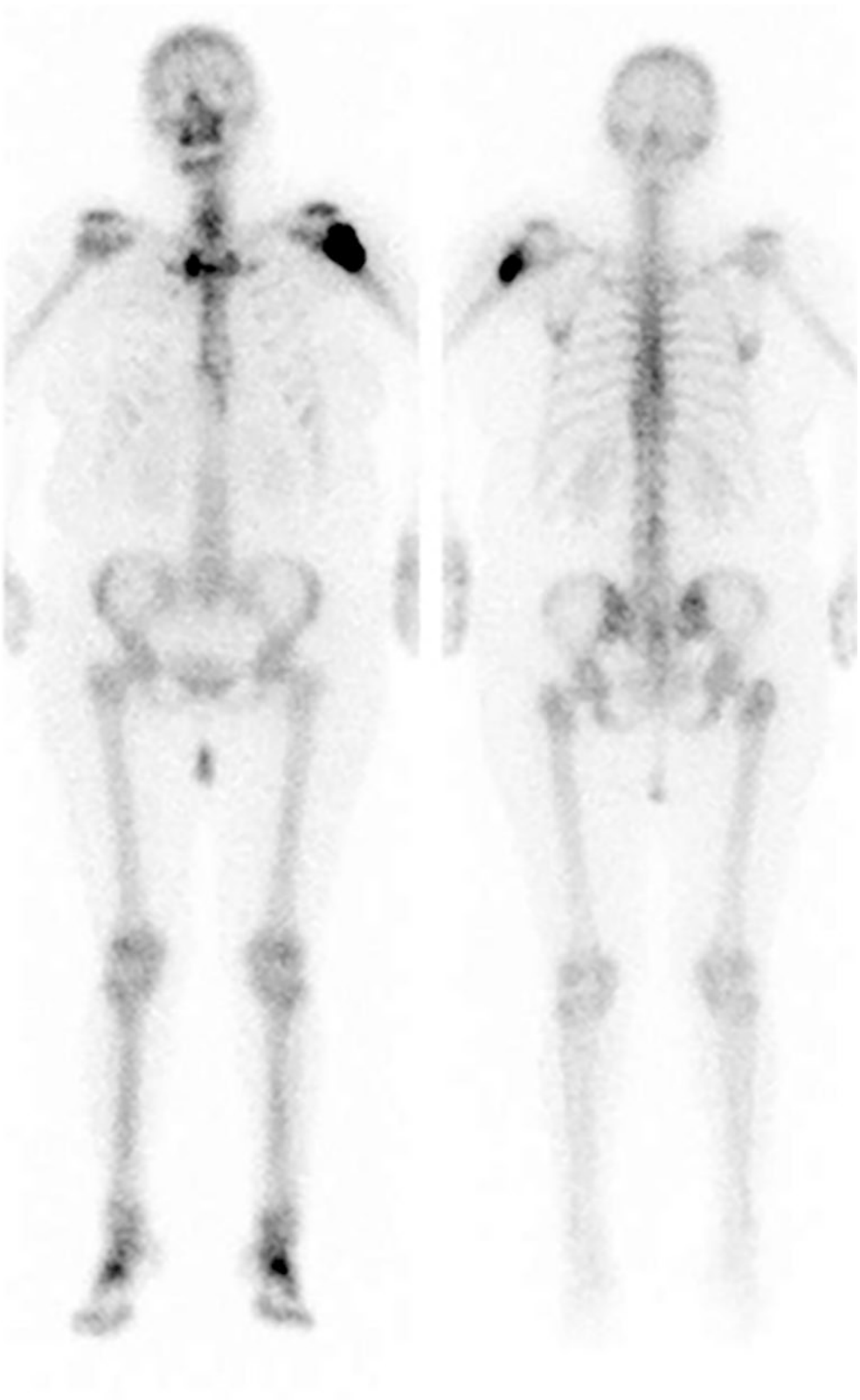

Fig. 24.30 Planar whole-body scintigraphy obtained about 3 h after administration of ^{99m}Tc-HDP in a patient with recent traumatic fracture just below the left humeral head. Markedly increased tracer uptake at the fracture site reflects active ongoing mineralization of the healing bone callus (*modified from: Volterrani D, Erba PA, Mariani G, Eds. Fondamenti di Medicina Nucleare – Tecniche e Applicazioni. Milan: Springer Italy; 2010*)

density places the female athlete at a significant risk for stress fractures.

Insufficiency fractures are the result of normal loading upon abnormally weakened bone. Several predisposing factors have been identified as the cause of insufficiency fractures, the common entity often being primary or secondary osteoporosis. Other risk factors include all the conditions where bone elasticity and mineral content are compromised, such as rheumatoid arthritis, metabolic bone disease, neurological disorders, prior irradiation, total hip replacement, corticosteroid therapy, high-dose fluoride therapy, and bisphosphonate therapy. Elderly and postmenopausal women are most at risk for developing insufficiency fractures.

Stress fractures almost universally present with pain upon activity and point tenderness. The pain is relieved with rest and worsens when the activity is continued. Typically, the presentation occurs when there has been a change in intensity of the activity. Insufficiency fractures of the pelvis frequently present as low back, buttock, and groin pain in the elderly. Subchondral insufficiency fractures may present with sudden onset of severe pain in the absence of or following only minor trauma and, therefore, may present in an emergency setting.

X-ray is a first-line imaging procedure, despite its low sensitivity in case of early stress fracture and difficulties of interpretation in the presence of osteopenia. Stress fractures may appear as subtle linear sclerosis (often perpendicular to major trabeculae), focal endosteal or periosteal reaction, and/or fracture through one cortex with superimposed periosteal reaction. MR imaging is extremely sensitive (100% sensitivity and 85% specificity), although typically a second-line modality, obtained when radiographs are normal and pain persists or in athletes requiring a definitive diagnosis. A linear hypointense fracture line on T1-weighted and T2-weighted images with adjacent bone marrow and soft tissue hyperintensity on T2 fat saturated or short tau inversion recovery (STIR) sequences (edema) are typical findings. Periosteal new bone will exhibit low signal in all sequences, and adjacent soft tissue edema may also be present. Fredericson et al. provided a classification into discrete grades based on fluid-sensitive and T1-weighted characteristics of the stress injury of the tibial bone in runners [74]. Further work by Kijowski et al. found a correlation between the grade of the lesions and the estimated time to return to sport activities [75]. MRI is also important for diagnosing subchondral insufficiency fractures, which are not apparent on radiographs unless there is linear subchondral lucency or collapse. The main limitation of MR is the possibility of misdiagnosis, since peripheral edema in the T2-weighted sequences can be present in case of infection and tumor. Therefore, MR imaging is currently reserved for the evaluation or follow-up of athletes performing sports activities at a competitive level or in combination with scintigraphic data, if they are not conclusive.

CT is useful for identification of longitudinal fracture lines, for the differential diagnosis with osteoid osteoma, and for the evaluation of stress injury of the spine, whereas has limited value in case of chronic lesions and for the evaluation of transverse fractures [76].

A repetitive stress on a given musculoskeletal tract causes a reabsorption and neoformation reaction of the bone tissue, mediated by the concerted action of osteoblasts and osteoclasts; this response is a functional adaptation of the bone tissue, which is constantly stretched under load. However, this process implies that there is a phase where osteoclast activity is predominant; the occurrence of further stress in this period can cause microfractures (or even macroscopic fractures).

Bone scintigraphy plays a well-defined role in the diagnosis of stress fractures, with 100% sensitivity even at an early stage when 80% of such lesions are not still evident in the conventional radiological examination. In fact, bone scintigraphy becomes positive about 2 weeks before the radiological appearance. Early diagnosis is very important, for example, for athletes who practice sports at an advanced level, both to prevent complications of an undiagnosed fracture and to allow a faster recovery. The most common fracture site is the tibia, followed by the metatarsal bones. On bone scintigraphy, the stress fracture appears as a focal area of hyperactivity in the 3-h image, variably associated with different degrees of changes in the flow blood and blood pool phase, depending on the time elapsed from the fracture or if it has been subjected to new stresses. Based on the scintigraphic pattern, a fracture can be classified as follows:

- Grade I—slightly increased tracer uptake localized to the cortex
- Grade II—more intense and extended increased uptake
- Grade III—increased uptake extended to more than half the bone amplitude
- Grade IV—increased uptake extended to the entire bone thickness

In general, stress fractures of the proximal tibia tend to heal earlier than those of the distal tract. Furthermore, fractures of the anterior aspect of the tibia and the malleolus are more frequently associated with complications (such as nonconjunction, poor positioning, and avascular necrosis) as compared to the corresponding posterior aspects. Femoral neck fractures are mostly diagnosed in athletes and in older people with osteoporosis and may be of two types: with compression (located at the lower margin of the femoral neck) and with loading (located at the top edge).

Pelvic occult fractures are mainly due to osteoporosis; they are usually located along the sacrum or pubis and can be misinterpreted as metastatic disease at scintigraphy. In 85% of patients with sacral osteoporosis, bone scintigraphy can

also detect other unknown fractures, located above all in the spine, ribs, and pubic bone.

Spondylolysis, characterized by a defect in the posterior arch of the vertebrae at the pars interarticularis, represents the primary diagnosis in 47% of young athletes with negative history for previous trauma but with lumbar back pain. Often it is bilateral and can, therefore, cause spondylolisthesis. For the diagnosis, in addition to the standard scintigraphic study (which shows an increased uptake at the lesion), SPECT and SPECT/CT acquisitions provide best results, especially for accurate localization of the site involved and as prognostic index for potential healing. In fact, a negative scintigraphy in presence of a positive radiography indicates either inactive disease or healed fracture and excludes spondylolysis as a cause of pain.

[^{18}F]FDG PET/CT can also demonstrate increased tracer uptake at the site of stress fracture. Some patterns of uptake, such as the "Honda sign" for sacral insufficiency fractures, can be diagnostic, with sensitivity and positive predictive value of up to 96% and 92%, respectively [77, 78].

Key Learning Points

- On bone scintigraphy, fractures are characterized by increased uptake of ^{99m}Tc-diphosphonates along the fracture lines.
- Fractures in the extremities usually become positive within the first 24 h after trauma, but fractures of the spine, pelvis, or femoral neck may become positive only after several days.
- In uncomplicated fractures scintigraphy normalizes over 1 or 2 years.
- In osteoporotic vertebral fractures, bone scintigraphy with SPECT/CT not only provides the diagnosis but can also assess their age and floridity.
- The *fatigue fracture* is the result of an abnormal load upon normal bone, while the *insufficiency fracture* is the result of normal loading upon abnormal bone (osteopenic bone).
- Bone scintigraphy plays a well-defined role in the diagnosis of stress fractures, with 100% sensitivity even at an early stage when 80% of such lesions are not yet obvious on conventional X-ray examination.

24.7 Vascular Disorders

Aseptic bone necroses are caused by acute disturbances in blood supply, the exact cause remaining unclear in most cases. In their very early phase, the necrotic bone is hypoperfused and hypometabolic, presenting therefore as a "cold spot" on bone scintigraphy. Reparative processes, starting at the periphery of the necrotic bone, begin several days after the insult and persist for months or years thereafter. In this process, the core of the necrosis remains hypometabolic; this creates a typical scintigraphic pattern of a "cold-in-hot" spot, often termed as halo or crescent sign.

Transient osteoporosis/bone marrow edema, a usually self-limiting condition, also affects the epiphysary bone; is painful, in its early stages markedly hypermetabolic; and thus raises the issue of differential diagnosis with femoral head necrosis. Aseptic necrosis may also affect other bones, such as the distal femur, the os lunatum, or the os scaphoideum. Bone infarctions are also due to vascular disturbances but—at variance with bone necrosis—in most cases are asymptomatic. They may be idiopathic or triggered by a variety of risk factors such as alcohol, sickle cell anemia, radiation therapy, cytotoxic medication, or steroids. Their scintigraphic appearance depends on the stage when they are imaged, similarly as in the case of bone necrosis. On CT imaging, they tend to have a sclerotic rim with a central lytic zone that may also feature calcifications.

In osteochondrosis dissecans, bone ischemia can lead to bone fragmentation of the joint end of a bone. This condition is found above all at the knee or talus. The involved zones are generally visible on planar/SPECT imaging as areas with increased ^{99m}Tc-diphosphonate uptake. SPECT/CT greatly increases the diagnostic accuracy.

24.7.1 Aseptic Necrosis of the Femoral Head

Osteonecrosis (often termed avascular necrosis with involvement of the epiphyseal regions) is a relatively common disease in which ischemic death of the cellular components of bone and marrow occurs. The femoral heads are the most commonly affected sites, with estimates of symptomatic femoral head osteonecrosis of 2–4.5 per patient-year, resulting in 10,000–20,000 new cases annually in the United States [79]. Since most patients are asymptomatic, most likely this incidence significantly underestimates the true prevalence of osteonecrosis. Osteonecrosis affects both children and adults, and the predisposing factors include dislocation of the hip, femoral neck fracture, corticosteroid usage, alcoholism, collagen vascular disease, hemoglobinopathies, Gaucher disease, caisson disease, and some skeletal dysplasias [80]. The spontaneous form (or Legg-Calvé-Perthes disease) affects children at an age of 4–8 years. Secondary forms are more common in adulthood. Nontraumatic osteonecrosis is bilateral in 70–80% of cases, which further increases the disability due to femoral head collapse.

No specific physical findings or laboratory tests can reliably establish the diagnosis of osteonecrosis. When sus-

pected on clinical ground, osteonecrosis must be confirmed by diagnostic imaging, or through biopsy. Imaging methods that can assist in establishing the diagnosis include planar X-rays, CT, bone scintigraphy, and MRI, with or without contrast enhancement. These methods vary considerably in their cost, diagnostic accuracy, and the information provided.

Although the optimal treatment for femoral head osteonecrosis is debated, early diagnosis is important both for excluding other causes of pain (infection, cancer, fracture, arthritis, femoro-acetabular impingement syndrome, etc.) and for assessing the efficacy of treatment.

X-ray should be always performed as the first-line imaging. In children, the earliest radiographic findings of osteonecrosis include a smaller ossific nucleus, increased radiodensity, subchondral fracture, and metaphyseal radiolucencies. Subsequently, fragmentation, resorption, reossification, and remodeling of the affected femoral head and neck are seen. The main role of CT is to determine the severity of articular collapse and its location and to detect early secondary degenerative joint disease. This information is useful for surgical planning, e.g., for rotational osteotomy, arthroplasty, resurfacing procedures, or joint replacement [81]. In the pediatric population, CT is not commonly used for assessment of osteonecrosis.

MRI is the most sensitive and specific imaging modality to detect osteonecrosis [82, 83]. In the adult population, the differential diagnosis should always be made versus transient osteoporosis and subchondral insufficiency fracture [84, 85]. In the pediatric population, there is a definite role for contrast-enhanced MRI [86, 87]. Using a dynamic technique, the disease can be detected at an earlier stage than with other MRI techniques; in particular, in Legg-Calvé-Perthes disease, there is increased peak enhancement and delayed time-to-peak enhancement [88]. Furthermore, this technique has been used to identify femoral heads at risk for the development of osteonecrosis subsequent to femoral neck fracture [89].

Although planar bone scintigraphy is less sensitive than MRI (90% versus 100%) [82], it remains a valid option in patients with suspected osteonecrosis. SPECT or preferably SPECT/CT improves overall sensitivity up to 97%. Different sensitivities reported by different studies are mainly due to the different etiopathogenetic factors that can cause aseptic necrosis and by the dynamic nature of the process. For example, osteonecrosis following fracture of the femoral neck is due to a sudden and substantial reduction of blood flow (the scintigraphic images, thus, show a photopenic area) (see Figs. 24.3 and 24.4). In the form secondary to corticosteroid therapy, the presence of small photopenic lesions with microfractures and repair might be visible in the bone scan as an area of increased uptake.

In addition, the diagnostic value of scintigraphy is less affected than CT and MR by artifacts due to recent surgical interventions. In Legg-Calvé-Perthes disease, a photopenic area can be seen in the early stages, followed by hyperactivity due to repair reaction in later stages.

24.7.2 Sympathetic Reflex Dystrophy

This is mainly a post-traumatic syndrome, characterized by pain, functional impotence, vasomotor instability, swelling, and skin dystrophy. Because of an altered neurovegetative balance, opening of vascular shunt occurs at the affected site, resulting in low blood flow resistances. Diagnostic sensitivity of the three-phase bone scintigraphy is very high (>90%), especially at an early stage when radiological imaging can still be completely negative. The characteristic scintigraphic pattern is represented by increased blood flow and increased capillary permeability (compared to the contralateral limb), usually only apparent in the first 2–3 months after the onset of the disease (Fig. 24.31). At later stages, increased uptake in the periarticular region at the affected limb, which can persist for up to 1 year from the onset of symptoms, is generally observed. A particular form, more common in childhood and adolescence, is characterized by low activity accumulation in the hip, both in the vascular phase and in the delayed, metabolic phase of the scan [90].

Key Learning Points

- Aseptic bone necroses are caused by acute disturbances in blood supply, the exact cause remaining unclear in most cases.
- In the very early phase, the necrotic bone is hypoperfused and hypometabolic, presenting therefore as a “cold spot” on bone scintigraphy.
- Reparative processes start at the periphery of the necrotic bone and begin several days after the insult, persisting for months or years thereafter. In this process, the core of the necrosis remains hypometabolic; this creates the typical scintigraphic pattern of a “cold-in-hot” spot, often termed halo or crescent sign.
- Sympathetic reflex dystrophy is a mainly post-traumatic syndrome, characterized by pain, functional impotence, vasomotor instability, swelling, and skin dystrophy.
- The characteristic scintigraphic pattern of sympathetic reflex dystrophy represented by increased blood flow, increased capillary permeability, and increased bone metabolism in the affected limb as compared to the contralateral.

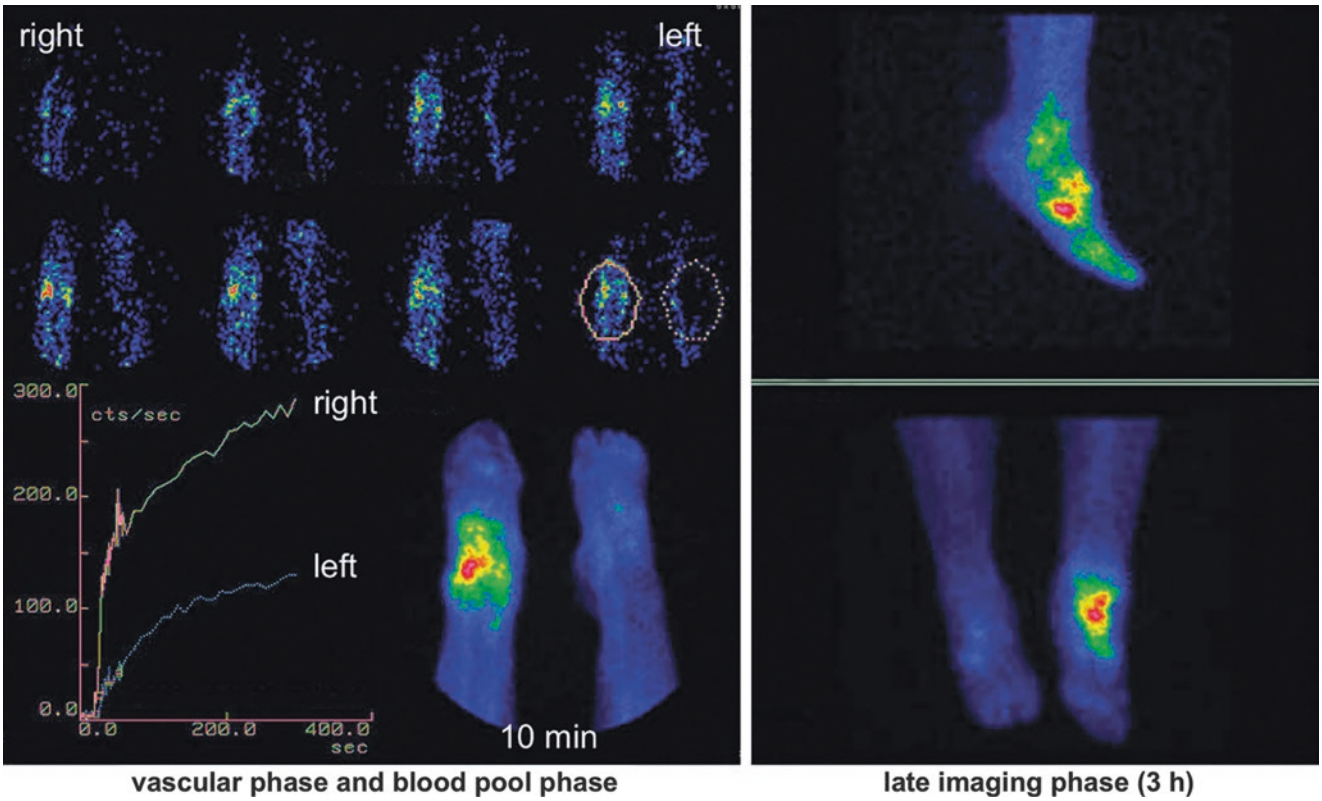

Fig. 24.31 Dynamic three-phase bone scintigraphy in a patient with recent sympathetic reflex dystrophy (also known as Sudeck's syndrome) of the right foot—evaluated in the subacute phase of recovery. The left panel depicts some selected initial frames from the dynamic acquisition, showing enhanced perfusion of right foot versus the left foot (ROIs defined on the two feet are depicted in last frame). The activity/time curves from 0 to 300 s reported in lower left panel show markedly increased blood perfusion of the right foot versus the left foot. The right panel depicts the late scintigraphic image (acquired about 3 h post-administration of the bone-seeking agent), showing markedly increased tracer uptake in right foot, reflecting ongoing remodeling of the involved bones

24.8 Inflammation

Inflammation usually leads to increased bone metabolism. Depending on its floridity, increased uptake can be visible in the first two phases of a three-phase bone scintigraphy. However, these findings are often nonspecific.

Because of its ability to produce whole-body images, bone scintigraphy can be helpful in evaluating the activity of rheumatic diseases. In patients with infection/inflammation, bone scintigraphy provides information on the floridity of individual lesions as well as important diagnostic information on the specific entity—based on the distribution pattern of the segments involved.

24.8.1 Rheumatoid Arthritis

Rheumatoid arthritis is an autoimmune inflammatory polyarthritis that affects about 1% of the Western population and is characterized by lymphocytic infiltration of the synovia that erodes the articular cartilage and the underlying bone. If not treated properly, this process leads to articular deformities with consequent pain and loss of function. The disease typically affects the small joints of the hands and feet symmetrically, with erosive arthritis that sometimes progresses to systemic involvement. The spine is affected late, with predominant cervical involvement of the atlanto-axial joint and of the inter-apophyseal joints.

The disease, easily diagnosed by clinical and laboratory parameters, is characterized by quiescent and exacerbation phases. Therefore, it is very important to define the state of activity of the disease to modulate therapy and prevent progression.

The radiological pattern is well defined, with alterations occurring isolated or in association (according to the stage), representing the key diagnostic signs. In the initial stages, swelling of the soft joints associated with effusion is observed, as well as juxta-articular subchondral corticospinal osteoporosis, symmetric reduction of articular interlines (as a consequence of cartilage damage), and bone erosions. CT imaging does not have specific indications, except in special cases to estimate bone damage of

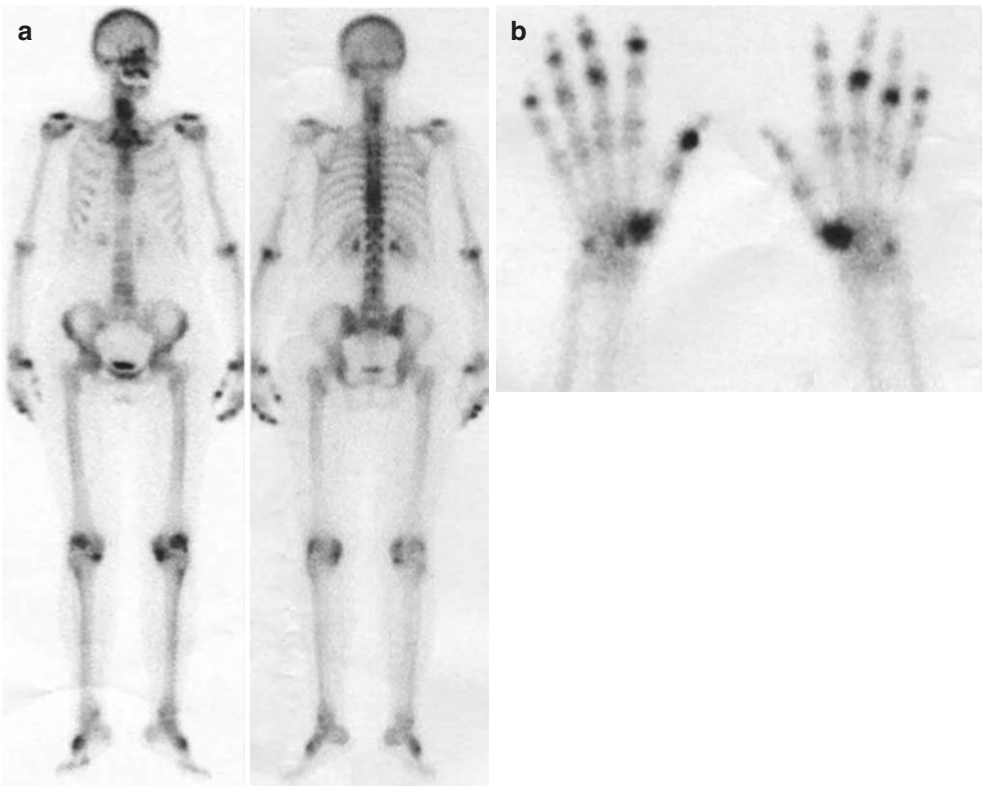

Fig. 24.32 Planar whole-body imaging (**a**) and spot acquisition of the hands (**b**) obtained about 3 h after administration of ^{99m}Tc-MDP in a patient with active rheumatoid arthritis involving both small and large joints (*reproduced with permission from: Versari A. Nuclear medicine imaging in chronic inflammatory diseases. In: Lazzeri E, Signore A, Erba PA, Prandini N, Versari A, D'Errico G, Mariani G, Eds. Radionuclide Imaging of Infection and Inflammation – A Pictorial Case-Based Atlas. Milan: Springer; 2013:289–331*)

large joints. Ultrasound is useful in the evaluation of the initial forms (which still do not involve the bone), thanks to its ability to detect early-stage arthrosynovitis and tenosynovitis; this method constitutes an optimal guide for endoarticular and infiltration procedures and monitoring the response to therapy over time. MR imaging can evaluate joint damage and extraarticular involvement, identifying the initial damage of the bone and bone compartment as capsular ligamentous. This technique also provides prognostic indications on disease severity and response to specific therapies. In addition, it permits to evaluate lesions of the atlanto-axial joint and, in particular, erosions of the epistropheus tooth.

The role of bone scintigraphy (which has been relevant in the past) is currently somewhat limited. However, the exam is still able to provide whole-body imaging and to detect early joint involvement. In particular, the degree of ^{99m}Tc-diphosphonate uptake in the juxta-articular area is proportional to the activity of the disease (Figs. 24.32 and 24.33) and is higher in recent acute lesions. Juxta-articular osteoporosis presents as a more or less intense bipole shaped diffusely increased uptake.

Bone erosion areas appear as areas of intense tracer uptake on a background of diffusely increased uptake. Identification of the involved joints is very early, before it can be detected by traditional radiology. In addition, the total-body imaging mode permits localization of disease in anatomic sites/joints that are difficult to explore with X-rays (sternoclavicular, acromioclavicular, temporomandibular, and atlanto-axial joints). Bone scintigraphy can be used to identify early rheumatoid arthritis, the form of recent onset (<3 months), in which the erosive bone damage has not yet developed and where proper therapy has the maximum probability of healing. At this stage, traditional radiological imaging is negative, and MR imaging is suboptimal. Instead, bone scintigraphy reveals a typical pattern of symmetrically increased tracer uptake in the affected joints.

Another important application concerns the identification of complications that may occur during the disease, such as fractures (e.g., during corticosteroid therapy). The sites most frequently affected are the vertebral bodies, femoral neck, proximal tibial metaphysis, sacrum, and metatarsal bone. In these cases traditional radiology is negative at an early stage and only later can reveal radiotransparency or thickening (linked to trabecular interpenetration) at the fracture fissures.

24.8.2 Seronegative Spondyloarthropathies

Seronegative spondyloarthropathies constitute a heterogeneous group of diseases that include ankylosing spondylitis, psoriatic arthropathy, Reiter's syndrome, and inflammatory bowel disease. They are called seronegative

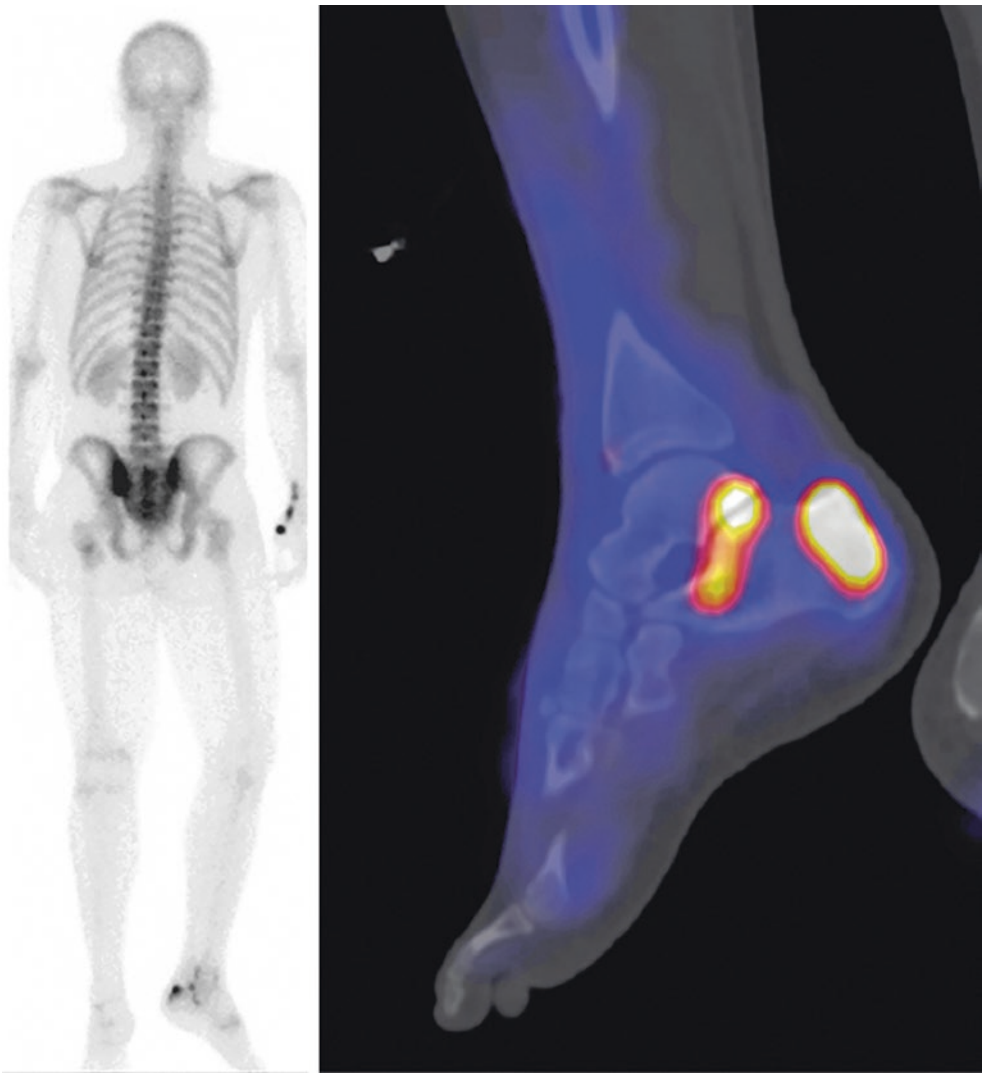

Fig. 24.33 Bone scintigraphy obtained in a 22-year-old man with pain in the right foot and pelvis. Planar anterior whole-body scan (left panel) shows increased tracer uptake in the calcanear region of the left foot. 3D-volume-rendered hybrid image (right panel) demonstrates Achilles enthesitis and calcaneo-talar arthritis. Spot dorsal view of the pelvis (not shown here) discloses predominantly left-sided sacroiliitis. The findings are due to psoriatic arthropathy

as they are not characterized by the production of anti-IgG antibodies as it occurs in rheumatoid arthritis. They are further characterized by HLA-B27 positivity. In these diseases, the spine is often affected, appearing on X-rays with the so-called syndesmophytes that resemble osteophytes but run in vertical direction. Sacroiliitis is also frequently found in these disorders and readily diagnosed by enhanced tracer uptake of these joints on the bone scan. Furthermore, these conditions are characterized by the common feature of enthesitis lesions, i.e., inflammation and degeneration of the insertion site of tendons, bands, and ligaments of the bone. These events create dystrophic ossification. The distribution of these lesions is quite typical, given the main involvement of the axial skeleton and the synchondrosis sacroiliac joints, which are invariably affected, although at different times. Less frequently the small joints of the wrists and of the hands are involved, in an asymmetrical way. The diagnostic workup is based on plain X-ray, although this imaging modality is less satisfactory than in rheumatoid arthritis, as the evolution of this group of pathologies is slower and with a minor inflammatory component. Moreover, axial joints are difficult to evaluate due to the complex three-dimensional geometry and overlapping with others skeletal structures. This diagnostic delay can be significantly reduced thanks to bone scintigraphy that, with a total body scan, is able to show multiple juxta-articular area of increased uptake with the typical spatial distribution in axial and appendicular segments and at the level of the enthesis.

Increased tracer uptake at the sternal, costotransverse, and sacroiliac bones and in the tendon insertion areas (such as posterior calcareous apophysis, large trochanter, ischial tuberosity) is highly characteristic and diagnostic of spondylarthritis.

Currently, MRI is the preferred modality for early assessment of these diseases, providing morphological evidence of degeneration. Bone scintigraphy allows the early diagnosis of sacroiliitis, which presents with atypical clinical signs.

Bone scintigraphy analyzed by calculating the uptake indexes of synchondrosis (on either planar and/or SPECT imaging) has a 100% negative predictive value. In contrast, an abnormal uptake index makes the diagnosis of sacroiliitis very likely already at the initial stage. SPECT increases by 20–50% the number of lesions detected in the lumbosacral region as compared to planar scintigraphy. Nonetheless, diagnostic confirmation of the synchondrosis by CT is necessary, due to the low specificity of scintigraphy since increased tracer uptake might be present also in case of osteoarthritis, functional overload in patients with scoliosis, and dissection of the limbs, and can be physiologically observed in subjects in prepuberal age with cartilages of florid growth. Intensity of uptake of the bone-seeking radiopharmaceutical declines over time, with the evolution of lesions to the chronic phase, in which the tendency to synostosis is manifested.

PET provides an alternative means that can elucidate molecular and cellular changes of the affected joints. Since changes in bone metabolism are present long before clear morphological signs develop, PET with either ^{18}F-fluoride or [^{18}F]FDG can identify and characterize early-stage disease, allowing for more timely treatment and closer monitoring of disease progression [91, 92]. Furthermore, ^{18}F-fluoride has greater accuracy and sensitivity than ^{99m}Tc-MDP scintigraphy and can reliably identify areas with associated inflammation-induced changes and high mechanical stress [93].

Key Learning Points

- Inflammation usually leads to increased bone metabolism.
- Depending on its floridity, increased uptake can be observed in the first two phases of a three-phase bone scintigraphy.
- Bone scintigraphy has a high sensitivity in detecting joint inflammation and may be used to visualize joint involvement in the rheumatic diseases.

24.9 Infection

Osteomyelitis (OM), the condition characterized by microorganisms infecting the bone and/or bone marrow, is not a single condition but rather a spectrum of different diseases that vary based on the host's immunological status, the pre-existing pathology in bone, and the type of the infectious microorganism. All of these factors affect the site of infection onset and the result of diagnostic investigations.

OM can be the result of direct infection after injury or can occur if microorganisms reach the bones via the bloodstream—from other infective foci in the body. Once the bone is infected, the activated leukocytes release enzymes (thereby causing osteolysis), pus can be formed, and the small vessels can be blocked causing sequesters and necrosis; with progressing infection, OM can become chronic, causing sclerosis and deformity. Although any bone may in principle be affected, the maxilla, mandible, long bones, and spine are most often involved, due to their high blood supply [94, 95]. Acute OM most often occurs in children and in adults with compromised host resistance (immunosuppressive therapy, i.v. drug abuse, infectious tooth-root canal teeth, etc.) [94]. The incidence of OM in developed countries is less than 2% of the general population per year (13/100,000 among children) [96]. OM requires prolonged antibiotic therapy (usually 6–12 weeks) and sometimes may require surgical debridement. Severe cases may even lead to amputation of a limb [97].

Imaging has the primary role of achieving a prompt diagnosis of OM and of evaluating its extent. Standard X-rays represent the first imaging modality used when OM is suspected; however, plain radiography may be normal up to 2–4 weeks after onset of OM. Although extremely variable values are reported, sensitivity and specificity of radiography for acute OM are generally considered to be rather low (28–93% and 50–91%, respectively). At later stages, reliable X-ray signs of OM are cortical erosions, bone resorption and/or destruction, and periosteal reaction. Even if rarely (depending on the specific bacteria responsible for the infection), gas can be seen in soft tissues.

Ultrasonography has no major role for evaluating bone involvement when OM is suspected, although it can be used (with power Doppler) to evaluate soft tissues involvement, presence of abscesses or sinus tracts, and periosteal reaction. In addition, ultrasound guidance can aid to guide needle aspiration of fluid or to place a drainage tube.

The diagnostic performance of CT imaging is clearly superior to plain X-rays, particularly by allowing an earlier diagnosis. Its use is, however, limited by the high amount of ionizing radiation and the impossibility of evaluating bone marrow edema.

MRI is superior to other radiological imaging modalities in evaluating patients with suspected OM, because of its ability to simultaneously assess soft tissues and bone/bone marrow structures. Sensitivity and specificity have been reported to reach up to 100% and 95%, respectively. In particular, MRI can be useful for distinguishing viable from necrotic tissues and for detecting the presence of air/gas bubbles within soft tissues. OM is usually characterized by low signal on T1-weighted images and bright signal on T2-weighted images, better appreciated when fat saturation is used. Increased signal on T2-weighted images without signal modification on T1-weighted images usually represents reactive edema of the surrounding soft tissues due to infection rather than bone infection itself. The

use of i.v. gadolinium-based contrast agents in conjunction with fat-saturated T1-weighted sequences increases the diagnostic accuracy. MRI is helpful in detecting septic involvement of the joint space and nearby soft tissues. MRI can also detect joint effusion and synovial thickening; in this instance, the absence of bone marrow changes on T1-weighed images and marrow changes confined to the subchondral bone indicate simple reactive edema rather than bone infection.

24.9.1 Radionuclide Imaging of Infection/Inflammation

Different radiopharmaceuticals can be used in the diagnostic flowchart of infection and/or inflammation of peripheral bones, including ^{99m}Tc-diphosponates, labeled autologous leukocytes, anti-granulocytes antibodies, [^{18}F]FDG, and ^{67}Ga-citrate [98]. A high or low clinical probability of OM dictates the choice of the radiopharmaceutical to be used.

In case of low probability of peripheral OM, dynamic three-phase bone scintigraphy with ^{99m}Tc-diphosponates represents the front-line nuclear medicine procedure of choice. As described above, dynamic bone scintigraphy permits evaluation of blood flow immediately following i.v. bolus injection of the radiopharmaceutical, as well as the presence of local edema (blood pool image at 5 min post-injection) and the level of osteoblastic activity (standard late imaging 3–4 h after tracer injection). A negative scan is sufficient to exclude presence of acute inflammation and/or infection. A positive scan, i.e., increased perfusion in early imaging and delayed increased tracer uptake in the region of suspected infection, suggests the presence of inflammation—but not necessarily infection. In the latter case, scintigraphy with labeled leukocytes will be useful to exclude the presence of infection. The pattern of increased uptake at bone scintigraphy is especially important in patients with chronic osteomyelitis, in whom it is crucial, for proper management, to distinguish between increased uptake caused by underlying infection and increased uptake due to bone remodeling. SPECT/CT acquisition can help define bone involvement (Fig. 24.34). Indeed, in the presence of orthopedic devices, the sensitivity and specificity of planar bone scintigraphy are relatively low (67% and 50%, respectively).

In patients with high clinical probability of OM, scintigraphy with labeled autologous leukocytes (usually ^{99m}Tc-HMPAO-leukocytes or ^{99m}Tc-HMPAO-WBCs—although ^{111}In-oxine-WBCs may be preferred in selected cases) represents the nuclear medicine procedure of choice [99] (see examples in Figs. 24.35–24.38). Nonetheless, in patients with neutropenia (caused by, e.g., chemotherapy or various immunodeficiencies), the use of [^{18}F]FDG PET/CT should be considered. The use of [^{18}F]FDG PET/CT can also be considered in patients with suspected OM in general, particularly if no fractures are present. Scintigraphy with labeled ^{99m}Tc-HMPAO-WBCs represents the gold standard for diagnosing neutrophil-mediated infectious diseases. The scintigraphic images should be acquired 30 min (early images), 3–4 h (delayed images), and 20–24 h (late images) post reinfusion of the labeled leukocytes. Time over which to acquire the images should be adjusted so as to accumulate counts with sufficient statistics according to radionuclide decay in the intervened time.

Scintigraphic images should be evaluated by adopting the correct interpretation criteria to distinguish infective from inflammatory disease of bone. The diagnostic accuracy of ^{99m}Tc-HMPAO-WBC scintigraphy is >95% [100].

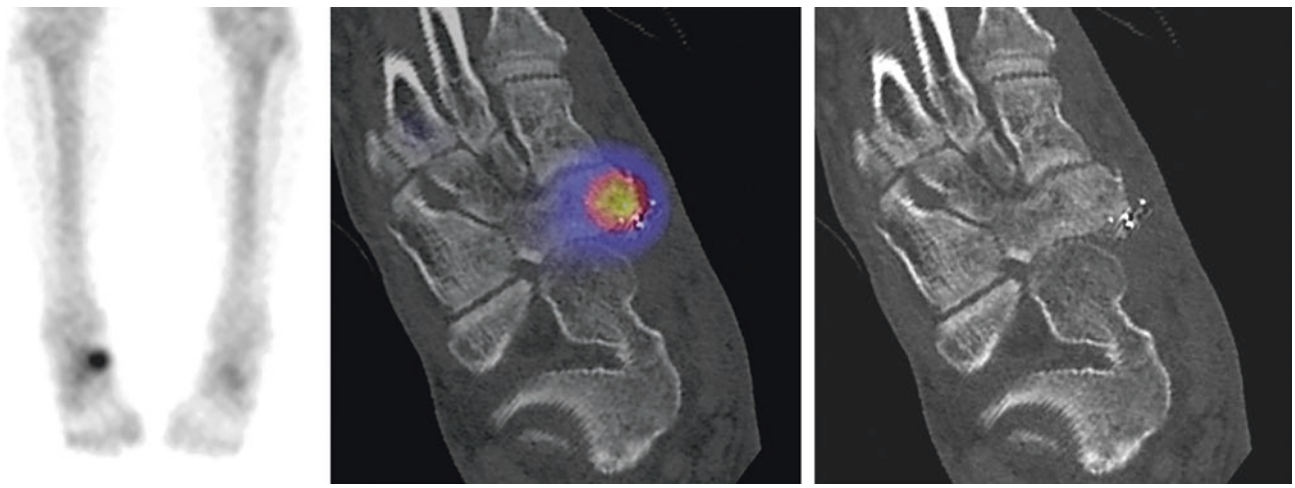

Fig. 24.34 ^{99m}Bone scintigraphy performed in a patient who had suffered a bullet injury to the right foot about 1 year earlier. Planar scan (left panel) discloses a hot spot in the right midfoot. On the fusion SPECT/CT image (center panel), an area of the navicular bone exhibits increased uptake. CT scan (right panel) discloses sclerotic as well as lytic changes in that bone. The findings are due to osteomyelitis. Note metallic remnants of bullet on the CT image

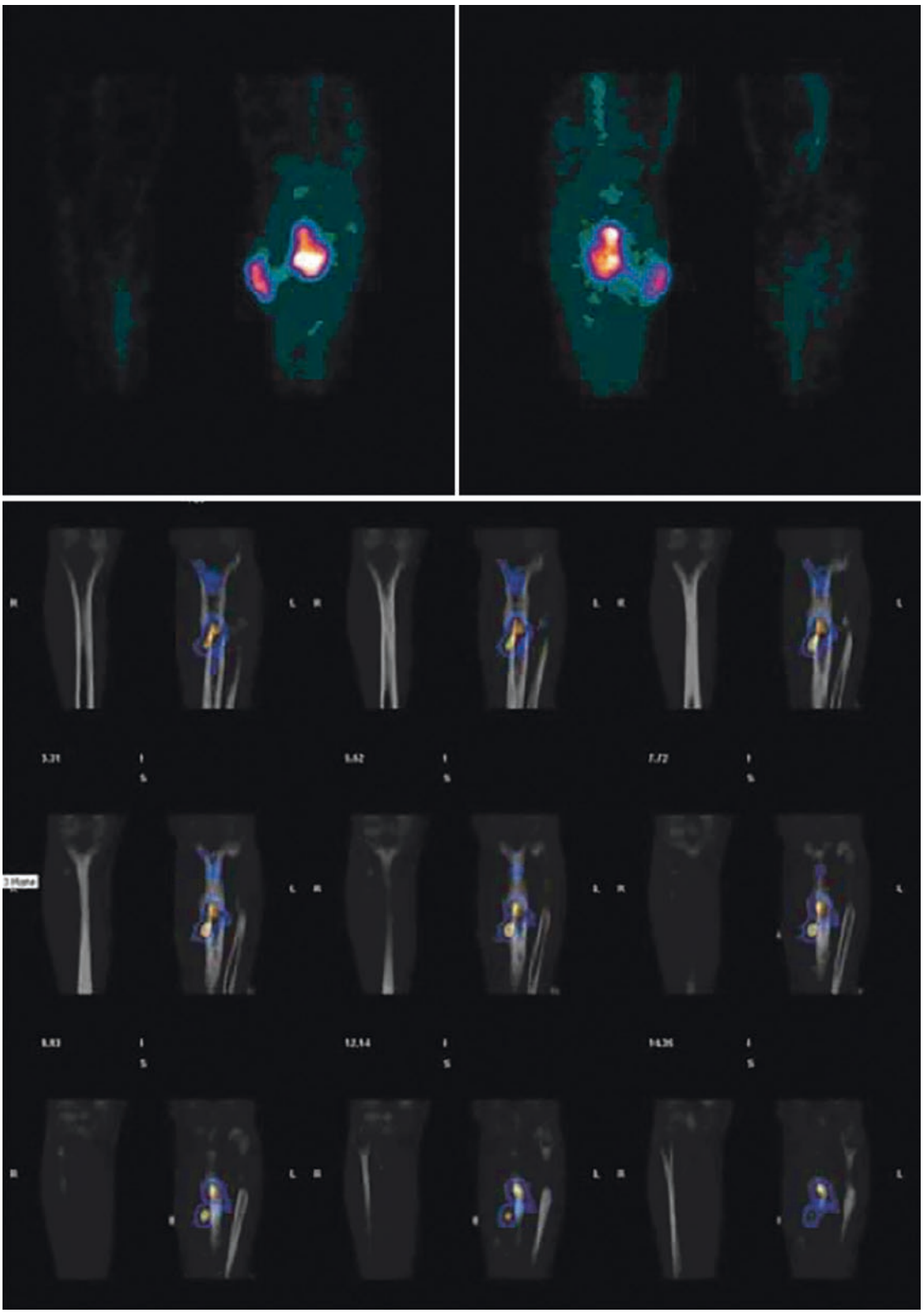

Fig. 24.35 ^{99m}Tc-HMPAO-WBC scintigraphy performed in a patient with osteomyelitis of the left tibia to evaluate the extent of infection. Top panel: the 24-h planar image (anterior and posterior, left and right) shows clear accumulation of labeled leukocytes in the diaphysis of the left tibia. Bottom panel: fused SPECT/CT images allow the precise assessment of the extent of the infection in the bone, extending to adjacent soft tissue (*modified from: Lazzeri E. Nuclear medicine imaging of bone and joint infection. In: Lazzeri E, Signore A, Erba PA, Prandini N, Versari A, D'Errico G, Mariani G, Eds. Radionuclide Imaging of Infection and Inflammation – A Pictorial Case-Based Atlas. Milan: Springer; 2013:39–80*)

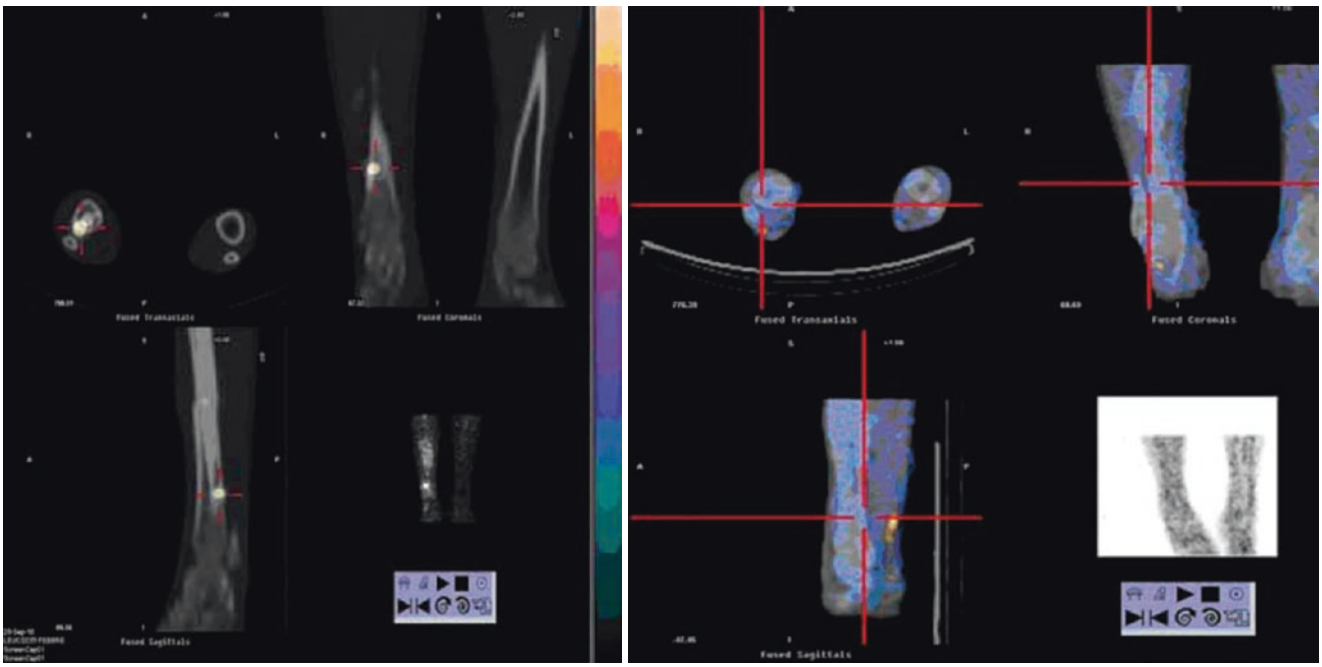

Baseline SPECT/CT Post-therapy SPECT/CT

Fig. 24.36 ^{99m}Tc-HMPAO-WBC scintigraphy performed at two different times in a patient with osteomyelitis of right tibia. Left panel: fused SPECT/CT acquired to confirm the clinical suspicion of osteomyelitis, showing clear accumulation of labeled leukocytes at the site of infection, confined to the bone and bone marrow. Right panel: fused SPECT/CT of the scan acquired after completion of antibiotic therapy, demonstrating disappearance of the abnormal focus of labeled leukocyte accumulation at the site of the prior infection (*modified from: Lazzeri E. Nuclear medicine imaging of bone and joint infection. In: Lazzeri E, Signore A, Erba PA, Prandini N, Versari A, D'Errico G, Mariani G, Eds. Radionuclide Imaging of Infection and Inflammation – A Pictorial Case-Based Atlas. Milan: Springer; 2013:39–80*)

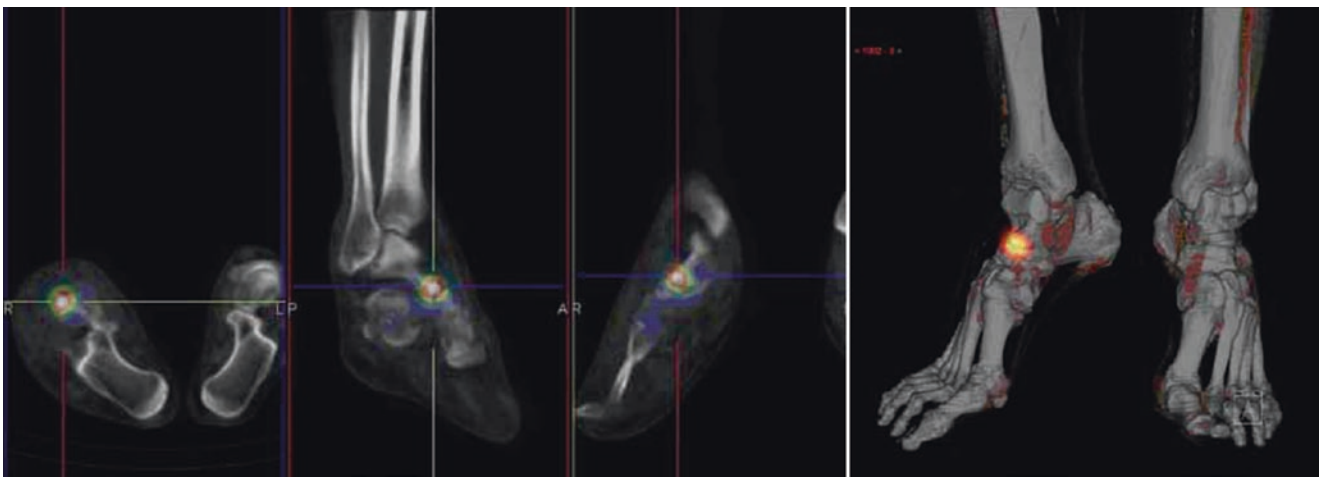

Fig. 24.37 ^{99m}Tc-HMPAO-WBC scintigraphy acquired 4 h post-injection in a patient with suspected infection of the right foot. Left panel: fused SPECT/CT images (transaxial, left; sagittal, middle; coronal, right) of the feet showing focal accumulation of labeled leukocytes in right talonavicular joint, consistent with septic arthritis. Right panel: 3D reconstruction of fused SPECT/CT images of lower limbs clearly depicting exact localization of the infection site (*modified from: Lazzeri E. Nuclear medicine imaging of bone and joint infection. In: Lazzeri E, Signore A, Erba PA, Prandini N, Versari A, D'Errico G, Mariani G, Eds. Radionuclide Imaging of Infection and Inflammation – A Pictorial Case-Based Atlas. Milan: Springer; 2013:39–80*)

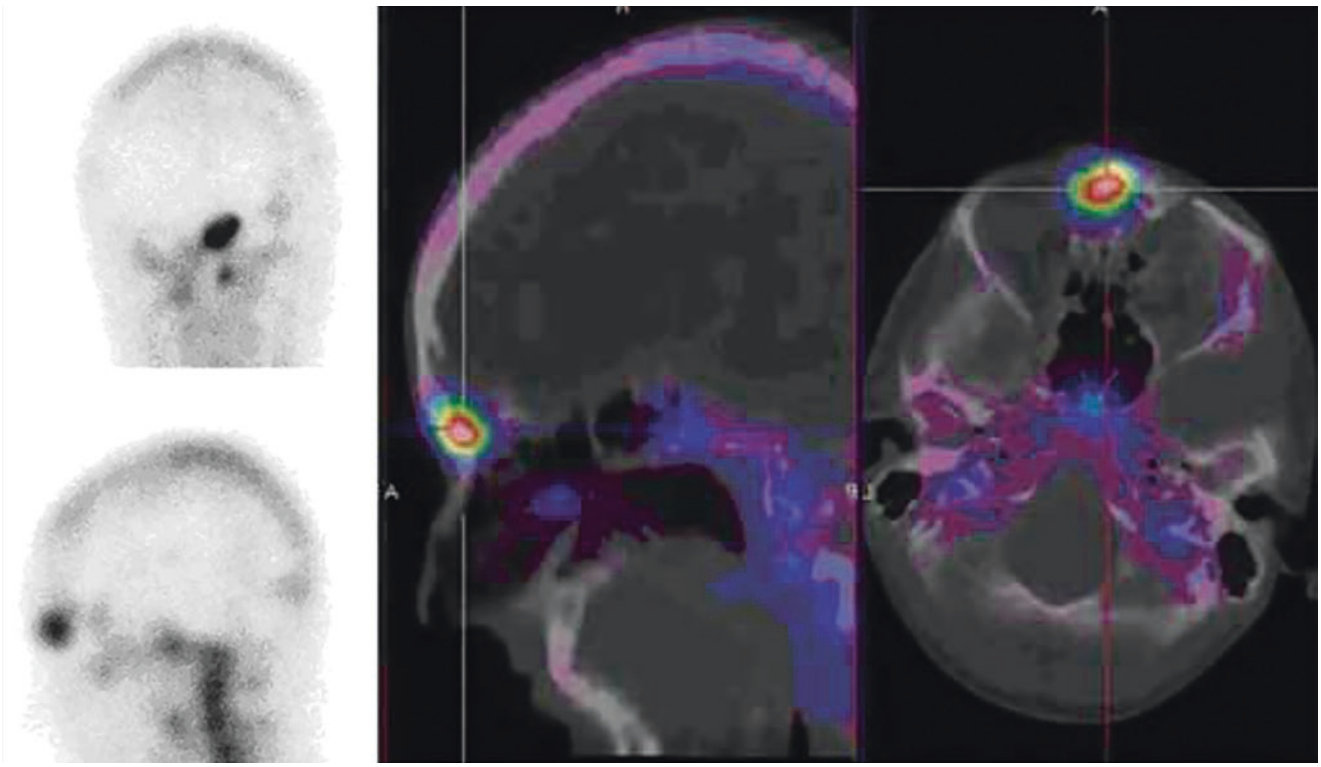

Fig. 24.38 ^{99m}Tc-HMPAO-WBC scintigraphy performed in a patient with suspected frontal osteomyelitis. Left panel: planar anterior (upper) and left lateral (lower) images acquired 4 h post-injection, showing focal accumulation of labeled leukocytes in the frontal region. Right panel: fused SPECT/CT images (sagittal, left; axial, right), showing intense accumulation of labeled leukocytes in frontal sinus (*modified from: Lazzeri E. Nuclear medicine imaging of bone and joint infection. In: Lazzeri E, Signore A, Erba PA, Prandini N, Versari A, D'Errico G, Mariani G, Eds. Radionuclide Imaging of Infection and Inflammation – A Pictorial Case-Based Atlas. Milan: Springer; 2013:39–80*)

SPECT/CT acquisition is crucial especially to evaluate the exact extension of infection, i.e., whether the infection is confined to the bone and bone marrow or it also involves the adjacent soft tissues. This evaluation is the optimal basis for proper clinical management, particularly in some conditions, e.g., the diabetic foot (see Figs. 24.39 and 24.40).

Scintigraphy with combined labeled leukocytes and a bone marrow agent (generally a ^{99m}Tc-colloid) can be used for diagnosing bone infection in case of equivocal findings at leukocyte scintigraphy, particularly in those cases where an expanded bone marrow activity is present. Both labeled leukocytes and radiocolloids accumulate in the healthy bone marrow, while in OM labeled leukocytes accumulate, whereas radiocolloids do not [101] (see Fig. 24.41).

Radiolabeled anti-granulocyte monoclonal antibody preparations can also be used, particularly for imaging chronic OM [102–105]. In this case, images should be acquired at 3–4 h and 20–24 h post i.v. injection of the radiopharmaceutical.

Biodistribution of the leukocytes labeled in vivo with the antibody agents is similar to that of ^{99m}Tc-HMPAO-WBCs, although in general bone marrow accumulation is higher when using radiolabeled anti-granulocyte antibodies than with the in vitro labeled leukocytes. Sensitivity of radiolabeled anti-granulocyte antibody scintigraphy for the diagnosis of peripheral bone OM is about 85%, with 83% specificity [106]. The combined scan with ^{99m}Tc-colloids can also be performed in case of equivocal findings at anti-granulocyte antibody scintigraphy [102].

Scintigraphy with ^{67}Ga-citrate (images being acquired at 6, 24, and 48 h after tracer injection) is an alternative option for radionuclide imaging where scintigraphy with labeled leukocytes or anti-granulocyte antibodies is not available. Nevertheless, this imaging technique has become obsolete in most Nuclear Medicine centres around the world.

PET/CT with [^{18}F]FDG and/or ^{18}F-fluoride are being increasingly used to investigate patients with suspected OM, although neither of these two tracers can be considered infection-specific [107, 108]. [^{18}F]FDG has also been suggested to label autologous leukocytes in vitro [109], although the short physical half-life of ^{18}F (110 min) does not allow satisfactory evaluation of the kinetics of labeled leukocyte accumulation at the site under investigation.

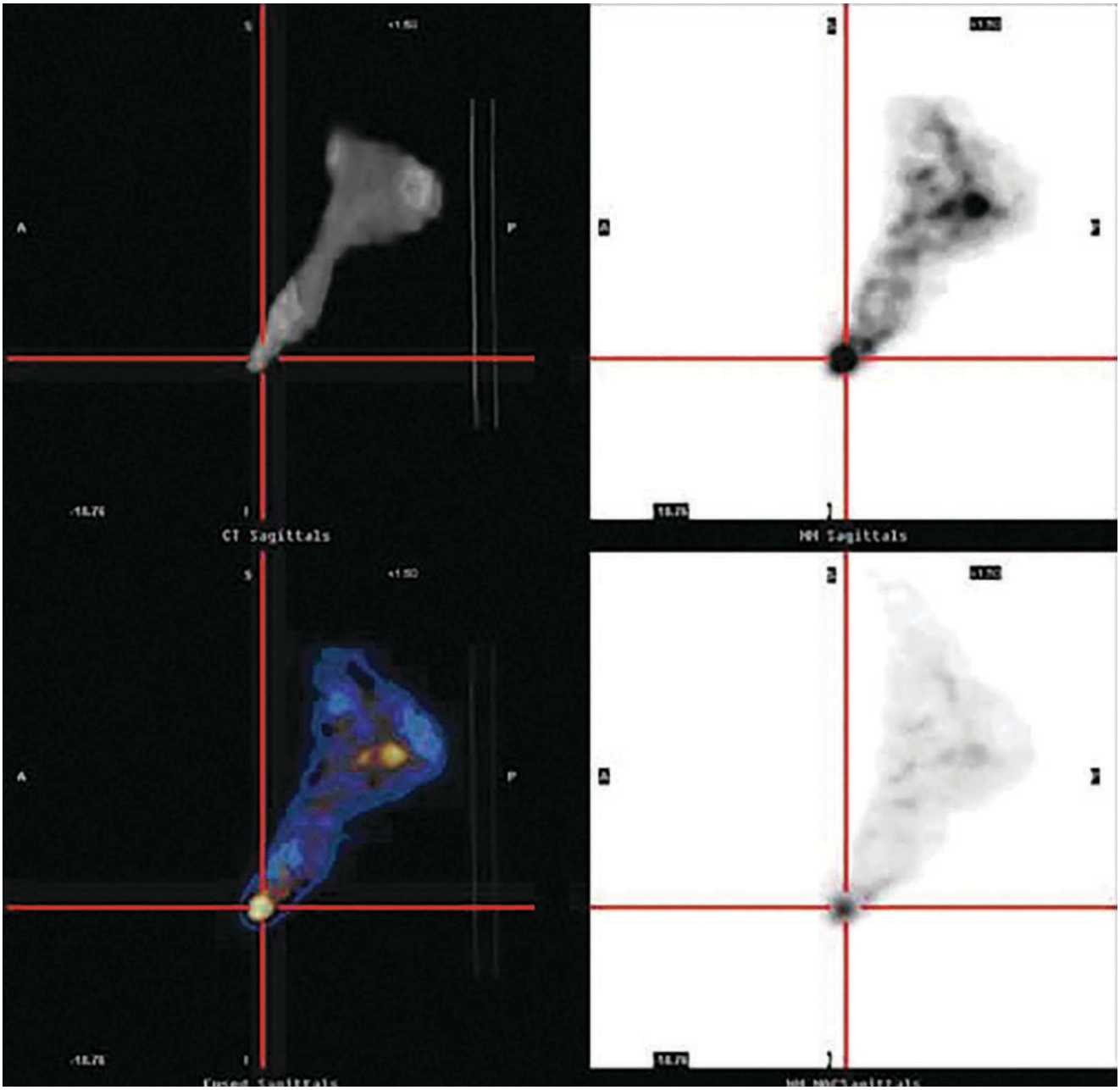

Fig. 24.39 SPECT/CT acquisition during ^{99m}Tc-HMPAO-WBC scintigraphy performed in a diabetic patient with suspected osteomyelitis of the right toe (MIP image in right lower panel). Sagittal section (CT, upper left; SPECT, upper right; fused SPECT/CT, lower left) demonstrating accumulation of labeled leukocytes selectively involving the bone structure of the toe (*reproduced with permission from: Prandini N, Beretta F. Nuclear medicine imaging of diabetic foot. In: Lazzeri E, Signore A, Erba PA, Prandini N, Versari A, D'Errico G, Mariani G, Eds. Radionuclide Imaging of Infection and Inflammation – A Pictorial Case-Based Atlas. Milan: Springer; 2013:253–269*)

The European Association of Nuclear Medicine (EANM), the European Society of Radiology (ESR), the European Bone and Joint Infection Society (EBJIS), and the European Society of Microbiology and Infectious Diseases (ESCMID) have recently released a Consensus Document for the diagnosis of peripheral bone infection in adults (see below under "Further reading"). According to their conclusions concerning radionuclide imaging, the pre-test probability of infection should be considered for choosing between three-phase bone scintigraphy and scintigraphy with labeled autologous WBCs. High probability of infection based on findings such as fracture, recent surgery, osteosynthesis, and highly positive serological tests favours the choice of scintigraphy with labeled autologous

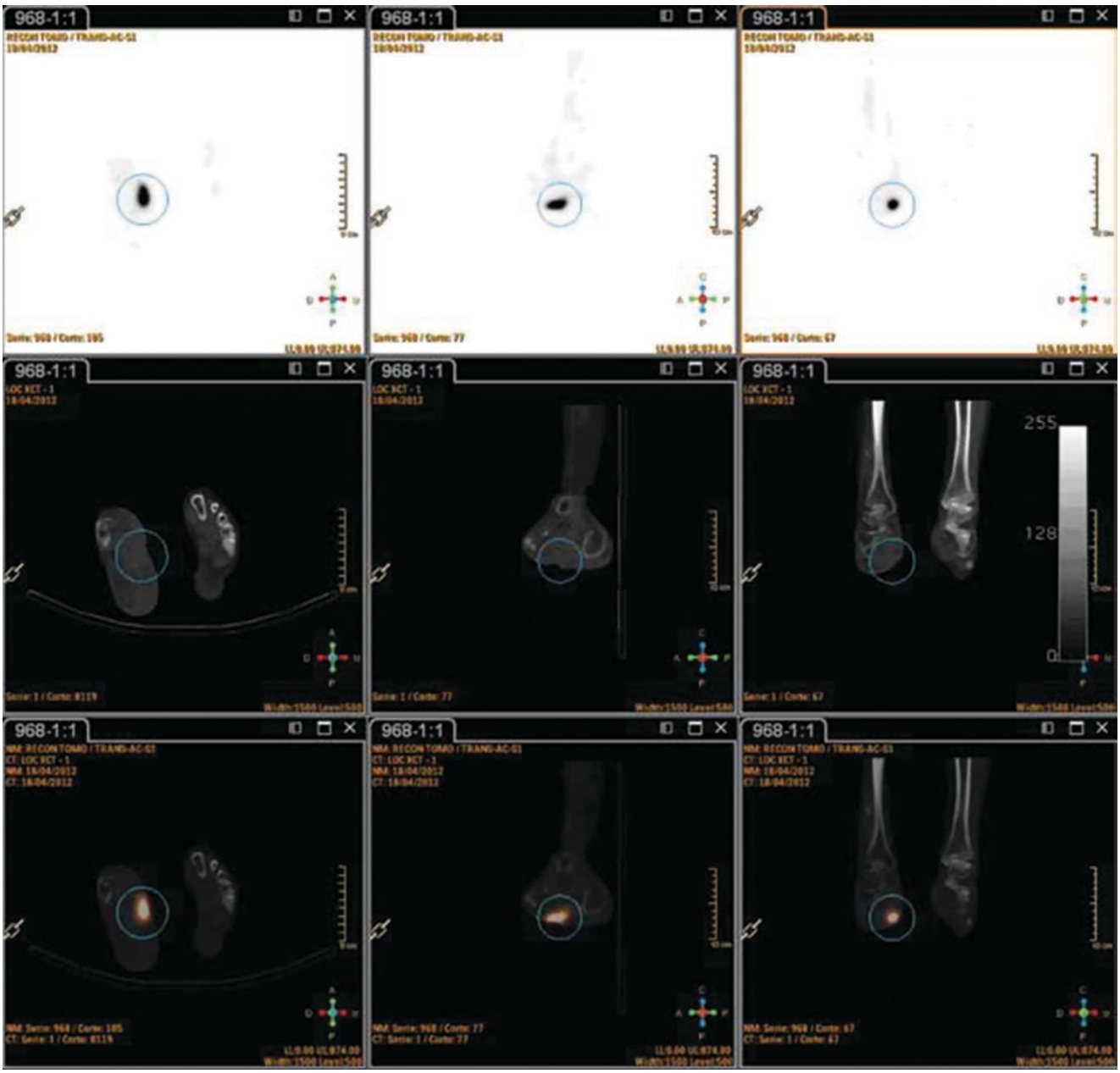

Fig. 24.40 SPECT/CT acquisition during ^{99m}Tc-HMPAO-WBC scintigraphy performed in a diabetic patient with right plantar ulcer and suspected osteomyelitis of the right foot (SPECT, upper row; CT, middle row; fused SPECT/CT, lower row). Sections in different planes demonstrate that the focus of labeled leukocyte accumulation involves only the soft tissues, thus ruling out osteomyelitis (*reproduced with permission from: Prandini N, Beretta F. Nuclear medicine imaging of diabetic foot. In: Lazzeri E, Signore A, Erba PA, Prandini N, Versari A, D'Errico G, Mariani G, Eds. Radionuclide Imaging of Infection and Inflammation – A Pictorial Case-Based Atlas. Milan: Springer; 2013:253–269*)

WBCs. Because of its high sensitivity and negative predictive value, three-phase bone scintigraphy is recommended as the first imaging modality of choice in patients with low pre-test probability of infection; in case of a positive three-phase bone scan, the next radionuclide imaging modality is either scintigraphy with autologous leukocytes or with anti-granulocyte antibodies (with both planar and SPECT/CT acquisitions). When autologous leukocyte scintigraphy (or anti-granulocyte antibody scintigraphy) turns out to be negative, [^{18}F]FDG PET/CT is generally the conclusive test for infection versus non infection. On the other hand, PET/CT with [^{18}F]FDG is recommended as the first imaging modality of choice especially in patients with high suspicion of hematogenous spread of the infection.

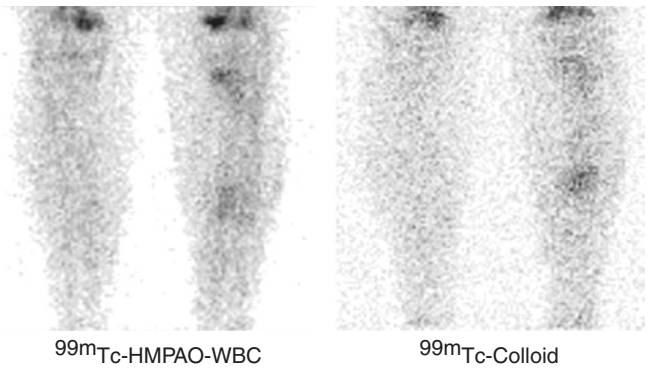

Fig. 24.41 Evaluation of a patient with suspected osteomyelitis of left tibia, to rule out the presence of acute infection. Left panel: ^{99m}Tc-HMPAO-WBC scintigraphy (planar image), showing mild accumulation of labeled leukocytes in proximal and middle portion of diaphysis of left tibia, suggesting the presence of inflammation without infection. Right panel: scintigraphy with ^{99m}Tc-nanocolloidal albumin, showing uptake at the same site of ^{99m}Tc-HMPAO-WBC accumulation. The overall scintigraphic pattern confirms the presence of normally functioning bone marrow, thus ruling out the presence of acute infection (*modified from: Lazzeri E. Nuclear medicine imaging of bone and joint infection. In: Lazzeri E, Signore A, Erba PA, Prandini N, Versari A, D'Errico G, Mariani G, Eds. Radionuclide Imaging of Infection and Inflammation – A Pictorial Case-Based Atlas. Milan: Springer; 2013:39–80*)

24.9.2 Spondylodiscitis

Spinal infections include vertebral osteomyelitis (infection of the vertebral body), discitis (infection of the intervertebral disk), and spondylodiscitis (SD) (infection of two adjacent vertebral bodies and their intervertebral disk) [110]. Incidence of SD in developed countries ranges from 4 to 24 per million per year [111], men being affected more frequently than women and the most frequently affected age being between 50 and 70 years. The most frequent site of vertebral infection is the lumbar spine (45%) followed by the dorsal (35%) and the cervical tract (20%) [111].

SD can be primary, i.e., when pathogens infect the spine by hematogenous spread. *Staphylococcus aureus* is the most frequently isolated pathogen (55–80% of cases), while 7–33% of pyogenic SDs are caused by *Enterobacteriaceae*, mostly *Escherichia coli* followed by *Proteus* spp. and *Klebsiella* spp. Coagulase-negative staphylococci (CoNS) account for 5–16% of cases, while brucellosis, a common zoonosis in endemic areas (Mediterranean basin, Latin America, the Middle East, parts of Africa, and Western Asia), can account for 21–48% of spinal infections. In developed countries, between 9 and 46% of SDs are due to tuberculosis (TB) infection.

Secondary SD is due to direct contamination of microorganisms during surgical or interventional procedures. The incidence of secondary SD varies according to the type of surgical procedure, ranging from 1% to 7% of patients undergoing surgery. Secondary SD is mainly caused by *Staphylococcus aureus*, isolated in almost 50% of cases and CoNS. Gram-negative bacteria may also cause postsurgical SD, the most frequently isolated Gram-negatives including *Escherichia coli*, *Pseudomonas aeruginosa*, *Klebsiella pneumoniae*, *Enterobacter cloacae*, *Bacteroides*, and *Proteus* species.

The diagnosis of SD may be challenging due to the nonspecific clinical presentation and laboratory findings and to the need of performing different diagnostic tests including serologic, radiographic, and microbiological examinations. Early diagnosis of SD, with the identification of the etiology and description of location, extent, and severity of the infective process, is crucial to choose appropriate management.

Radiologic imaging is important to define the correct diagnosis as early as possible, to assist in the percutaneous biopsy (if needed), for follow-up of the disease, and to evaluate possible complications. Plain X-ray imaging has low sensitivity and specificity, even if it is usually the first imaging modality requested when SD is suspected. The detection of signs and abnormalities depends on their entity and can be seen only when bone destruction exceeds 30–50% of cortical bone. Erosion of the anterior corner of the vertebral endplate, progressive loss of disk height, narrowing of inter-vertebral space, and osteolysis with further destruction of the subchondral plate can be seen in case of advanced disease—associated with soft tissue swelling and pre- or paravertebral soft tissue densities, occasionally with fluid level. Erosions can involve the entire vertebral endplate and signs of new bone formation (including peripheral sclerosis, osteophytosis, and a buildup of osteolytic lesions) can coexist. Reactive sclerosis may sometimes produce an "ivory" sign as the only evident change.

MRI has high diagnostic sensitivity, specificity, and accuracy (reported as 96%, 92%, and 94%, respectively) for SD due to its high contrast resolution, direct multiplanar imaging capability, and high sensitivity for soft tissue and bone marrow abnormalities. MRI is generally positive in the early stages (first 2 weeks) after the onset of infection in >50% of cases, when other radiologic imaging modalities are still normal; these features currently make MR the gold standard for imaging of spinal infections.

The MRI examination should include the following sequences:

- STIR or fat saturation T2-weigthed, which detect inflammatory edema with high sensitivity
- T1-weighted SE fat saturation pre- and post-administration of i.v. contrast media, for evaluation of morphology and vascularization of lesions.

Usually vertebral infection and inflammation cause marrow edema, with ensuing signal reduction in T1-weighted sequences and increase in T2-weighted sequences, associated with contrast enhancement in T1-weighted sequences after i.v. contrast. When erosion of the vertebral endplates occurs, the hypointense band of

cortical bone appears thinned or even absent. The MRI pattern referred to as "Modic change" corresponds to abnormal bone signals under the vertebral endplate suggesting lesions of vertebral endplate as well as of the adjacent bone marrow in the vertebral body. Loss of the internuclear cleft in T2-weighted sequences is an early sign of discitis. If the infection involves all the vertebral body and also the intervertebral disk and the nearby soft tissues, T2-weighted sequences show a hyperintense signal and a moderate and adjacent tissue enhancement in the T1-weighted sequences that can be seen post i.v. contrast injection. Abscesses, seen as fluid collection, show heterogeneous signal in T1-weighted sequences with ring-enhancing thickened walls. Granulation tissue causes diffuse enhancement throughout the mass.

The main limitations of MRI are related to overestimation of the extent of infection (as some of the signal changes are reactive) and to false-positive results (e.g., in presence of severe degenerative disk disease and postsurgery—due to the increased T2-weighted signal and contrast enhancement at the surgery site). Since some MR changes may persist or even worsen during treatment (even with clinical improvement and negative lab tests), they may lead to unnecessary surgery.

CT is readily available, easy to perform, and faster than MRI and represents the best modality to detect bony abnormalities (such as minimal erosion of the endplates—before they become visible on plain X-ray) and small vertebral foci of infection as well as sequestration or pathological calcification suggesting TB. In spine infection CT shows loss of bone architecture with areas of transparency and soft tissue replacement, endplate erosion, and collapse of the disk space with abscess formation.

Furthermore, CT is currently used for guiding percutaneous needle biopsy and percutaneous drainage of abscesses. Image quality may suffer from artifacts related to implants. Image-guided biopsy of the infected tissue is indeed important for diagnosing SD. Histopathological and microbiological examinations of biopsy specimens can establish definite diagnosis of SD and identify the causative pathogen. A CT or fluoroscopy-guided biopsy is the first invasive diagnostic step since it identifies the bacterial agent in up to 91% of patients. Biopsy is the principal investigation in patients with postoperative spondylodiscitis since in these patients, blood cultures are frequently negative.

24.9.2.1 Radionuclide Imaging of Spondylodiscitis

Scintigraphy with ^{99m}Tc-HMPAO-leukocytes has virtually no role in the diagnosis of spondylodiscitis. In fact, both the vertebral bodies and the intervertebral disks are spaces enclosed in a virtually non-expandable structure; therefore, all pathological events inducing local edema increase the interstitial pressure and thus prevent efficient accumulation of labeled leukocytes at the site of infection/inflammation within the useful imaging time window. Based on the above considerations, it follows that the available radiopharmaceuticals to diagnose spine infection are: ^{99m}Tc-diphosphonates (^{99m}Tc-MDP/HDP), ^{67}Ga-citrate, and [^{18}F]FDG. Each of them has *pros* and *cons*.

Scintigraphy with ^{99m}Tc-MDP/HDP and/or ^{67}Ga-citrate

Bone scintigraphy with ^{99m}Tc-MDP/HDP has a sensitivity of 81.4% and 40.7% specificity for diagnosing spine infection (see example in Fig. 24.27). This imaging procedure has the advantages of low cost, low radiation burden, and single-day imaging procedure, whereas low specificity is its main limitation [112].

^{67}Ga-citrate scintigraphy has a sensitivity of 86.3% and 35.8% specificity. ^{99m}Tc-diphosphonate bone scintigraphy combined with ^{67}Ga-citrate can be used for increased diagnostic accuracy, particularly in case of postsurgical infections or to complement equivocal MRI findings in primary infections [113–115].

Although ^{67}Ga-citrate and ^{99m}Tc-MDP are widely available, the ^{67}Ga-citrate scan is time-consuming (with image acquisitions up to 48–72 h post-injection) and results in a relatively high radiation burden to patients.

If the uptake of ^{67}Ga-citrate is higher than ^{99m}Tc-MDP/HDP uptake, the vertebral lesion is most likely due to infection, whereas degenerative changes are most likely when ^{99m}Tc-diphosphonate uptake is higher [113]. The overall accuracy of combined ^{99m}Tc-MDP/^{67}Ga-citrate imaging ranges between 65% and 80% [113, 114]. Nevertheless, it should be considered that, except circumstances where the use of other radionuclide imaging procedures is problematic, the use of ^{67}Ga-citrate has markedly declined both because of a relatively high radiation dose and because of poor quality images, linked to the suboptimal energies of the gamma emission generated by ^{67}Ga.

PET/CT with [^{18}F]FDG

The role of PET (currently used as hybrid PET/CT) with [^{18}F]FDG for diagnosing spinal infection has been extensively investigated. The degree of [^{18}F]FDG uptake is related to the metabolic rate, therefore to the expression of glucose transporters on the cell membrane [116]. Similarly as in tumor cells, in activated inflammatory cells (such as neutrophils, lymphocytes, monocytes, and macrophages), both the number of glucose transporters and affinity of these transporters for glucose (or its analog—deoxyglucose) are enhanced [117–119]. These features explain the very high sensitivity of PET (especially PET/CT) with [^{18}F]FDG in diagnosing spine infections—which is however associated with relatively low specificity (see Fig. 24.42).

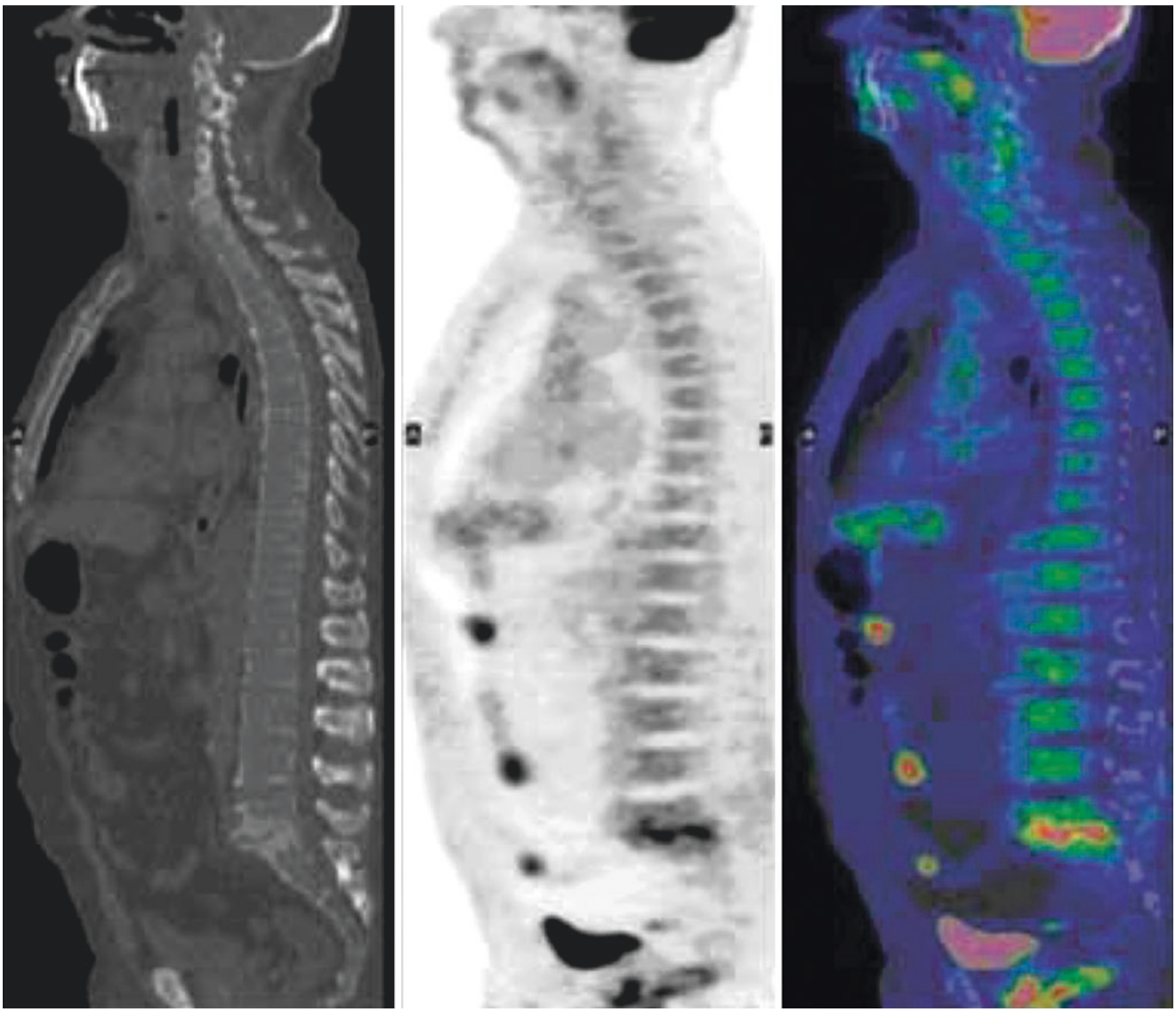

Fig. 24.42 PET/CT with [^{18}F]FDG in a patient with suspected lumbosacral spondylodiscitis. The sagittal sections (CT, left; PET, middle; fused PET/CT, right) of the lumbosacral skeleton show increased uptake of [^{18}F]FDG (SUV_{max} 3.6) at the vertebral body of L5 with involvement of the disk interposed between L5 and S1, confirming the clinical suspicion of spondylodiscitis (*modified from: Lazzeri E. Nuclear medicine imaging of bone and joint infection. In: Lazzeri E, Signore A, Erba PA, Prandini N, Versari A, D'Errico G, Mariani G, Eds. Radionuclide Imaging of Infection and Inflammation – A Pictorial Case-Based Atlas. Milan: Springer; 2013:39–80*)

Ohtori et al. showed that a definitive diagnosis of spine infection was achieved more often when [^{18}F]FDG was utilized specifically in patients with spinal infections presenting as Modic type 1 signal on MRI—a condition where distinguishing between common Modic changes and spine infection is challenging [120]. [^{18}F]FDG PET is useful also in the evaluation of patients with metallic implants, since this imaging modality is not affected by artifacts.

[^{18}F]FDG PET/CT imaging has an important role especially for the evaluation of response to treatment in patients with spine infections; it is therefore recommended to acquire a scan in baseline conditions as the reference for a repeat scan following (medical) therapy to assess disease activity [121–123]. After reporting their experience demonstrating 86% sensitivity and 95% specificity for assessing disease activity, Hungenbach et al. have proposed some interpretation criteria based on the [^{18}F]FDG uptake patterns, classified into different scores (from 0 to 4) related to different states of spine infection [124]:

- Score 0: normal findings and physiological [^{18}F]FDG distribution (consistent with no infection)
- Score 1: slightly enhanced uptake in the inter- or paravertebral region (consistent with no infection)
- Score 2: clearly enhanced uptake with a linear or disciform pattern in the intervertebral space (consistent with discitis)

- Score 3: clearly enhanced uptake with a linear or disciform pattern in the intervertebral space and involvement of ground or cover plate or both plates of the adjacent vertebrae (consistent with spondylodiscitis)
- Score 4: clearly enhanced uptake with a linear or disciform pattern in the intervertebral space and involvement of ground or cover plate or both plates of the adjacent vertebrae + surrounding soft tissue abscess (consistent with spondylodiscitis)

Alternative interpretation criteria proposed by Riccio et al. state that [^{18}F]FDG uptake in bone or soft tissue is consistent with active infection, while uptake confined to the edges of a destroyed disk, after antibiotic therapy of pyogenic spine infection, must not be considered indicative of persistent infection and likely represents mechanically induced inflammation. On the other hand, semiquantitative analysis could not reliably distinguish patients with active infection from those without active infection and those who had had a successful response to therapy [125]. Whereas, according to some authors, SUV_{max} reflects the activity of infectious spondylitis, although this conclusion is based on limited observations [126].

The findings at [^{18}F]FDG PET/CT have been reported to complement the MRI findings for distinguishing pyogenic from tuberculous spondylitis [126]. It should also be noted that the combination of MRI with [^{18}F]FDG PET/CT results in detection of spinal infection in 100% of patients [127–129].

On the other hand, it has consistently been shown that [^{18}F]FDG PET/CT is superior to ^{67}Ga-citrate scintigraphy for detecting spinal infection and paraspinal soft tissue infection and could be used in selected cases as an alternative to MRI.

In summary, the advantages of [^{18}F]FDG PET/CT are a very high negative predictive value, high-quality imaging, and short time for completing the acquisition. Limitations of [^{18}F]FDG PET/CT are its relatively low specificity (ranging from 35.8% to 87.9%) and its relative inability to distinguish infection from neoplastic lesions or pronounced degenerative vertebral disease [130].

24.9.3 Infection/Inflammation of Prosthetic Joint Implants

Arthroplasty has revolutionized treatment of patients with advanced degenerative joint disease, especially of the hip and knee. The introduction of modular prostheses made of metal (cobalt, chrome, or titanium), plastic, or ceramic has made it possible to adapt the prosthetic implant to the individual patient's needs. These components can be assembled on bone tissue with different techniques: cemented prostheses are fixed with polymethylmethacrylate, while non-cemented prostheses use a porous surface between the prosthesis itself and adjacent bone tissue. The prosthesis can be also fixed by applying a hydroxyapatite-based compound to the prosthetic surface, on which new bone tissue is formed. Acetabular components can be placed under pressure within the acetabulum and, if necessary, further assured with orthopedic nails.

Clinical outcomes of these procedures in terms of pain relief and restoration of function are usually very satisfactory. However, complications may arise due to detachments, dislocations, fractures, infections, and/or heterotopic ossification. These conditions must be diagnosed and adequately treated. About 10 years post-implant, 50% of the prostheses show clear radiographic signs of mobilization, and about 30% must be reimplanted/replaced. Aseptic mobilization is often due to an immune/inflammatory reaction that causes the formation of a pseudomembrane similar to synovium (constituted mainly by giant cells), which is located between the prosthesis and bone; lymphocytes and plasma cells are present in 25% of cases and neutrophils in <10%. Material (debris) produced from fragmentation of the prosthetic components attracts and activates tissue phagocytes which, however, cannot destroy with their lithic enzymes this material; this process results in the secretion of inflammatory cytokines and proteolytic enzymes (which damage the surrounding bone tissue and cartilage), in turn resulting in the activation of immune cells, osteolysis, and mobilization of the prosthesis.

The incidence of prosthetic joint infection (PJI) of primary implants is approximately 2%, increasing to 20% after revision surgery [131–134]. Once microorganisms reach the prosthetic region, they can attach to the biomaterials and within 2 days form a biofilm on the implants, which makes them hard to detect and to eradicate. Furthermore, osteolysis induced by the inflammatory cells results in loosening of the prosthesis, which can become painful. Due to the often low-grade nature of the infection, it is very difficult to establish whether there is a septic or aseptic loosening [133, 134].

The onset of symptoms after implantation can be classified as early, delayed, or late infection. Early infection (<3 months) is predominantly acquired during implant surgery (or over the following 2–4 days) and is caused by highly virulent organisms (e.g., *Staphylococcus aureus* or Gram-negative bacilli). Delayed or low-grade infection is predominantly acquired during implant surgery and caused by less virulent organisms (3–24 months) (e.g., coagulase-negative staphylococci or *Propionibacterium acnes*). Late infection (>24 months) is predominantly caused by hematogenous seeding from remote infections [135]. The inflammatory reaction induced by infection is similar to aseptic mobilization, except for a fundamental feature: neutrophils are invariably present. The main inflammation indices (ESR and PCR) can be altered both during aseptic mobilization and during infection.

Management of patients with aseptic loosening differs from that of patients with prosthetic infection. In fact, while in

case of aseptic loosening direct replacement of the prosthesis with a new one might be directly performed, in case of infection dual-time surgery is required, consisting of removal of the prosthesis followed by antibiotic therapy and/or antibiotic-loaded spacer and subsequent implant of new prosthesis.

24.9.4 Non-radionuclide Imaging for Infection/Inflammation of Prosthetic Joint Implants

X-ray constitutes the first-line diagnostic approach in case of suspected PJI, even if it is well known that plain radiography may be negative up to 4 weeks after onset of infection and does not allow early diagnosis. At later stages, X-ray may show loosening signs, such as the presence of a radiolucent area around the prosthesis. Other signs such as erosions, periosteal reaction, and soft tissue swelling can be seen in case of PJI. One advantage of plain X-ray is that image quality is not affected by the presence of metallic implants.

Ultrasonography can be effectively used to detect the presence of periprosthetic fluid collections and to track the presence of sinus tracts within soft tissues. The main advantages of ultrasonography are its wide availability, low cost, and the possibility of being performed at bedside. It can also be repeated whenever needed. Furthermore, it can be used to guide interventional procedures, such as needle aspiration.

CT imaging can be used to evaluate bone abnormalities and loosening of the prosthesis, although the presence of implant-related striking artifacts constitutes an important limitation. Nonetheless, recent technical developments, such as specific algorithms for artifact reduction, partly overcome these limitations. Other limitations of CT imaging are represented by suboptimal evaluation of periprosthetic soft tissues and by the relatively high ionizing radiation burden to patients.

Prosthetic implants do not constitute an absolute contraindication to MRI. In fact, specific MR sequences (metal artifact reduction sequences, *MARS*) have been developed to overcome these problems. Among the various sequences, turbo spin-echo and short tau inversion recovery sequences appear to be affected by minor artifacts than gradient-echo-based sequences. MRI is excellent for evaluating involvement of the skin, subcutaneous or deep soft tissues adjacent to the prosthesis, as well as the presence of a fistula and soft tissue edema. MRI is also helpful in characterizing the nature of a collection as serous, purulent, or hematic.

24.9.5 Radionuclide Imaging for Infection/Inflammation of Prosthetic Joint Implants

In patients with low probability of PJI, the radionuclide imaging procedure of choice is a dynamic three-phase bone scintigraphy with ^{99m}Tc-diphosphonates. The specificity of bone scintigraphy in hip prosthesis infection ranges from 50% to 70%, and it is related to the time elapsed after the implant. The ^{99m}Tc-diphosphonate late phase findings alone cannot distinguish between aseptic loosening and infection. In fact, periprosthetic increased tracer uptake reflects increased bone turnover, which can occur in both conditions—infection and inflammation. When bone scintigraphy fails to visualize enhanced periprosthetic bone metabolism, it is very unlikely that the patient's symptoms are caused by the implant (i.e., the scan has a very high negative predictive value). In these cases, referred pain from other regions of the body might be the cause of the problem, which in some cases can be diagnosed at bone scintigraphy (e.g., degenerative disease of the spine leading to pain projecting to the hip in patients).

When increased uptake of ^{99m}Tc-diphosphonates is observed near or around the prosthetic implant, differential diagnoses must be considered. In particular, physiologic bone remodeling may occur up to at least 1 year after implantation; this implies that bone scintigraphy performed within such time window has a high yield of false-positive results, therefore resulting in quite difficult interpretation. Loosening of the metallic implants is scintigraphically characterized by increased uptake at the bone/metal interface. Inflammation (not necessarily caused by infection) is defined as very likely when increased tracer accumulation is observed in all three phases of a three-phase bone scintigraphy.

In addition, the presence and pattern of uptake around a prosthetic implant vary depending on the time elapsed since implantation surgery. In the case of cemented implants, most asymptomatic patients have a normal bone scan pattern 1 year after the implant. However, up to 10% of patients shows persistently increased uptake even in the absence of complications. For non-cemented prostheses, nonspecific increased uptake persists for even longer periods. In patients with knee prosthesis, increased tracer uptake may be observed for more than 1 year after the implant (in 63% of cases for the femoral component, in 89% for the tibial component).

Most of the prosthetic infections occur within the first year after the implant (i.e., when bone scintigraphy is mostly affected by the limitations described above), only the presence of a normal pattern can provide useful information (i.e., to exclude the presence of infection and/or inflammation). It follows that the overall accuracy of bone scintigraphy for diagnosing prosthetic joint infection is suboptimal—at 50–70%. In particular, while a negative three-phase bone scintigraphy can reasonably rule out prosthetic infection, a positive bone scintigraphy is generally not sufficiently specific to diagnose prosthetic infection. In this case scintigraphy with radiolabeled autologous leukocytes is required to distinguish between aseptic prosthetic loosening and PJI (see Figs. 24.43 and 24.44).

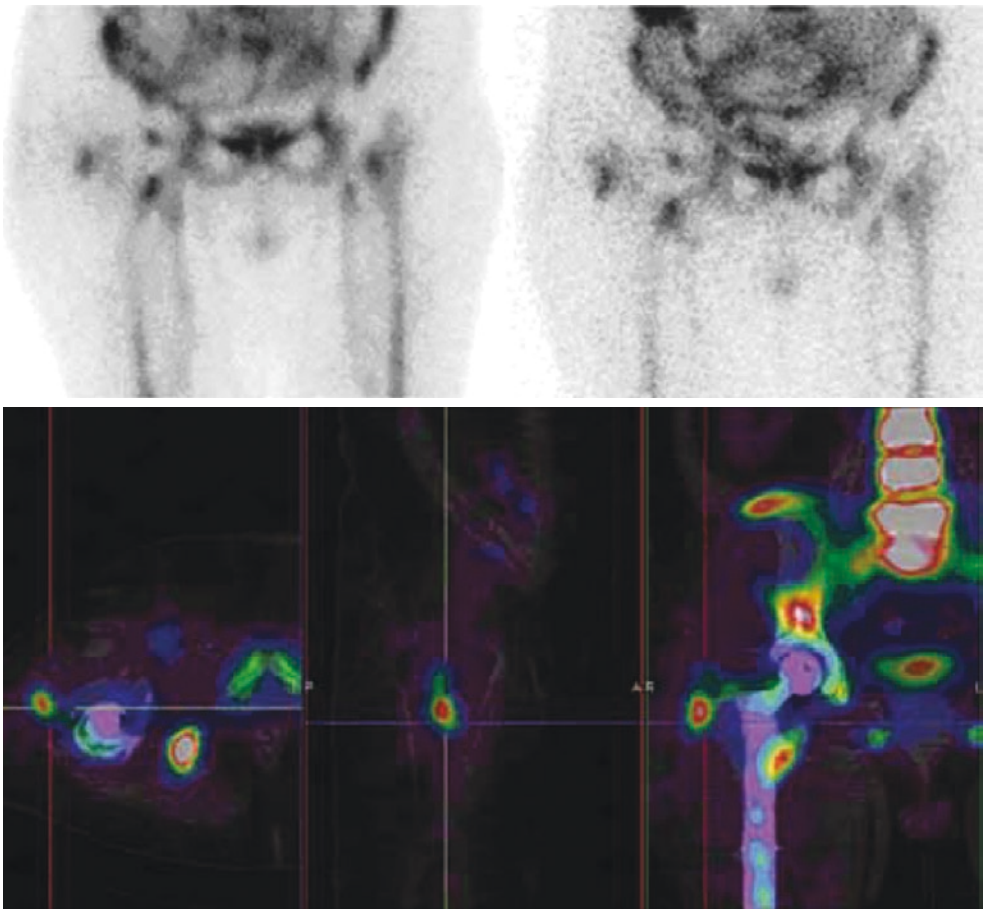

Fig. 24.43 ^{99m}Tc-HMPAO-WBC scintigraphy performed in a patient with bilateral total hip prosthesis and persisting pain associated with functional impairment of right hip. The planar images acquired at 3 and 20 h post-injection (upper panel) show accumulation of labeled leukocytes in soft tissues around the right hip. The fused SPECT/CT images shown in lower panel (axial, left; sagittal, middle; coronal, right) demonstrate that the infection of soft tissues of the hip is in continuity with the prosthesis, consistent with an abscess (*modified from: Prandini N, Caruso G. Nuclear medicine imaging of joint prosthesis infection. In: Lazzeri E, Signore A, Erba PA, Prandini N, Versari A, D'Errico G, Mariani G, Eds. Radionuclide Imaging of Infection and Inflammation – A Pictorial Case-Based Atlas. Milan: Springer; 2013:81–106*)

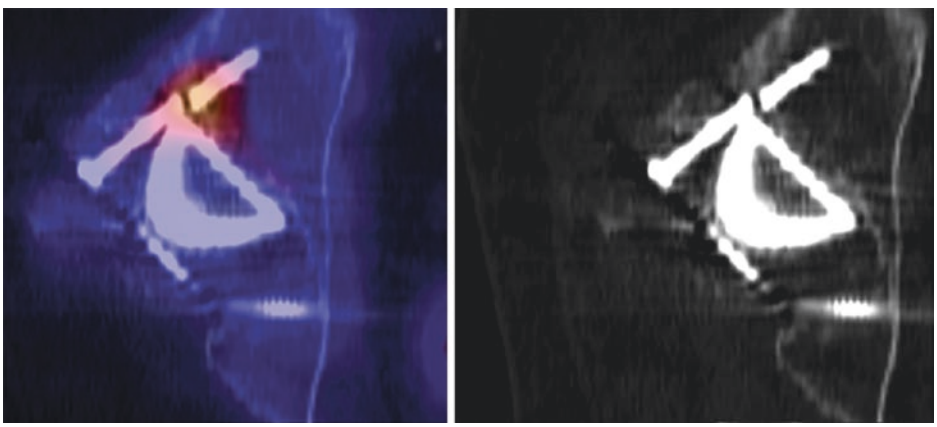

Fig. 24.44 Bone scintigraphy in a patient previously submitted to right hip prosthesis. Broken screw and enhanced tracer uptake in the upper acetabulum indicate loosening of a cup of the endoprosthesis as visualized on fused SPECT/CT image (left panel) and on low-dose CT image (right panel)

In hip prosthesis, extraarticular calcifications may also be found. Their removal only makes sense when they are no longer metabolically active. In loosened knee prosthesis, large resorptive cysts that are not hypometabolic and are easily identifiable on CT may produce false-positive results. When lumbar implants do not stabilize the joint, spondylosis and facet's arthritis may progress in the instrumented region. Furthermore, spinal degeneration occurring below or above the instrumented region can be the cause of ongoing pain and is recognized on scintigraphic imaging, preferably performed with SPECT/CT, especially because in patients treated with metallic implants planar imaging and even stand-alone SPECT imaging cannot reliably localize the anatomic sites of abnormalities observed on the scan.

On the other hand, the changing pattern of tracer uptake in the case of knee prosthesis differs somewhat from hip

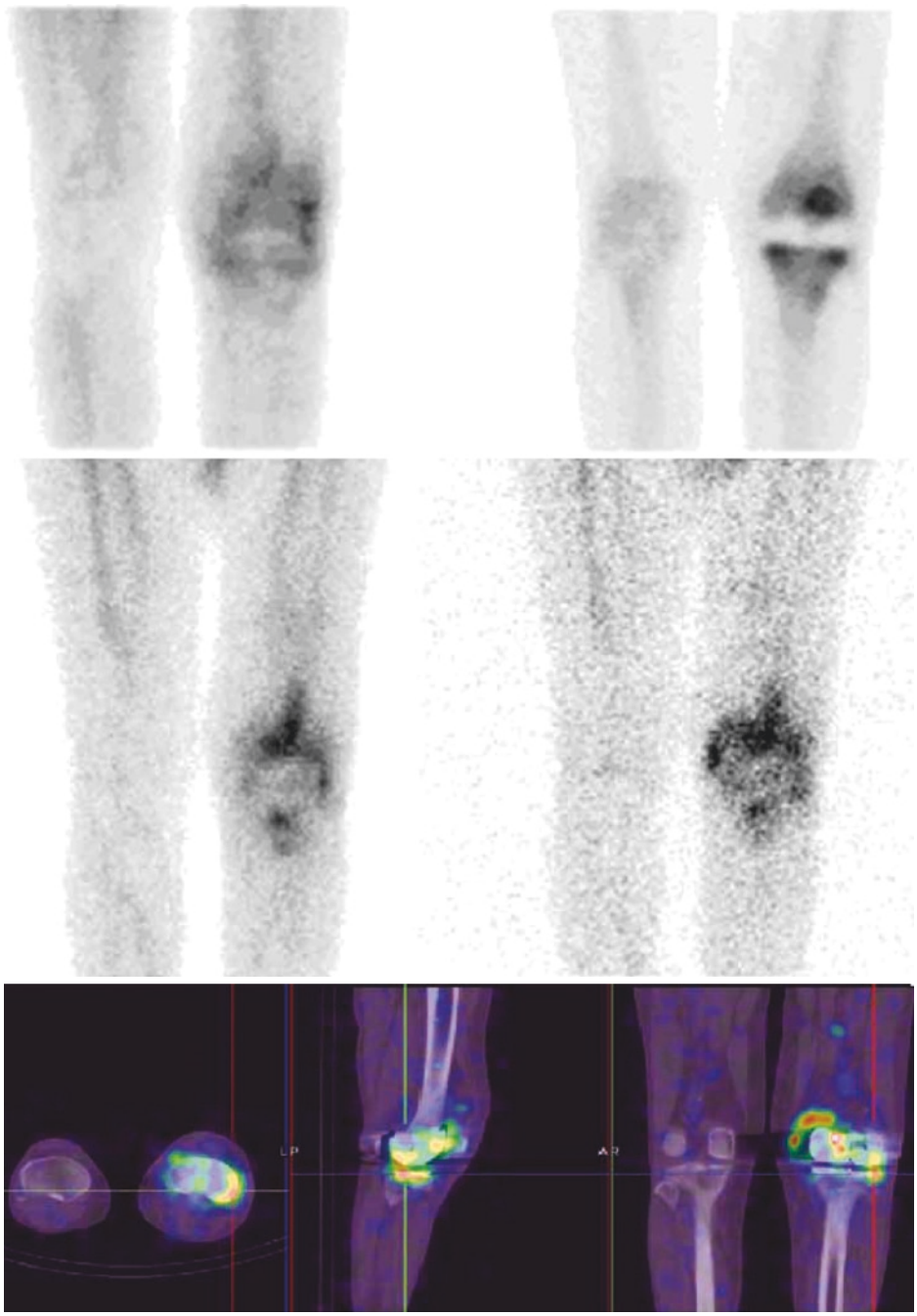

Fig. 24.45 Scintigraphic evaluation of a patient submitted 1 year earlier to total left knee prosthesis, presenting with pain of left knee, edema, and local signs of inflammation. Upper panel: "blood pool" phase (left) and delayed 3-h (right) acquisitions from three-phase bone scintigraphy with ^{99m}Tc-MDP, indicating the presence of edema and active bone remodeling. These findings are consistent with ongoing inflammation, but not conclusive as to the presence of infection. Middle panel: 3- and 20-h acquisitions (left and right, respectively) during ^{99m}Tc-HMPAO-WBC scintigraphy, showing accumulation of labeled leukocytes at the left knee. Bottom panel: fused transaxial (left), sagittal (center), and coronal (right) SPECT/CT images acquired during showing involvement ^{99m}Tc-HMPAO-WBC scintigraphy, showing bone involvement of the lateral compartment of left knee, of the lateral portion of the tibial plateau, of the lateral femoral condyle, and also in the infrapatellar bursae (*modified from: Prandini N, Caruso G. Nuclear medicine imaging of joint prosthesis infection. In: Lazzeri E, Signore A, Erba PA, Prandini N, Versari A, D'Errico G, Mariani G, Eds. Radionuclide Imaging of Infection and Inflammation – A Pictorial Case-Based Atlas. Milan: Springer; 2013:81–106*)

prosthesis, as increased uptake of ^{99m}Tc-diphosphonates reflecting bone remodeling can persist much longer than in patients with hip prosthesis—up to several years. Therefore, dynamic three-phase bone scintigraphy is less useful in these patients than in patients with hip prosthesis [136]. In case of clinical high probability of periprosthetic knee infection (Fig. 24.45) or in the evaluation of response to treatment (antibiotic therapy), scintigraphy with labeled autologous leukocytes constitutes the radionuclide imaging procedure of choice [100]. SPECT/CT acquisition and the use of correct interpretation criteria allow the differential diagnosis between infective and inflammatory periprosthetic processes. In case of doubtful/equivocal findings at labeled leukocyte scintigraphy, bone marrow scintigraphy can usefully be added to achieve the correct diagnosis [100], based on the rationale that, while both labeled leukocytes and radiocolloids accumulate in the healthy bone marrow, only labeled leukocytes accumulate in infection.

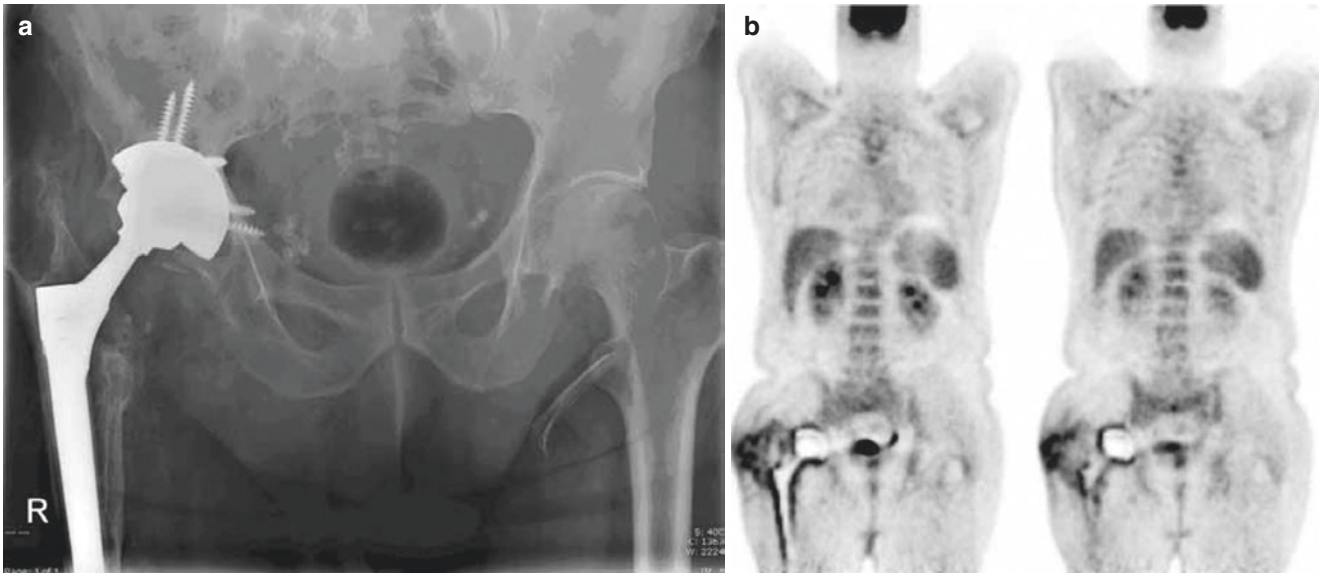

Fig. 24.46 Patient with right hip arthroplasty, presenting with pain and fistula around the right hip. (**a**) X-rays show radiolucent lines around the shaft of the prosthesis consistent with hip loosening. (**b**) [^{18}F]FDG PET (coronal sections at two different levels) shows irregularly increased tracer uptake around both components (acetabulum and femur) of the total hip arthroplasty, in continuity with the fistula in lateral side of the hip. Enhanced tracer uptake can also be seen in the right inguinal lymph nodes, consistent with infection diagnosis of right hip prosthesis (*modified from: Prandini N, Caruso G. Nuclear medicine imaging of joint prosthesis infection. In: Lazzeri E, Signore A, Erba PA, Prandini N, Versari A, D'Errico G, Mariani G, Eds. Radionuclide Imaging of Infection and Inflammation – A Pictorial Case-Based Atlas. Milan: Springer; 2013:81–106*)

Radiolabeled anti-granulocyte monoclonal antibody preparations can also be used if periprosthetic OM is suspected, with the same imaging acquisition modes as described above for peripheral OM. This imaging approach has 85% sensitivity and 83% specificity for the diagnosis of PJI [102–104]. The combination with bone marrow scintigraphy appears to increase specificity of scintigraphy with labeled anti-granulocyte antibody agents [137].

Controversial results have been reported on the diagnostic accuracy of [^{18}F]FDG PET/CT for diagnosing PJI (Fig. 24.46), and its utility is still debated [107, 138]. In particular, while a negative PET/CT scan can certainly rule out the presence of PJI (because of its very high negative predictive value), a positive scan does not permit to distinguish with certainty between infection and inflammation [139].

Key Learning Points

- Different radiopharmaceuticals can be used in the diagnostic flowchart of infection and/or inflammation of peripheral bones, including ^{99m}Tc-diphosponates, labeled autologous leukocytes, anti-granulocytes antibodies, [^{18}F]FDG, and ^{67}Ga-citrate.
- A negative bone scan is sufficient to exclude presence of inflammation associated with infection.
- Scintigraphy with labeled leukocytes or radiolabeled anti-granulocyte antibodies is useful to exclude or prove the presence of infection.
- Spinal infections include vertebral osteomyelitis (infection of the vertebral body), discitis (infection of the intervertebral disk) and spondylodiscitis (SD) (infection of two adjacent vertebral bodies and their intervertebral disk).
- Unlike osteomyelitis at other sites, diagnostic imaging of spine infection relies mostly on MR and PET/CT with [^{18}F]FDG.
- Radionuclide imaging for suspected infection/inflammation of prostetic joint implants is based on specific protocols to discriminate aseptic loosening from infection.

The European Association of Nuclear Medicine (EANM), the European Society of Radiology (ESR), the European Bone and Joint Infection Society (EBJIS), and the European Society of Microbiology and Infectious Diseases (ESCMID) have recently released a Consensus Document for the diagnosis of prosthetic joint infections (see below under "Further reading"). According to their conclusions concerning radionuclide imaging, the time elapsed since prosthesis implant

and the beginning of symptoms suggesting prosthetic joint infection is the first discriminant for the choice of the initial imaging modality. In particular, due to continuing bone remodeling for the majority of the implant sites, more than two years (but up to five years for knee prosthetic implants) must elapse for either three-phase bone scintigraphy or PET/CT with [^{18}F]FDG to have a high negative predictive value for infection and/or inflammation – thus to rule out the diagnosis of infection. In case either of these two imaging modality turns out to be positive, the clinical presentation must be carefully considered to stratify patients with regard to the suspicion of either acute or chronic infection. When acute infection is suspected, the first imaging modality of choice is labeled autologous WBC scintigraphy, the use of labeled anti-granulocyte scintigraphy remaining the second choice. When instead chronic infection is suspected, anti-granulocyte antibody scintigraphy is the first imaging modality of choice, autologous WBC scintigraphy remaining the second choice. If instead the clinical suspicion of infection arises within two years after prosthetic joint implant, the first imaging modality of choice is scintigraphy with autologous WBCs, possibly combined with bone marrow scintigraphy; nonetheless, the use of [^{18}F]FDG PET/CT can also be considered – keeping in mind however its low specificity associated with possible false-positive findings due to inflammation in the case of aseptic loosening and/or recent surgery.

24.10 Paget's Disease of the Bone

Paget's disease of the bone is a focal, progressive alteration of the remodeling processes of the bone, described in 1876 by James Paget. It is characterized initially by excessive bone resorption, followed by a secondary increase of osteoblast activity with bone reconstitution. The fundamental histological lesion is an excessive amount of fibrotic connective tissue inside the medullary space, with hyper-vascularization. The prevalence of Paget's disease is 1.5–3% in subjects over the age of 60 years, more common in men than in women (with a 1.8:1 ratio). Although the etiology of Paget's disease is unknown, it is believed that there is some interaction between genetic factors and environmental factors (viral infections) at the basis of the disease. A family history is present in about 15% of patients, with a higher risk than in the general population to develop the disease in the first-degree relatives. Typically, three phases of disease are described: lytic, mixed, and sclerotic phases. The initial lytic phase is characterized by geographic map osteolysis with advancing sharp edge bone resorption. In the long bones, the disease starts in the metaphyseal region and extends to the diaphyseal region with the appearance described as resembling a "blade of grass" or "flame-shaped." In the skull, the initial lytic phase is often referred to as "osteoporosis circumscripta." The intermediate phase is a mixed lytic-sclerotic phase. In this phase the margins of resorption might further expand; coarse trabeculae and thickened cortical bones with a cotton wool appearance are hallmarks of the latter stage.

Paget's disease is generally asymptomatic, so often the disease is detected incidentally during radiologic imaging performed for unrelated reasons or because of blood chemistry tests revealing increased alkaline phosphatase values. In the clinically manifest cases, pain or onset of bone deformity are the most frequent manifestations. Pain is due to the increased bone remodeling that characterizes the disease or, more frequently, by indirect complications of the disease such as degenerative osteoarthritis, nerve compression, or osteosarcoma.

Other causes of pain include increased vascularization, periosteum distortion caused by disorganized bone structure during remodeling, and the consequences of microtraumatic stress to which the bone is most exposed. Bone hypertrophy in the subchondral region can cause osteoarthritis, and this phenomenon can make the differential diagnosis between articular pain caused by Paget's disease and pain caused by a flogistic degenerative osteoarticular process very difficult.

Diagnosis of Paget's disease is often radiological, and the pathognomonic aspect is bone deformation; other radiological patterns include thickening of cortical bone and the presence of areas of osteolysis with alternating areas of osteosclerosis. Lytic lesions are clearly evident in the initial phase and occur as focal lesions (restricted osteoporosis) or appear as a "flame" on plain X-ray. In the later stages, areas of sclerosis appear and lithic and sclerotic lesions coexist. Although plain X-rays may allow a correct diagnosis, it may sometimes be difficult to distinguish between pagetic lesions and other skeletal lesions, such as metastases—either lytic or sclerotic.

Bone scintigraphy is the most sensitive imaging procedure for identifying Paget's disease, and it is mainly indicated in the initial diagnostic workup of patients affected by this condition. In fact, bone scintigraphy is crucial to define overall distribution of the disease, to identify the affected bone segments and the possible development of bone complications. The most affected bone segments belong to the axial skeleton: pelvis (65%), spine (42%), femur (37%), tibia (37%), sacrum (30%), and skull (29%). The humerus (13%), clavicle (5%), and forearm (5%) are less frequently affected. The disease may be monostotic (when only one bone segment is involved) or polyostotic (when more bone segments are affected), in a continuum spectrum, with 65% probability of identifying new disease localizations during follow-up. To assist in the diagnosis of Paget's disease, relatively specific signs have been described on both X-rays and bone scintigraphy [140]. On bone scintigraphy, the "picture frame sign" represents cortical thickening associated with radiolucent center of an enlarged, flattened vertebra body. The "Ivory sign" is typical of the sclerotic phase and is characterized by

enlarged and homogenously dense vertebra body. The "Mickey Mouse" sign describes the specific increased uptake in the vertebral body, posterior elements, and its spinous process. This same sign has been reported under different names such as the "T-sign" or "champagne glass" sign [141].

Bone scintigraphy can be also used for assessing possible complications of Paget's disease, for instance, in the case of fractures, which are frequently complicated by nonunion. Insufficiency fractures are usually seen in the cortex of abnormally bowed long bones and have been defined as "banana fracture" [142]. The altered biomechanics of the affected joints can lead to cartilaginous and bone abnormalities resulting in osteoarthritis.

Malignant transformation of bone affected by Paget's disease can occur, most commonly in patients with widespread osseous involvement, however with an incidence <1% [143]; sarcomatous Paget transformation may occur simultaneously at different sites. This condition has a very poor prognosis, yet it is difficult to diagnose, because several reports noted unexpectedly low [^{18}F]FDG uptake in these tumors [144]. Other rarer tumors possibly complicating Paget's disease are fibrosarcoma, chondrosarcoma, malignant fibrous histiocytoma, and even giant cell tumor [145].

Figure 24.47 shows some examples of ^{99m}Tc-diphosphonate bone scans observed in case of mono- and polyostotic Paget's disease.

The most common conditions that are considered in the differential diagnosis with Paget's disease are metastasis and fibrous dysplasia. Paget's disease and fibrous dysplasia are frequently difficult to distinguish on the basis of the bone scan, because both lesions may have intense tracer uptake. However, clinical data and other radiologic techniques can contribute to the correct diagnosis; in particular, young age, bowing deformities and ground-glass appearance are more typical of fibrous dysplasia. When the head is involved, fibrous dysplasia tends to spare the skull, while Paget's disease often involves skull bones. Furthermore, MRI and [^{18}F]FDG PET/CT can help distinguish metastatic disease from Paget's disease. In the lytic phase of Paget's lesion, the fatty marrow signal is preserved on MR imaging because the destruction of bone is due to resorption and not to infiltration as in metastatic disease [146]. However, in the sclerotic phase, this MRI feature cannot help the differential diagnosis, because the signal would be low in all sequences. [^{18}F]FDG PET/CT has some additional value in this differential diagnosis, since pagetic lesions are often non-[^{18}F]FDG-avid (or mildly avid when the alkaline phosphatase is markedly elevated), while metastases are usually hypermetabolic [147].

Paget's disease represents a pitfall also when using new PET tracers, such as ^{68}Ga-PSMA ligand [148] and labeled choline [149], radiopharmaceuticals that are commonly used in patients with recurrent and/or metastatic prostate cancer. Several reports describe nonspecific uptake of these two tracers in Paget's disease. ^{18}F-fluoride PET/CT has been used to quantify bone turnover in Paget's disease, particularly for assessing response to treatment with bisphosphonates [150]; however, this technique is not used routinely in clinical practice.

Key Learning Points

- Bone scintigraphy is the most sensitive imaging procedure for identifying Paget's disease, and it is mainly indicated in the initial diagnostic workup of patients affected by this condition.
- Bone scintigraphy is useful also to detect possible transformation of pagetic lesions into a malignant condition.

24.11 Treatment of Skeletal Metastases with Bone-Seeking Radiopharmaceuticals

24.11.1 Generalities on Metastatic Disease to the Skeleton

Skeletal metastases constitute one of the most feared events in patients with cancer, not only because they generally indicate advanced disease but also because they translate into markedly reduced quality of life [151]. Some of the cancers that more frequently give rise to skeletal metastases are also those with the highest incidence (e.g., prostate, breast, and lung cancers), whereas other less frequent cancers do exhibit a certain propensity to metastasize to the skeleton (e.g., thyroid and bladder cancers or melanoma and myeloma) [152].

Except rare instances where tumors directly infiltrate adjacent bony structures (e.g., in case of an intrapelvic cancer infiltrating the sacrum), most of the skeletal metastases arise because tumor cells circulating in the blood home into the bone marrow. Therefore, skeletal segments that are more frequently involved by metastasis are those with a more important component of active bone marrow—that receive a higher fraction of blood flow, such as the axial skeleton (from the skull to pelvis) and the proximal portions of the humeri and femora [153].

The most frequent complications of skeletal metastases are bone pain (initially of moderate intensity—but then proceeding to excruciating pain), pathologic bone fractures, and spinal cord compression. The combined effects of these events result in loss of mobility, while the most important

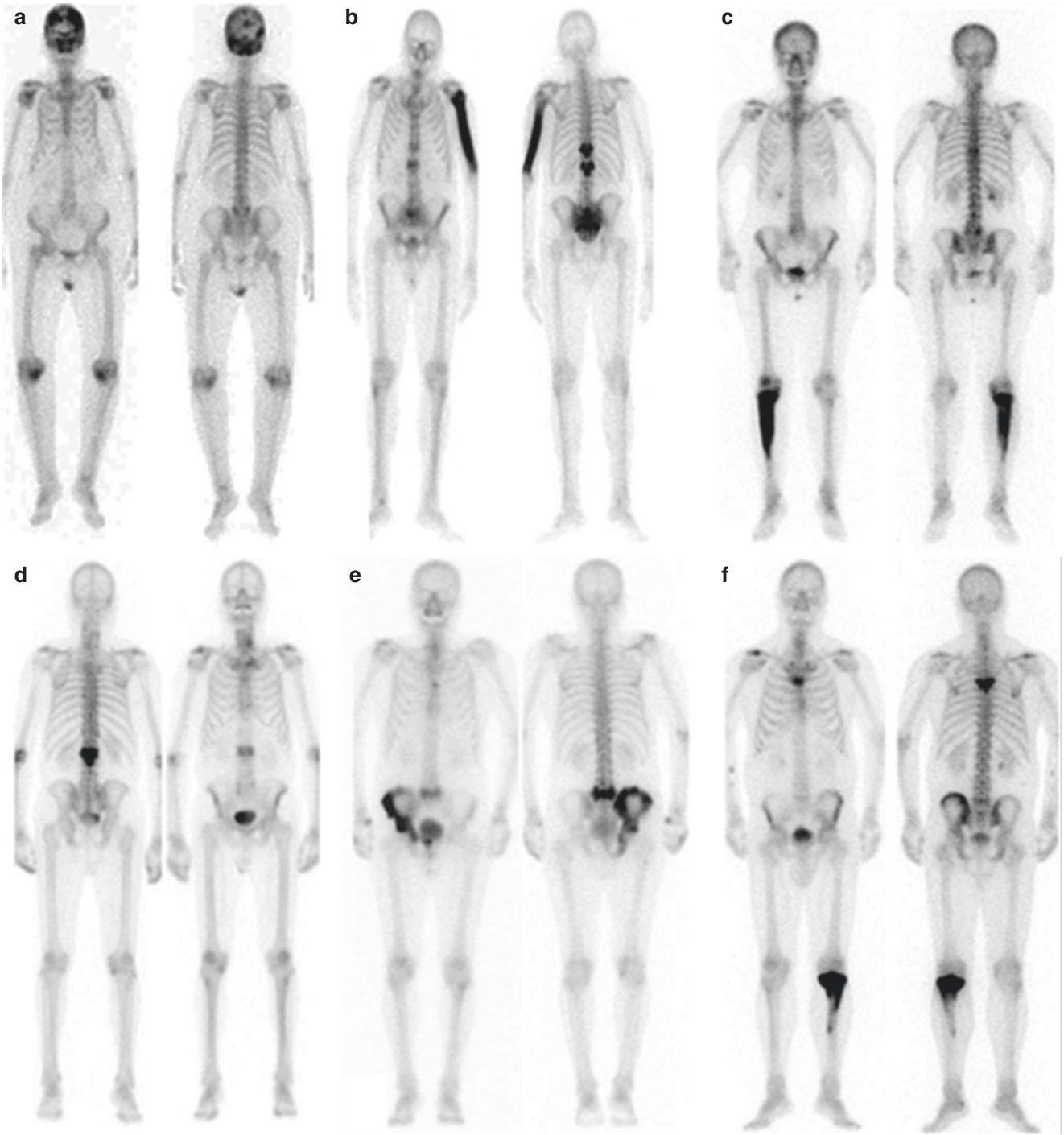

Fig. 24.47 Different patterns observed at ^{99m}Tc-HDP scintigraphy in patients with Paget's disease of the bone; planar whole-body scans in the anterior and posterior views are depicted for each patient. (**a**) Predominant involvement of the skull. (**b**) Polyostotic disease involving the left humerus and two nonadjacent vertebral bodies with the typical "Mickey Mouse" appearance. (**c**) Monostotic disease affecting the right tibia. (**d**) Monostotic disease involving a lumbar vertebral body. (**e**) Polyostotic disease involving the entire right pelvis and the lumbosacral passage. (**f**) Polyostotic disease involving a thoracic vertebral body, the left pelvis, and the proximal left tibia (*reproduced with permission from: Volterrani D, Erba PA, Mariani G, Eds. Fondamenti di Medicina Nucleare – Tecniche e Applicazioni. Milan: Springer Italy; 2010*)

biochemical derangement associated with skeletal metastasis is hypercalcemia and bone marrow aplasia.

Bone pain is due to the combined effects of several factors, some of which are related to anatomic changes caused by the growth of a tumor mass within the bone marrow causing expansion and increased intramedullary pressure, periosteal stress, or compression of nerves. Nonetheless, the most important determinants of bone pain appear to be chemical mediators, such as prostaglandins, interleukins, and other cytokines inducing inflammation (with recruitment of

inflammatory cells) and stimulation of sensory nerve endings [154].

Treatment of skeletal metastasis per se is based on a multifaceted approach that includes effective antitumor regimens (chemotherapy, hormonal therapy when appropriate, other newer forms of therapy), local treatments (external beam radiation therapy and/or surgery in case of highly localized disease or of impending fracture in weight-bearing segments), and different systemic therapies including pain-killing medications, bisphosphonates, and radiolabeled agents. The latter category includes both specific tumor-targeting agents (e.g., ^{131}I-iodide in case of metastases from differentiated iodine-avid thyroid cancers, ^{131}I-MIBG, or ^{90}Y/^{177}Lu-DOTA-somatostatin analogs in case of metastases from neuroendocrine tumors) and, more commonly, bone-seeking radiopharmaceuticals that localize at sites of enhanced turnover of the mineral component of the bone.

24.11.2 Pathophysiologic Bases for the Use of Bone-Seeking Radiopharmaceuticals

Bone-seeking radiopharmaceuticals used for treatment of bone pain localize at the site(s) of skeletal metastasis based on mechanisms that are similar to those taking place when diagnostic radiopharmaceuticals are used for bone scintigraphy, i.e., ^{99m}Tc-diphosphonates for conventional gamma camera imaging or ^{18}F-fluoride for PET imaging. In particular, the intensity of uptake of these agents is directly correlated with the degree of osteoblastic reaction to osteolysis induced by the growth of cancer cells in bone. Therefore, a more favorable outcome regarding bone pain palliation can be predicted for those painful skeletal sites that exhibit more intense uptake of the diagnostic agent when performing bone scintigraphy as a preliminary to treatment with the therapeutic radiopharmaceutical (see Fig. 24.48).

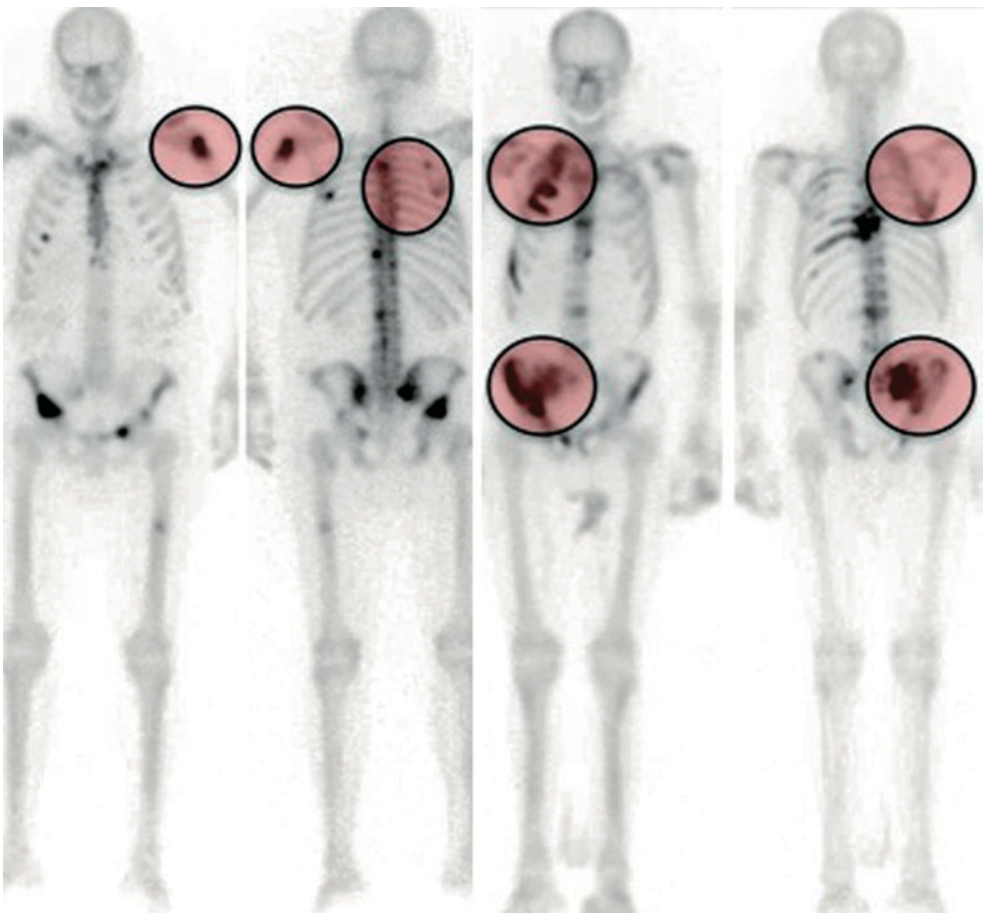

Fig. 24.48 Conventional gamma camera bone scintigraphy obtained about 3 h post-administration of ^{99m}Tc-MDP in two patients with painful bone metastases who were subsequently treated with ^{153}Sm-EDTMP (which ensued palliation of bone pain). The areas highlighted with pink color are the metastatic sites that are also the site of bone pain. Both these patients are good candidates for therapy with bone-seeking radiopharmaceuticals, since the painful areas correspond to metastatic sites with avid uptake of ^{99m}Tc-MDP. Case in left panel is a 67-year-old patient already treated with surgery and adjuvant chemotherapy because of non-small cell lung cancer. Case in right panel is a 72-year-old man already treated for prostatic adenocarcinoma, currently resistant to hormonal therapy and with progressing metastatic skeletal disease during chemotherapy (*reproduced with permission from: Volterrani D, Erba PA, Mariani G, Eds. Fondamenti di Medicina Nucleare – Tecniche e Applicazioni. Milan: Springer Italy; 2010*)

The clinical benefits of external beam radiation therapy in patients with skeletal metastases have long been known in terms of both bone pain palliation and accelerated healing of pathologic fractures [155, 156]. In this form of therapy, ionizing radiation is delivered to the metastatic site as a whole volume, including both the mineral component of the bone and the bone marrow space, where metastatic tumor cells colonize and grow. Therefore, the efficacy of treatment is linked, among other factors, to an important antitumor effect of radiation which leads to reduced local production of the inflammatory/algogenic compounds released in the presence of tumor cells, such as prostaglandins, interleukins, and other cytokines.

The mechanism of bone pain palliation induced by bone-seeking radiopharmaceuticals is somewhat similar to that following external beam radiation therapy regarding the local production of inflammatory/algogenic compounds [157]; instead, the mode of energy release by ionizing radiation following administration of therapeutic bone-seeking radiopharmaceuticals is somewhat different from external beam radiation therapy regarding both the distribution of energy in the target lesion and time-related release of energy. Bone-seeking radiopharmaceuticals localize at the surface of the trabecular bone (the osteoid layer surface) undergoing active remodeling, and the ionizing particles emitted during their decay travel a certain distance depending on their physical properties; in particular, β^- particles travel in water/tissue longer distances than α^{++} particles (2–8 mm depending on maximum energy versus 0.1 mm, respectively); therefore their linear energy transfer (LET) is lower than that of α^{++} particles. Since electrically charged particles are emitted and travel in a 3D space (see Fig. 24.49), part of their energy is absorbed by the trabecular structure of the bone, while a certain fraction of the energy is absorbed by cells in the intertrabecular space, i.e., the bone marrow—which includes the normal hematopoietic cells, the tumor cells, and the inflammatory cells. These events translate into some radiobiological effects not only on the mineral component but also on the cellular component of the affected bone, thus exerting some antitumor activity and at the same time some myelotoxicity—which is indeed the main dose-limiting factor for therapy with bone-seeking radiopharmaceuticals emitting β^- particles. Instead, the much shorter tissue penetration of the α^{++} particles emitted by ^{223}Ra (the only α-emitting radionuclide currently approved for treatment of skeletal metastases) limits bone marrow toxicity following treatment with this agent.

Concerning time-related issues of therapy with bone-seeking radiopharmaceuticals versus external beam radiation therapy, it must be considered that the latter is administered typically as treatments with high-dose rate (either with the conventional multiple fraction protocols or with the more recent hypofractionated protocols), whereas therapy with bone-seeking radiopharmaceuticals is characterized by release of ionizing energy over an extended period, therefore with dose rates that vary according to physical decay of the radionuclide and are in general lower than those involved in external beam radiation therapy.

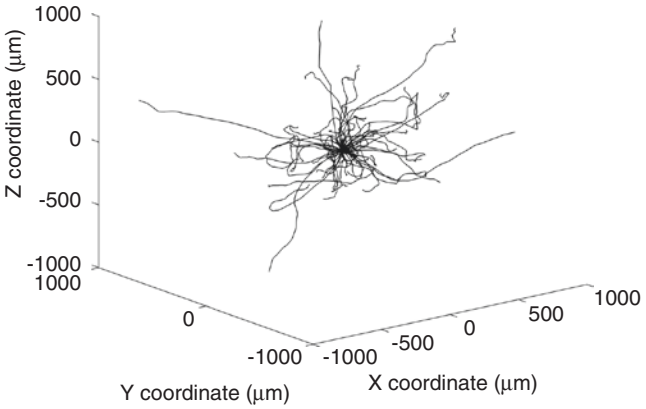

Fig. 24.49 Simulation of the tracks in water of β^- particles emitted by a point source of ^{131}I (full-energy spectrum); simulation has been performed for only 100 particles, a number too limited to show the whole spectrum of possibilities (including the maximum range, which is reached only by an extremely small fraction of the particles emitted). Due to interactions with surrounding matter, the β^- particles deviate repeatedly from their initial direction. Most of the energy (about 90%) associated with the emissions is deposited within about 20% of the maximum path range reported for each radionuclide. The maximum energy of the β^- particles emitted by ^{131}I (0.606 MeV) is somewhat intermediate between those of the β^- particles emitted by ^{89}Sr (0.585 MeV) and by ^{32}P (0.696 MeV), respectively, used for treatment of painful skeletal metastases (*image provided by courtesy of Prof. Alberto Del Guerra, Department of Physics "E. Fermi," University of Pisa and National Institute of Nuclear Physics (INFN), Pisa Section, Pisa (Italy)*)

24.11.3 Bone-Seeking Radiopharmaceuticals for Therapy

According to the main localization mechanism, bone-seeking radiopharmaceuticals used for therapy can be classified into (1) those that localize at sites of enhanced bone mineral turnover because of their affinity/chemisorption onto the newly formed hydroxyapatite crystals and (2) those that localize at sites of enhanced bone mineral turnover because they behave in vivo as chemical analogs of calcium. As described in details in Chap. 4, the first group includes emitters of β^- particles such as bisphosphonates labeled with different radionuclides, most notably ^{153}Sm-EDTMP and ^{186}Re-HEDP or ^{188}Re-HEDP (and more recently ^{177}Lu-EDTMP). The second group includes ^{89}Sr-chloride (a β^- emitter) and ^{223}Ra-dichloride (an α^{++} emitter). On the other hand, ^{32}P-phosphate (a β^- emitter still used clinically in some low-income countries because of low cost—despite a non-negligible bone marrow toxicity) distributes widely throughout the bone mineral component because of the natural distribution of phosphate.

Most of the clinical experience with the use of this category of bone-seeking radiopharmaceuticals has been acquired with ^{89}Sr-chloride and with ^{153}Sm-EDTMP. Therefore, most of the comprehensive analyses of the published literature concerning β^- emitters (see further below) refer to these two therapeutic agents.

24.11.4 Clinical Use of β^- Particle-Emitting Bone-Seeking Radiopharmaceuticals

There has been a constant update of guidelines developed by professional societies throughout the years for the use of bone-seeking radiopharmaceuticals emitting β^- particles in the management of patients with skeletal metastases [158–160]. In this chapter we will refer to the most recently updated guidelines on the use of β^--emitting radiopharmaceuticals, developed by the European Association of Nuclear Medicine [160]. Although these guidelines formally regard the three approved β^--emitting radiopharmaceuticals (^{32}P-sodium phosphate, ^{89}Sr-chloride, ^{153}Sm-EDTMP), similar considerations apply to the use of other bone-seeking radiopharmaceuticals that have been clinically validated and are available in certain institutions under approval by the local Institutional Review Board (e.g., ^{186}Re-HEDP, ^{188}Re-HEDP, ^{177}Lu-EDTMP).

24.11.4.1 Indications

As simply stated by Handkiewicz-Junak et al. [160], the chief indication for therapy of skeletal metastases with this class of radiopharmaceuticals is for "Painful metastatic bone lesions with osteoblastic response, as indicated by areas of intense uptake on radionuclide bone scans." Furthermore, clinical experience has cumulated on the beneficial effect of this therapy also in patients with primary painful bone malignancies with similarly enhanced uptake on the radionuclide bone scan, although not at sufficient level for the proper authorization bodies to approve this indication for routine clinical use.

Moreover, although not mentioned in the published guidelines the role of high-dose ^{153}Sm-EDTMP in patients with multiple myeloma has been investigated. The results obtained indicate that there are no additional hematological or non-hematological toxicities following this treatment in combination with other therapies—even when administered with multiple cycles [161, 162]. Furthermore, clinical benefit has been demonstrated following administration of ^{153}Sm-EDTMP combined with bortezomib (a proteasome inhibitor, used in this regimen as a radiosensitizing agent) in patients with relapsed or refractory multiple myeloma [163].

24.11.4.2 Contraindications

The only two absolute contraindications for therapy with β^--emitting bone-seeking radiopharmaceuticals are pregnancy and breastfeeding.

There are several relative contraindications that require tailoring of therapy after careful consideration of the whole clinical scenario of each individual patient. They include conditions related to compromised bone marrow function (due to either diffuse infiltration of the bone marrow by metastatic cancer cells or prior chemo- or radiotherapy regimens) and life expectancy.

Concerning bone marrow function, a certain reduction of blood cell counts (usually affecting platelets and/or leukocytes) is expected following therapy with β^- emitting bone-seeking radiopharmaceuticals. Such reductions may reach the levels of hematological toxicity in patients with evidence of compromised bone marrow function prior to treatment. Although the scenario has changed after the introduction of colony-stimulating factors to support/stimulate the production of granulocytes in particular, the following blood cell count values have been defined as the threshold above which administration of β^--emitting bone-seeking radiopharmaceuticals for therapy of skeletal metastases is expected to be safe:

- Hemoglobin >90 g/L
- Total leukocyte count >3.5 × 10^9/L
- Platelet count >100 × 10^9/L

Stability of blood cell counts should be ascertained prior to treatment, in order to rule out the occurrence of deteriorating bone marrow function before administering therapy with β^--emitting bone-seeking radio-pharmaceuticals. Furthermore, since the main route of clearance for these radiopharmaceuticals is through renal excretion, poor renal function results in prolonged blood retention and therefore possibly increasing bone marrow toxicity. As a consequence, treatment with β^--emitting bone-seeking radiopharmaceuticals should not be performed in patients with serum creatinine >180 μmol/L (or >2.05 mg/dL) and/or estimated glomerular filtration rate <30 mL/min.

Moreover, the coagulation profile should be investigated prior to treatment in order to rule out subclinical disseminated intravascular coagulation, a condition that constitutes a risk factor for severe thrombocytopenia following therapy with these radiolabeled agents.

Concerning life expectancy, it must be considered that the palliative effect of this form of therapy typically takes place up to 4 weeks after administration. Therefore, therapy with bone-seeking radiopharmaceuticals is expected to be more beneficial in patients with longer life expectancy as well as in patients with earlier stages of skeletal metastatic disease.

A final consideration concerning selection of patients with bone pain from skeletal metastases for palliative therapy with bone-seeking radiopharmaceuticals has to do with special features of the metastatic lesions, as it may occur when such lesions cause spinal cord compression or imply the risk of impending fracture. In these cases the critical lesions must be treated with modalities that ensue faster control of the lesions, such as surgery or external beam radiation therapy. This approach does not preclude concomitant treatment of other noncritical lesions with administration of bone-seeking radiopharmaceuticals.

24.11.4.3 Efficacy

Several meta-analyses and systematic reviews have evaluated the results of a vast number of clinical studies that have been published on this matter [164–173]. Such results consistently demonstrate the beneficial effects of therapy with bone-seeking agents in patients with osteoblastic or mixed-pattern skeletal metastases. Since predominantly osteoblastic metastases are observed primarily in patients with prostate cancer, most of the studies have focused on these patients; nonetheless, this therapy is equally effective in patients with skeletal metastases originating from other cancers (e.g., breast cancer, lung cancer, etc.), provided that patients are adequately selected on the basis of bone scintigraphy demonstrating increased tracer uptake at the sites of painful bone metastases.

Overall response rates for palliation of bone pain average 70% of the patients treated, with reports up to 90%, are reported; these figures are remarkably consistent regardless of the radiopharmaceutical used—^{153}Sm-EDTMP or ^{89}Sr-chloride. In about one out of the three patients responding to treatment, there is complete relief of bone pain, while in the remaining patients there is partial response, i.e., marked reduction of bone pain which becomes therefore amenable to treatment with minor analgesic drugs rather than opioid medications. Similar results have been reported regarding bone pain palliation following administration of ^{188}Re-HEDP, with an average 32% of complete responses and 44% of partial responses.

The onset of bone pain palliation varies between about 1 and 4 weeks post-administration, the shorter interval occurring when radionuclides with shorter physical half-life are used (i.e., ^{153}Sm and ^{186}Re, 1.9 and 3.8 days, respectively) versus ^{89}Sr (50.5 days). This difference is due to the higher dose rate for shorter-lived radionuclides compared to longer-lived radionuclides (see Fig. 24.50). Duration of pain palliation is generally reported in the 6–15-month range. In case of recurrence of bone pain, treatment can be repeated, and efficacy of such therapy is maintained throughout several cycles, provided that all indications for therapy with β^--emitting bone-seeking radiopharmaceuticals are met—with special attention to the pattern of bone scintigraphy and to the criteria of bone marrow function [174].

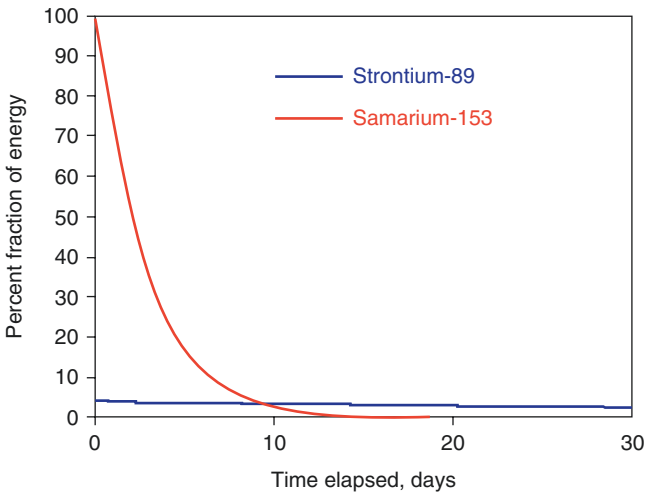

Fig. 24.50 Comparison of the time-related pattern of energy release over a certain period between ^{153}Sm and ^{89}Sr. The plot has been drawn in such a way that the areas (or integrals) under the two curves (i.e., the total energy released from time zero to total decay) are identical for the two radionuclides. Thus, the two curves basically correspond to the dose rates for the two radionuclides. The plot shows that, with the same total radiation dose released, the dose rate of ^{153}Sm (physical half-life 1.9 days) is much higher than that of ^{89}Sr (physical half-life 50.5 days), but it declines to virtually zero over approximately 20 days. Whereas, ^{89}Sr continues to release radiation energy (though lower than that of ^{153}Sm) over a much longer period (*reproduced with permission from: Volterrani D, Erba PA, Mariani G, Eds. Fondamenti di Medicina Nucleare – Tecniche e Applicazioni. Milan: Springer Italy; 2010*)

Studies on the quality of life following treatment of painful skeletal metastases with bone-seeking radiopharmaceuticals indicate that these treatments can be recommended to improve the quality of life of patients with skeletal metastases characterized by high tracer uptake on conventional bone scintigraphy.

Besides symptomatic relief of bone pain, treatment with β^--emitting bone-seeking radiopharmaceuticals has been shown to induce also objective tumor responses, as demonstrated by, e.g., reduction in the serum levels of tumor-associated antigens, improved imaging patterns (see Fig. 24.51), and/or reduction in new skeletal-related serious events. Furthermore, several reports have shown improved survival after treatment with these agents, either alone or especially in combination with chemotherapy in patients with cancers of either the prostate or breast.

24.11.4.4 Administration Protocols and Possible Side Effects

The standard administration route for ^{32}P-phosphate, ^{89}Sr-chloride, ^{153}Sm-EDTMP, and ^{186}Re- or ^{188}Re-HEDP is by intravenous injection; slow infusion is recommended, especially when administering ^{89}Sr-chloride. Nonetheless, ^{32}P-phosphate can also be administered orally—but in this case the activity to be administered is about twofold the activity administered intravenously. Particular attention

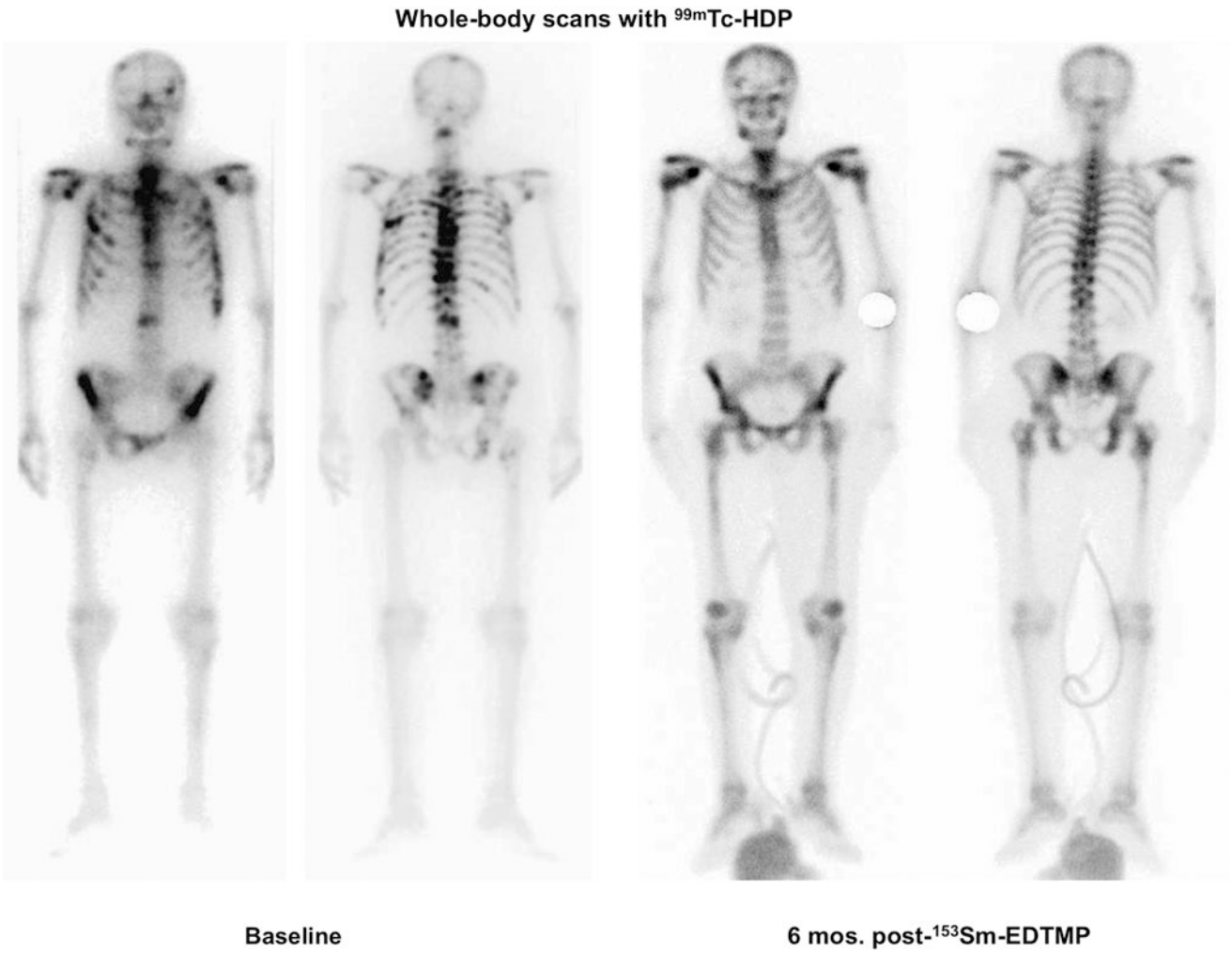

Fig. 24.51 Efficacy of treatment with ^{153}Sm-EDTMP administered for bone pain palliation purposes to a patient with progressing castration-resistant prostate cancer. Left panel shows the baseline bone scintigraphy (prior to therapy with the bone-seeking radiopharmaceutical) obtained about 3 h after injection of ^{99m}Tc-HDP: at this time serum PSA was 540 ng/mL. Right panel shows the bone scan obtained about 6 months posttreatment, without any intervening chemotherapy; at this time serum PSA was 45 ng/mL, and the bone scan shows marked improvement of the scintigraphic pattern (*reproduced with permission from: Volterrani D, Erba PA, Mariani G, Eds. Fondamenti di Medicina Nucleare – Tecniche e Applicazioni. Milan: Springer Italy; 2010*)

must be paid to avoid extravasation of the β⁻-emitting radiopharmaceutical, because the high local concentration of the therapeutic agent in interstitial space may cause tissue necrosis.

No special preparation of the patient is required before administration of the radiopharmaceutical, including recent, prior, or subsequent therapy with latest generation bisphosphonates (such as zoledronic acid), considering that no competition was found for bone localization between such bisphosphonates and ^{153}Sm-EDTMP or ^{89}Sr-chloride.

Recommended activities of the β⁻-emitting bone-seeking radiopharmaceuticals administered for palliation of bone pain from osteoblastic or mixed-pattern skeletal metastases are listed here below, as derived from either the EANM guidelines or from other sources:

- ^{32}P-phosphate: 185–370 MBq (or 5–10 mCi) when administered intravenously (or about twofold this activity when administered orally)
- ^{89}Sr-chloride: 1.5–2.2 MBq/kg body weight (or 40–60 μCi/kg)
- ^{153}Sm-EDTMP: 37 MBq/kg (or 1 mCi/kg)
- ^{186}Re-HEDP: 1110–3515 MBq (or 30–95 mCi)
- ^{188}Re-HEDP: 2500–5500 MBq (or 67–148 mCi)

Although distribution of these therapeutic radiopharmaceuticals is in general expected to mirror the pattern observed on conventional bone scintigraphy with any ^{99m}Tc-labeled bone-seeking phosphonate agent, it may be useful to acquire scintigraphic images after administration of the β⁻-emitting radiopharmaceutical, to depict in the individual patient actual

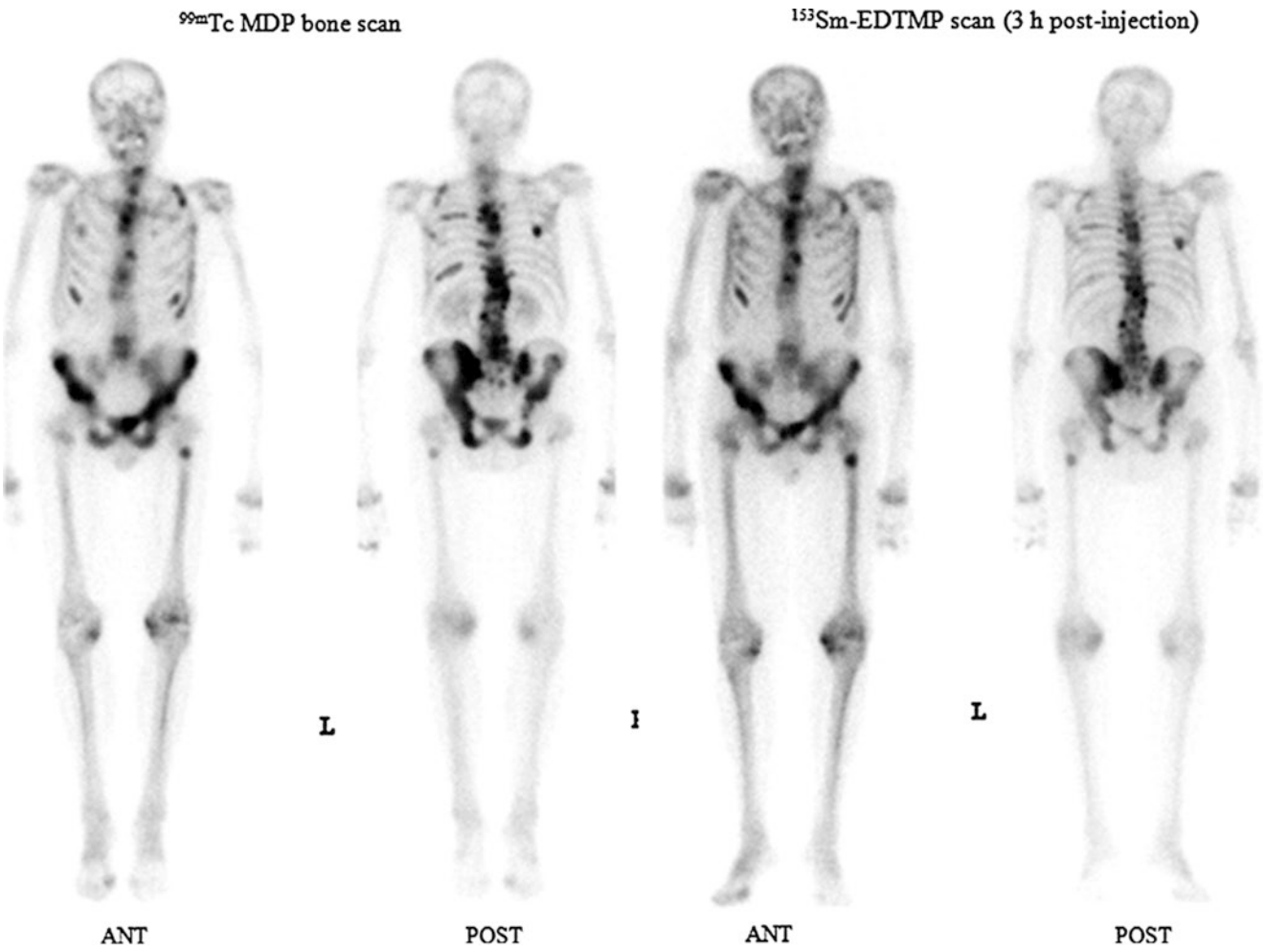

Fig. 24.52 Whole-body imaging: ^{99m}Tc-MDP bone scan and ^{153}Sm-EDTMP scan. Bone scan (left) shows multiple areas of abnormally increased uptake in the bones consistent with metastatic disease. Targeting of all sites by ^{153}Sm-EDTMP is seen on the whole-body scan obtained 3 h post-therapy (right) (*reproduced with permission from: Pandit-Taskar N, Divgi CR. Targeted radionuclide therapy for bone metastases. In: Strauss HW, Mariani G, Volterrani D, Larson SM, Eds. Nuclear Oncology: From Pathophysiology to Clinical Applications. New York: Springer; 2017:1307–1336*)

distribution of the therapeutic agent throughout the skeleton. When ^{89}Sr-chloride is administered, gamma camera imaging can be recorded by taking advantage of the photon emission associated with the bremsstrahlung effect caused by interaction with tissues of the high-energy β^- particles emitted by ^{89}Sr. However, the images so obtained are in general of rather poor quality. Instead, good-quality gamma camera images are obtained after administration of radiopharmaceuticals labeled with either ^{153}Sm, ^{188}Re, ^{186}Re, or ^{177}Lu, since the modes of decays of these radionuclides include the emission of γ-rays with energies suitable for gamma camera imaging. Imaging can be acquired either few hours post-administration (Fig. 24.52) or, for better scintigraphic contrast, 24 h post-administration.

Therapy with β^--emitting bone-seeking radiopharmaceuticals implies some side effects that are in general mild and exhibit a rather predictable pattern. The earliest side effect (occurring within approximately 72 h post-administration and affecting about 10% of the patients treated) is the so-called "flare" phenomenon, i.e., a transitory self-limiting and readily managed increase in bone pain which is in the majority of cases associated with good clinical response.

The second side effect, which is consistently observed in the majority of patients treated with β^--emitting bone-seeking radiopharmaceuticals, is some degree of myelotoxicity, which is in general mild and recovers spontaneously without requiring special additional therapies. In particular, as a result of irradiation of the hemopoietic cells in the bone marrow by the β^- particles emitted by the radiopharmaceutical adsorbed on the surfaces of trabecular bone, there is drop in leukocyte and especially in platelet counts, with a nadir that is observed at 3–5 weeks post-administration when using the agents labeled with the shorter-lived radionuclides

(^{153}Sm, ^{186}Re, or ^{188}Re); recovery is usually complete within 3 months. When using instead the longer-lived ^{89}Sr or ^{32}P, the nadir in leukocyte/platelet counts can occur at 12–16 weeks post-administration. Myelotoxicity is usually more pronounced when patients have received prior myelosuppressive chemotherapy regimens.

24.11.5 Clinical Use of the α^{++} Emitter ^{223}Ra-dichloride

This radiopharmaceutical constitutes the most recent addition to the list of approved bone-seeking agents for therapy of patients with skeletal metastases. It should be noted that, while other radiopharmaceuticals have been approved with mention of the palliative effects of such treatment, FDA and EMA approvals of ^{223}Ra-dichloride read as follows: "For the treatment of patients with castration-resistant prostate cancer, symptomatic bone metastases and no known visceral metastatic disease." This definition, which is based on the results of a large-scale randomized seminal study by Parker et al. [175] subsequently supported by additional reports [176, 177], implies not only a mere palliation effect on bone pain but also an additional clinical benefit in terms of new serious skeletal-related events and overall survival following therapy with ^{223}Ra-dichloride.

In this chapter we will refer to the recently published guidelines on the use of ^{223}Ra-dichloride, developed by the European Association of Nuclear Medicine [178].

Similarly as other bone-seeking radiopharmaceuticals utilized for either diagnostic or therapeutic purposes, ^{223}Ra (a member of the second main group of elements, which possess chemical and physiological similarities with calcium) selectively accumulates in the bone, particularly in areas of high bone turnover—as typically are the border zones of bone and bone metastases. ^{223}Ra decays with physical half-life of 11.43 days, emitting α^{++} particles that have a very limited penetration in tissue (less than 100 μm, which corresponds to about 10 cell diameters). This results in a very high linear energy transfer and therefore in high probability of inducing lethal DNA damage (double-strand breaks) in the adjacent cells that are mostly represented by osteoblasts and osteoclasts in addition to metastatic tumor cells. On the other hand, the limited tissue penetration of the α^{++} particles minimizes irradiation of the normal hemopoietic components of the bone marrow, thus resulting in hematological toxicity of therapy with ^{223}Ra-dichloride considerably lower than that observed following therapy with the β^--emitting bone-seeking radiopharmaceuticals.

24.11.5.1 Indications

The approved indication for ^{223}Ra-dichloride is "… the treatment of adult patients with castration-resistant prostate cancer, symptomatic bone metastases and no known visceral metastases" [178]. Thus, it should be noted that in the clinical routine skeletal metastases originating from tumors other than prostate cancer are not amenable to treatment with ^{223}Ra-dichloride.

Although not specifically mentioned in the approval document, it is common practice to verify the presence of predominantly osteoblastic metastases with either a conventional gamma camera bone scintigraphy or with ^{18}F-fluoride PET/CT.

Furthermore, the term "visceral metastases" does not apply to the presence of lymph node metastases as a criterion for exclusion from therapy with ^{223}Ra-dichloride.

24.11.5.2 Contraindications

Considering that prostate cancer in children and adolescents under the age of 18 years is an exceptionally rare occurrence, no safety and efficacy of treatment with ^{223}Ra-dichloride has ever been investigated in this age group. There are no absolute contraindications to the use of ^{223}Ra-dichloride, provided that the indications are correctly adopted, chiefly the absence of visceral metastases.

Although hematological toxicity following the use of ^{223}Ra-dichloride is lower than with the β^--emitting agents, the bone marrow reserve must be carefully investigated before administration. Before the first administration/cycle, the minimum threshold values for treatment are listed as follows:

- Hemoglobin >10.0 g/dL
- Absolute neutrophil count >1.5 × 10^9/L
- Platelet count >100 × 10^9/L

For all subsequent administrations/cycles, the following minimum threshold values for treatment are required:

- Absolute neutrophil count >1.0 × 10^9/L
- Platelet count >50 × 10^9/L

Regarding the overall clinical condition of patients who are candidates for treatment with ^{223}Ra-dichloride in an outpatient setting, their Karnofsky score should be >50% or their ECOG performance status <2. If patients do not meet these criteria, hospitalization should be considered. Furthermore, fecal incontinence requires hospitalization, since ^{223}Ra undergoes fecal excretion (13% of the injected activity within 48 h post-administration versus 2% for renal excretion) and incontinence would imply an increased risk of contamination for the attending caregivers/household and for the environment.

24.11.5.3 Efficacy

Treatment with ^{223}Ra-dichloride is generally followed by rapid and marked reduction of bone pain, although pain

relief alone is not a reliable indicator of response to treatment in terms of survival benefit [175, 179, 180]. Objective markers of response to treatment are represented by the serum levels of PSA and alkaline phosphatase, although fluctuations in serum PSA levels may be observed throughout the six therapy cycles and make this marker a somewhat unreliable predictor of long-term response.

^{223}Ra-dichloride is the first bone-seeking radiopharmaceutical that has shown a definite survival benefit in the patients treated with this radiopharmaceutical as a single therapeutic agent, with median overall survival of 14.9 months versus 11.3 months for the group treated with placebo. Investigations of the possible synergistic effect of ^{223}Ra-dichloride used concomitantly with chemotherapy are currently under way.

24.11.5.4 Administration Protocol and Possible Side Effects

According to the EANM guidelines (based on key consensus recommendations developed among 11 nuclear medicine centers across six European countries [181]), fasting is not required prior to administration of ^{223}Ra-dichloride, and patients should be well hydrated. Although in general patients should take their medications as usual, the only recommended precaution is to temporarily discontinue supplementation with calcium, phosphates, or vitamin D for at least 4 days before and after each administration of the radiopharmaceutical. A careful benefit/risk evaluation should be performed in case patients are receiving concomitant chemotherapy.

Patients with urinary or fecal incontinence should be handled in such a way so as to minimize the risk of contamination, through bladder catheterization or with other padding devices, respectively. Although therapy with ^{223}Ra-dichloride is generally performed on an outpatient basis, hospitalization should be considered for seriously ill patients of for patients with fecal incontinence.

^{223}Ra-dichloride is administered by slow intravenous injection (over approximately 1 min), paying special attention to avoid extravasation. The standard protocol for this treatment is based on administration of ^{223}Ra-dichloride in the amount of 55 kBq/kg of body weight, corresponding to 3.85 MBq (or 104 μCi) for a 70 kg patient. At variance with the β^--emitting bone-seeking radiopharmaceuticals described in the prior section (for which the rule is a single administration—considering repeat administration after several weeks or months in case of recurrence of bone pain), the standard protocol for therapy with ^{223}Ra-dichloride involves six administrations at 4-week intervals. Before each administration, the hematological profile of patients must be carefully evaluated in order to verify that the requisites for treatment are maintained throughout.

The risk of hematological adverse events (e.g., neutropenia and thrombocytopenia) is increased in patients whose bone marrow reserve is reduced because of prior cytotoxic chemotherapies and/or radiation therapy or in patients with advanced diffuse metastatic infiltration of the bone—appearing as "superscan" on conventional bone scintigraphy.

The most frequent adverse side effects observed after treatment with ^{223}Ra-dichloride (occurring in ≥10% of the patients treated) are diarrhea, nausea, vomiting, and thrombocytopenia, the most serious adverse reactions being represented by thrombocytopenia and neutropenia.

Since ^{223}Ra is excreted mainly through the gastrointestinal route, the intestine may be exposed to radiation exposure sufficient to cause detrimental effects. Therefore, the possible risks caused by administration of ^{223}Ra-dichloride in patients with inflammatory bowel disease should carefully be considered in terms of benefit/risk ratio.

A few patients treated concomitantly with ^{223}Ra-dichloride and bisphosphonates combined with chemotherapy have developed osteonecrosis of the jaw. However, it is currently unclear whether this occurrence was attributable to prior treatment with bisphosphonates and chemotherapy or whether therapy with ^{223}Ra-dichloride further increased the risk of osteonecrosis of the jaw.

Key Learning Points

- The skeleton is the most frequent site of metastases arising from cancers originating at other sites.
- Metastatic tumor cells home in the bone marrow mostly by the hematogenous route.
- The complications of skeletal metastases include bone pain, pathologic bone fractures, spinal cord compression, hypercalcemia, and bone marrow aplasia.
- Bone pain is due mainly to local production of chemical mediators produced in the bone marrow environment both by the tumor cells and by inflammavtory cells.
- Treatment of skeletal metastases includes systemic antitumor regimens, local treatment (radiation therapy and/or surgery), pain-killing medications, bisphosphonates, and bone-seeking radiopharmaceuticals.
- The mechanism of bone pain palliation induced by bone-seeking radiopharmaceuticals is mostly due to reduced local production of inflammatory/algogenic compounds.
- The radiobiological effects caused by bone-seeking radiopharmaceuticals affect not only the mineral

component but also the cellular component of the affected bone, thus exerting some antitumor activity and at the same time some myelotoxicity.

- The basic indication for therapy with bone-seeking radiopharmaceuticals is that the lesions to be treated show a predominant osteoblastic pattern on conventional bone scintigraphy with ^{99m}Tc-phosphonates.
- Bone-seeking radiopharmaceuticals utilized for therapy include agents labeled with or carrying radionuclides emitting β^- particles (^{32}P, ^{89}Sr, ^{153}Sm, ^{18}6Re, ^{188}Re, ^{177}Lu) or α^{++} particles (^{223}Ra).
- While indications for the approved β^--emitting radiopharmaceuticals (^{32}P-phosphate, ^{89}Sr-chloride, ^{153}Sm-EDTMP) state their clinical use for palliation of bone pain, the indications for the use of ^{223}Ra-dichloride state its use for therapy of skeletal metastatic disease from prostate cancer with the purpose of prolonging overall survival.
- All bone-seeking radiopharmaceuticals are effective not only in terms of bone pain palliation but also in terms of objective tumor responses to treatment.
- There are specific indications, contraindications, possible adverse side effects, and expected clinical outcomes for each category of bone-seeking radiopharmaceuticals used for therapy of metastatic skeletal disease.

References

1. Van den Wyngaert T, Strobel K, Kampen WU, Kuwert T, van der Bruggen W, Mohan HK, et al. The EANM practice guidelines for bone scintigraphy. Eur J Nucl Med Mol Imaging. 2016;43(9):1723–38.
2. Treves ST, Lassmann M, EANM/SNMMI Pediatric Dosage Harmonization Working Group. International guidelines for pediatric radiopharmaceutical administered activities. J Nucl Med. 2014;55(6):869–70.
3. Ayres KL, Spottswood SE, Delbeke D, Price R, Hodges PK, Wang L, et al. Dose optimization of the administered activity in pediatric bone scintigraphy: validation of the North American consensus guidelines. J Nucl Med. 2015;56(9):1391–4.
4. Cachovan M, Vija AH, Hornegger J, Kuwert T. Quantification of ^{99m}Tc-DPD concentration in the lumbar spine with SPECT/CT. EJNMMI Res. 2013;3(1):45. https://doi.org/10.1186/2191-219X-3-45.
5. Beck M, Sanders JC, Ritt P, Reinfelder J, Kuwert T. Longitudinal analysis of bone metabolism using SPECT/CT and ^{99m}Tc-diphosphono-propanedicarboxylic acid: comparison of visual and quantitative analysis. EJNMMI Res. 2016;6(1):60. https://doi.org/10.1186/s13550-016-0217-4.
6. Beheshti M, Mottaghy FM, Payche F, Behrendt FFF, Van den Wyngaert T, Fogelman I, et al. ^{18}F-NaF PET/CT: EANM procedure guidelines for bone imaging. Eur J Nucl Med Mol Imaging. 2015;42:1767–77.
7. Segall G, Delbeke D, Stabin MG, Even-Sapir E, Fair J, Sajdak R, et al. SNM practice guideline for sodium ^{18}F-fluoride PET/CT bone scans 1.0. J Nucl Med. 2010;51:1813–20.
8. Blake GM, Siddique M, Puri T, Frost ML, Moore AE, Cook GJ, et al. A semipopulation input function for quantifying static and dynamic ^{18}F-fluoride PET scans. Nucl Med Commun. 2012;33(8):881–8.
9. Blake GM, Siddique M, Frost ML, Moore AE, Fogelman I. Imaging of site specific bone turnover in osteoporosis using positron emission tomography. Curr Osteoporos Rep. 2014;12(4):475–85.
10. Hawkins RA, Choi Y, Huang SC, Hoh CK, Dahlbom M, Schiepers C, et al. Evaluation of the skeletal kinetics of fluorine-18-fluoride ion with PET. J Nucl Med. 1992;33(5):633–42.
11. Patlak CS, Blasberg RG, Fenstermacher JD. Graphical evaluation of blood-to-brain transfer constants from multiple-time uptake data. J Cereb Blood Flow Metab. 1983;3(1):1–7.
12. Pfannkuchen N, Meckel M, Bergmann R, Bachmann M, Bal C, Sathekge M, et al. Novel radiolabeled bisphosphonates for PET diagnosis and endoradiotherapy of bone metastases. Pharmaceuticals (Basel). 2017;10(2). pii: E45. https://doi.org/10.3390/ph10020045.
13. Holub J, Meckel M, Kubicek V, Rosch F, Hermann P. Gallium(III) complexes of NOTA-bis (phosphonate) conjugates as PET radiotracers for bone imaging. Contrast Media Mol Imaging. 2015;10(2):122–34.
14. Bastiaannet E, Groen H, Jager PL, Cobben DC, van der Graaf WT, Vaalburg W, et al. The value of FDG-PET in the detection, grading and response to therapy of soft tissue and bone sarcomas; a systematic review and meta-analysis. Cancer Treat Rev. 2004;30(1):83–101.
15. Biermann S, Chow W, Reed DR, Lucas D, Adkins DR, Agulnik M, et al. NCCN Guidelines® insights – bone cancer, Version 2.2017. Featured updates to the NCCN guidelines. J Natl Compr Cancer Netw. 2017;15(2):155–67.
16. Charest M, Hickeson M, Lisbona R, Novales-Diaz JA, Derbekyan V, Turcotte RE. FDG PET/CT imaging in primary osseous and soft tissue sarcomas: a retrospective review of 212 cases. Eur J Nucl Med Mol Imaging. 2009;36(12):1944–51.
17. Fuglo HM, Jorgensen SM, Loft A, Hovgaard D, Petersen MM. The diagnostic and prognostic value of ^{18}F-FDG PET/CT in the initial assessment of high-grade bone and soft tissue sarcoma. A retrospective study of 89 patients. Eur J Nucl Med Mol Imaging. 2012;39(9):1416–24.
18. Mirabello L, Troisi RJ, Savage SA. Osteosarcoma incidence and survival rates from 1973 to 2004: data from the Surveillance, Epidemiology, and End Results Program. Cancer. 2009;115(7):1531–43.
19. Peller PJ. Role of positron emission tomography/computed tomography in bone malignancies. Radiol Clin North Am. 2013;51(5):845–64.
20. Quartuccio N, Treglia G, Salsano M, Mattoli MV, Muoio B, Piccardo A, et al. The role of Fluorine-18-Fluorodeoxyglucose positron emission tomography in staging and restaging of patients with osteosarcoma. Radiol Oncol. 2013;47(2):97–102.
21. Schulte M, Brecht-Krauss D, Heymer B, Guhlmann A, Hartwig E, Sarkar MR, et al. Grading of tumors and tumor-like lesions of bone: evaluation by FDG PET. J Nucl Med. 2000;41(10):1695–701.
22. Tateishi U, Yamaguchi U, Seki K, Terauchi T, Arai Y, Kim EE. Bone and soft-tissue sarcoma: preoperative staging with fluorine 18 fluorodeoxyglucose PET/CT and conventional imaging. Radiology. 2007;245(3):839–47.
23. London K, Stege C, Cross S, Onikul E, Graf N, Kaspers G, et al. ^{18}F-FDG PET/CT compared to conventional imaging modalities in pediatric primary bone tumors. Pediatr Radiol. 2012;42(4):418–30.

24. Hongtao L, Hui Z, Bingshun W, Xiaojin W, Zhiyu W, Shuier Z, et al. ^{18}F-FDG positron emission tomography for the assessment of histological response to neoadjuvant chemotherapy in osteosarcomas: a meta-analysis. Surg Oncol. 2012;21(4):e165–70.
25. Gaston LL, Di Bella C, Slavin J, Hicks RJ, Choong PF. ^{18}F-FDG PET response to neoadjuvant chemotherapy for Ewing sarcoma and osteosarcoma are different. Skelet Radiol. 2011;40(8):1007–15.
26. Cheon GJ, Kim MS, Lee JA, Lee SY, Cho WH, Song WS, et al. Prediction model of chemotherapy response in osteosarcoma by ^{18}F-FDG PET and MRI. J Nucl Med. 2009;50(9):1435–40.
27. Healey JH, Ghelman B. Osteoid osteoma and osteoblastoma. Current concepts and recent advances. Clin Orthop Relat Res. 1986;(204):76–85.
28. Kransdorf MJ, Stull MA, Gilkey FW, Moser RP Jr. Osteoid osteoma. Radiographics. 1991;11(4):671–96.
29. Iyer RS, Chapman T, Chew FS. Pediatric bone imaging: diagnostic imaging of osteoid osteoma. AJR Am J Roentgenol. 2012;198(5):1039–52.
30. Saccomanni B. Osteoid osteoma and osteoblastoma of the spine: a review of the literature. Curr Rev Musculoskelet Med. 2009;2(1):65–7.
31. Chotel F, Franck F, Solla F, Dijoud F, Kohler R, Berard J, et al. Osteoid osteoma transformation into osteoblastoma: fact or fiction? Orthop Traumatol Surg Res. 2012;98(6 Suppl):S98–S104.
32. Kole AC, Nieweg OE, Hoekstra HJ, van Horn JR, Koops HS, Vaalburg W. Fluorine-18-fluorodeoxyglucose assessment of glucose metabolism in bone tumors. J Nucl Med. 1998;39(5):810–5.
33. Al-Muqbel KM, Al-Omari MH, Audat ZA, Alqudah MA. Osteoblastoma is a metabolically active benign bone tumor on ^{18}F-FDG PET imaging. J Nucl Med Technol. 2013;41(4):308–10.
34. Brenner W, Bohuslavizki KH, Eary JF. PET imaging of osteosarcoma. J Nucl Med. 2003;44(6):930–42.
35. Volker T, Denecke T, Steffen I, Misch D, Schonberger S, Plotkin M, et al. Positron emission tomography for staging of pediatric sarcoma patients: results of a prospective multicenter trial. J Clin Oncol. 2007;25(34):5435–41.
36. Bredella MA, Caputo GR, Steinbach LS. Value of FDG positron emission tomography in conjunction with MR imaging for evaluating therapy response in patients with musculoskeletal sarcomas. AJR Am J Roentgenol. 2002;179(5):1145–50.
37. Hyun OJ, Luber BS, Leal JP, Wang H, Bolejack V, Schuetze SM, et al. Response to early treatment evaluated with ^{18}F-FDG PET and PERCIST 1.0 predicts survival in patients with Ewing sarcoma family of tumors treated with a monoclonal antibody to the insulin-like growth factor 1 receptor. J Nucl Med. 2016;57(5):735–40.
38. Eary JF, Conrad EU, Bruckner JD, Folpe A, Hunt KJ, Mankoff DA, et al. Quantitative [F-18]fluorodeoxyglucose positron emission tomography in pretreatment and grading of sarcoma. Clin Cancer Res. 1998;4(5):1215–20.
39. Hwang JP, Lim I, Kong CB, Jeon DG, Byun BH, Kim BI, et al. Prognostic value of SUV_{max} measured by pretreatment fluorine-18 fluorodeoxyglucose positron emission tomography/computed tomography in patients with Ewing sarcoma. PLoS One. 2016;11(4):e0153281. https://doi.org/10.1371/journal.pone.0153281.
40. Hawkins DS, Schuetze SM, Butrynski JE, Rajendran JG, Vernon CB, Conrad EU III, et al. [^{18}F]Fluorodeoxyglucose positron emission tomography predicts outcome for Ewing sarcoma family of tumors. J Clin Oncol. 2005;23(8834):8828–34.
41. Lee FY, Yu J, Chang SS, Fawwaz R, Parisien MV. Diagnostic value and limitations of fluorine-18 fluorodeoxyglucose positron emission tomography for cartilaginous tumors of bone. J Bone Joint Surg Am. 2004;86-A(12):2677–85.
42. Feldman F, Van Heertum R, Saxena C, Parisien M. ^{18}FDG-PET applications for cartilage neoplasms. Skelet Radiol. 2005;34(7):367–74.
43. Kransdorf MJ, Moser RP Jr, Gilkey FW. Fibrous dysplasia. Radiographics. 1990;10(3):519–37.
44. Fitzpatrick KA, Taljanovic MS, Speer DP, Graham AR, Jacobson JA, Barnes GR, et al. Imaging findings of fibrous dysplasia with histopathologic and intraoperative correlation. AJR Am J Roentgenol. 2004;182(6):1389–98.
45. D'Souza MM, Jaimini A, Khurana A, Tripathi M, Sharma R, Mondal A, et al. Polyostotic fibrous dysplasia on F-18 FDG PET/CT imaging. Clin Nucl Med. 2009;34(6):359–61.
46. Case DB, Chapman CN Jr, Freeman JK, Polga JP. Best cases from the AFIP: atypical presentation of polyostotic fibrous dysplasia with myxoma (Mazabraud syndrome). Radiographics. 2010;30(3):827–32.
47. Berrebi O, Steiner C, Keller A, Rougemont AL, Ratib O. F-18 fluorodeoxyglucose (FDG) PET in the diagnosis of malignant transformation of fibrous dysplasia in the pelvic bones. Clin Nucl Med. 2008;33(7):469–71.
48. Qu N, Yao W, Cui X, Zhang H. Malignant transformation in monostotic fibrous dysplasia: clinical features, imaging features, outcomes in 10 patients, and review. Medicine (Baltimore). 2015;94(3):e369.
49. Murphey MD, Nomikos GC, Flemming DJ, Gannon FH, Temple HT, Kransdorf MJ. From the archives of AFIP. Imaging of giant cell tumor and giant cell reparative granuloma of bone: radiologic-pathologic correlation. Radiographics. 2001;21(5):1283–309.
50. Aoki J, Watanabe H, Shinozaki T, Takagishi K, Ishijima H, Oya N, et al. FDG PET of primary benign and malignant bone tumors: standardized uptake value in 52 lesions. Radiology. 2001;219(3):774–7.
51. Strauss LG, Dimitrakopoulou-Strauss A, Koczan D, Bernd L, Haberkorn U, Ewerbeck V, et al. ^{18}F-FDG kinetics and gene expression in giant cell tumors. J Nucl Med. 2004;45(9):1528–35.
52. O'Connor W, Quintana M, Smith S, Willis M, Renner J. The hypermetabolic giant: ^{18}F-FDG avid giant cell tumor identified on PET-CT. J Radiol Case Rep. 2014;8(6):27–38.
53. Davila D, Antoniou A, Chaudhry MA. Evaluation of osseous metastasis in bone scintigraphy. Semin Nucl Med. 2015;45:3–15.. Erratum in: Semin Nucl Med. 2015;45:266
54. Even-Sapir E. Imaging of malignant bone involvement by morphologic, scintigraphic, and hybrid modalities. J Nucl Med. 2005;46:1356–67.
55. Mariani G, Bruselli L, Kuwert T, Kim EE, Flotats A, Israel O, et al. A review on the clinical uses of SPECT/CT. Eur J Nucl Med Mol Imaging. 2010;37(10):1959–85.
56. Schmitz A, Risse JH, Textor J, Zander D, Biersack HJ, Schmitt O, et al. FDG-PET findings of vertebral compression fractures in osteoporosis: preliminary results. Osteoporos Int. 2002;13(9):755–61.
57. Bush LA, Chew FS. Subtrochanteric femoral insufficiency fracture in woman on bisphosphonate therapy for glucocorticoid-induced osteoporosis. Radiol Case Rep. 2009;4(1):261.
58. Patel RN, Ashraf A, Sundaram M. Atypical fractures following bisphosphonate therapy. Semin Musculoskelet Radiol. 2016;20(4):376–81.
59. Raynor W, Houshmand S, Gholami S, Emamzadehfard S, Rajapakse CS, Blomberg BA, et al. Evolving role of molecular imaging with ^{18}F-sodium fluoride PET as a biomarker for calcium metabolism. Curr Osteoporos Rep. 2016;14(4):115–25.
60. Siddique M, Blake GM, Frost ML, Moore AE, Puri T, Marsden PK, et al. Estimation of regional bone metabolism from whole-body ^{18}F-fluoride PET static images. Eur J Nucl Med Mol Imaging. 2012;39(2):337–43.

61. Siddique M, Frost ML, Moore AE, Fogelman I, Blake GM. Correcting ^{18}F-fluoride PET static scan measurements of skeletal plasma clearance for tracer efflux from bone. Nucl Med Commun. 2014;35(3):303–10.
62. Fogelman I, McKillop JH, Bessent RG, Boyle IT, Turner JG, Greig WR. The role of bone scanning in osteomalacia. J Nucl Med. 1978;19(3):245–8.
63. Chakraborty PP, Bhattacharjee R, Mukhopadhyay S, Chowdhury S. 'Rachitic rosary sign' and 'tie sign' of the sternum in tumour-induced osteomalacia. BMJ Case Rep. 2016. pii: bcr2016214766. https://doi.org/10.1136/bcr-2016-214766.
64. Kaneuchi Y, Hakozaki M, Yamada H, Hasegawa O, Tajino T, Konno S. Missed causative tumors in diagnosing tumor-induced osteomalacia with ^{18}F-FDG PET/CT: a potential pitfall of standard-field imaging. Hell J Nucl Med. 2016;19(1):46–8.
65. Jain AS, Shelley S, Muthukrishnan I, Kalal S, Amalachandran J, Chandran S. Diagnostic importance of contrast enhanced ^{18}F-fluorodeoxyglucose positron emission computed tomography in patients with tumor induced osteomalacia: our experience. Indian J Nucl Med. 2016;31(1):14–9.
66. Breer S, Brunkhorst T, Beil FT, Peldschus K, Heiland M, Klutmann S, et al. ^{68}Ga DOTA-TATE PET/CT allows tumor localization in patients with tumor-induced osteomalacia but negative ^{111}In-octreotide SPECT/CT. Bone. 2014;64:222–7.
67. Agrawal K, Bhadada S, Mittal BR, Shukla J, Sood A, Bhattacharya A, et al. Comparison of ^{18}F-FDG and ^{68}Ga DOTATATE PET/CT in localization of tumor causing oncogenic osteomalacia. Clin Nucl Med. 2015;40(1):e6–e10.
68. Bhavani N, Reena Asirvatham A, Kallur K, Menon AS, Pavithran PV, Nair V, et al. Utility of Gallium-68 DOTANOC PET/CT in the localization of Tumour-induced osteomalacia. Clin Endocrinol. 2016;84(1):134–40.
69. Gahier Penhoat M, Drui D, Ansquer C, Mirallie E, Maugars Y, Guillot P. Contribution of 18-FDG PET/CT to brown tumor detection in a patient with primary hyperparathyroidism. Joint Bone Spine. 2017;84(2):209–12.
70. Niemann KE, Kropil F, Hoffmann MF, Coulibaly MO, Schildhauer TA. A 23-year-old patient with secondary tumoral calcinosis: regression after subtotal parathyroidectomy: a case report. Int J Surg Case Rep. 2016;23:56–60.
71. Ando T, Mochizuki Y, Iwata T, Nishikido M, Shimazaki T, Furumoto A, et al. Aggressive pulmonary calcification developed after living donor kidney transplantation in a patient with primary hyperparathyroidism. Transplant Proc. 2013;45(7):2825–30.
72. Hwang GJ, Lee JD, Park CY, Lim SK. Reversible extraskeletal uptake of bone scanning in primary hyperparathyroidism. J Nucl Med. 1996;37(3):469–71.
73. Terry DW Jr, Isitman AT, Holmes RA. Radionuclide bone images in hypertrophic pulmonary osteoarthropathy. Am J Roentgenol Radium Ther Nucl Med. 1975;124(4):571–6.
74. Fredericson M, Bergman AG, Hoffman KL, Dillingham MS. Tibial stress reaction in runners. Correlation of clinical symptoms and scintigraphy with a new magnetic resonance imaging grading system. Am J Sports Med. 1995;23(4):472–81.
75. Kijowski R, Choi J, Shinki K, Del Rio AM, De Smet A. Validation of MRI classification system for tibial stress injuries. AJR Am J Roentgenol. 2012;198(4):878–84.
76. Sofka CM. Imaging of stress fractures. Clin Sports Med. 2006;25(1):53–62.
77. Fujii M, Abe K, Hayashi K, Kosuda S, Yano F, Watanabe S, et al. Honda sign and variants in patients suspected of having a sacral insufficiency fracture. Clin Nucl Med. 2005;30(3):165–9.
78. Joshi P, Lele V, Gandhi R, Parab A. Honda sign on 18-FDG PET/CT in a case of lymphoma leading to incidental detection of sacral insufficiency fracture. J Clin Imaging Sci. 2012;2:29.
79. Murphey MD, Foreman KL, Klassen-Fischer MK, Fox MG, Chung EM, Kransdorf MJ. From the radiologic pathology archives imaging of osteonecrosis: radiologic-pathologic correlation. Radiographics. 2014;34(4):1003–28.
80. Lavernia CJ, Sierra RJ, Grieco FR. Osteonecrosis of the femoral head. J Am Acad Orthop Surg. 1999;7(4):250–61.
81. Beckmann J, Matsuura M, Grässel S, Kock F, Grifka J, Tingart M. A μCT analysis of the femoral bone stock in osteonecrosis of the femoral head compared to osteoarthrosis. Arch Orthop Trauma Surg. 2009;129(4):501–5.
82. Theodorou DJ, Malizos KN, Beris AE, Theodorou SJ, Soucacos PN. Multimodal imaging quantitation of the lesion size in osteonecrosis of the femoral head. Clin Orthop Relat Res. 2001;386:54–63.
83. Yeh LR, Chen CK, Huang YL, Pan HB, Yang CF. Diagnostic performance of MR imaging in the assessment of subchondral fractures in avascular necrosis of the femoral head. Skelet Radiol. 2009;38(6):559–64.
84. Balakrishnan A, Schemitsch EH, Pearce D, McKee MD. Distinguishing transient osteoporosis of the hip from avascular necrosis. Can J Surg. 2003;46(3):187–92.
85. Ikemura S, Yamamoto T, Motomura G, Nakashima Y, Mawatari T, Iwamoto Y. MRI evaluation of collapsed femoral heads in patients 60 years old or older: differentiation of subchondral insufficiency fracture from osteonecrosis of the femoral head. AJR Am J Roentgenol. 2010;195(1):W63–8.
86. Kim HK, Kaste S, Dempsey M, Wilkes D. A comparison of non-contrast and contrast-enhanced MRI in the initial stage of Legg-Calve-Perthes disease. Pediatr Radiol. 2013;43(9):1166–73.
87. Du J, Lu A, Dempsey M, Herring JA, Kim HK. MR perfusion index as a quantitative method of evaluating epiphyseal perfusion in Legg-Calve-Perthes disease and correlation with short-term radiographic outcome: a preliminary study. J Pediatr Orthop. 2013;33(7):707–13.
88. Chan WP, Liu YJ, Huang GS, Lin MF, Huang S, Chang YC, et al. Relationship of idiopathic osteonecrosis of the femoral head to perfusion changes in the proximal femur by dynamic contrast-enhanced MRI. AJR Am J Roentgenol. 2011;196(3):637–43.
89. Kaushik A, Sankaran B, Varghese M. Prognostic value of dynamic MRI in assessing post-traumatic femoral head vascularity. Skelet Radiol. 2009;38(6):565–9.
90. Goldsmith DP, Vivino FB, Eichenfield AH, Athreya BH, Heyman S. Nuclear imaging and clinical features of childhood reflex neurovascular dystrophy: comparison with adults. Arthritis Rheum. 1989;32:480–5.
91. Kobayashi N, Inaba Y, Tateishi U, Yukizawa Y, Ike H, Inoue T, et al. New application of ^{18}F-fluoride PET for the detection of bone remodeling in early-stage osteoarthritis of the hip. Clin Nucl Med. 2013;38(10):e379–83.
92. Kobayashi N, Inaba Y, Tateishi U, Ike H, Kubota S, Inoue T, et al. Comparison of ^{18}F-fluoride positron emission tomography and magnetic resonance imaging in evaluating early-stage osteoarthritis of the hip. Nucl Med Commun. 2015;36(1):84–9.
93. Hirata Y, Inaba Y, Kobayashi N, Ike H, Yukizawa Y, Fujimaki H, et al. Correlation between mechanical stress by finite element analysis and ^{18}F-fluoride PET uptake in hip osteoarthritis patients. J Orthop Res. 2015;33(1):78–83.
94. Lew DP, Waldvogel FA. Osteomyelitis. N Engl J Med. 1997;336(14):999–1007.
95. Lew DP, Waldvogel FA. Osteomyelitis. Lancet. 2004;364(9431):369–79.
96. Riise OR, Kirkhus E, Handeland KS, Flato B, Reiseter T, Cvancarova M, et al. Childhood osteomyelitis-incidence and differentiation from other acute onset musculoskeletal features in a population-based study. BMC Pediatr. 2008;8:45.

97. Cierny G III, Mader JT, Penninck JJ. A clinical staging system for adult osteomyelitis. Clin Orthop Relat Res. 2003;414:7–24.
98. Chianelli M, Boerman OC, Malviya G, Galli F, Oyen WJ, Signore A. Receptor binding ligands to image infection. Curr Pharm Des. 2008;14(31):3316–25.
99. Weon YC, Yang SO, Choi YY, Shin JW, Ryu JS, Shin MJ, et al. Use of Tc-99m HMPAO leukocyte scans to evaluate bone infection: incremental value of additional SPECT images. Clin Nucl Med. 2000;25(7):519–26.
100. Palestro CJ, Swyer AJ, Kim CK, Goldsmith SJ. Infected knee prosthesis: diagnosis with In-111 leukocyte, Tc-99m sulfur colloid, and Tc-99m MDP imaging. Radiology. 1991;179(3):645–8.
101. Palestro CJ, Love C, Tronco GG, Tomas MB, Rini JN. Combined labeled leukocyte and technetium 99m sulfur colloid bone marrow imaging for diagnosing musculoskeletal infection. Radiographics. 2006;26(3):859–70.
102. Pakos EE, Trikalinos TA, Fotopoulos AD, Ioannidis JP. Prosthesis infection: diagnosis after total joint arthroplasty with antigranulocyte scintigraphy with ^{99m}Tc-labeled monoclonal antibodies – a meta-analysis. Radiology. 2007;242(1):101–8.
103. Meller J, Liersch T, Oezerden MM, Sahlmann CO, Meller B. Targeting NCA-95 and other granulocyte antigens and receptors with radiolabeled monoclonal antibodies (Mabs). Q J Nucl Med Mol Imaging. 2010;54(6):582–98.
104. Ruf J, Oeser C, Amthauer H. Clinical role of anti-granulocyte MoAb versus radiolabeled white blood cells. Q J Nucl Med Mol Imaging. 2010;54(6):599–616.
105. Richter WS, Ivancevic V, Meller J, Lang O, Le Guludec D, Szilvazi I, et al. ^{99m}Tc-besilesomab (Scintimun) in peripheral osteomyelitis: comparison with ^{99m}Tc-labelled white blood cells. Eur J Nucl Med Mol Imaging. 2011;38(5):899–910.
106. Prandini N, Feggi L, Massari L. Diagnosis of bone infections using ^{99m}Tc-HMPAO labelled leukocytes. Nucl Med Commun. 2002;23(12):1245–8.
107. Chen SH, Ho KC, Hsieh PH, Lee MS, Yen TC. Potential clinical role of ^{18}F FDG-PET/CT in detecting hip prosthesis infection: a study in patients undergoing two-stage revision arthroplasty with an interim spacer. Q J Nucl Med Mol Imaging. 2010;54(4):429–35.
108. Gemmel F, Van den Wyngaert H, Love C, Welling MM, Gemmel P, Palestro CJ. Prosthetic joint infections: radionuclide state-of-the-art imaging. Eur J Nucl Med Mol Imaging. 2012;39(5):892–909.
109. Rini JN, Palestro CJ. Imaging of infection and inflammation with ^{18}F-FDG-labeled leukocytes. Q J Nucl Med Mol Imaging. 2006;50(2):143–6.
110. Calderone RR, Larsen JM. Overview and classification of spinal infections. Orthop Clin North Am. 1996;27(1):1–8.
111. Gouliouris T, Aliyu SH, Brown NM. Spondylodiscitis: update on diagnosis and management. J Antimicrob Chemother. 2010;65(Suppl 3):iii11–24.
112. Prandini N, Lazzeri E, Rossi B, Erba P, Parisella MG, Signore A. Nuclear medicine imaging of bone infections. Nucl Med Commun. 2006;27(8):633–44.
113. Gratz S, Dorner J, Oestmann JW, Opitz M, Behr T, Meller J, et al. ^{67}Ga-citrate and ^{99}Tc^{m}-MDP for estimating the severity of vertebral osteomyelitis. Nucl Med Commun. 2000;21(1):111–20.
114. Fuster D, Sola O, Soriano A, Monegal A, Setoain X, Tomas X, et al. A prospective study comparing whole-body FDG PET/CT to combined planar bone scan with ^{67}Ga SPECT/CT in the diagnosis of spondylodiskitis. Clin Nucl Med. 2012;37(9):827–32.
115. Love C, Palestro CJ. Nuclear medicine imaging of bone infections. Clin Radiol. 2016;71(7):632–46.
116. Pauwels EK, Ribeiro MJ, Stoot JH, McCready VR, Bourguignon M, Maziere B. FDG accumulation and tumor biology. Nucl Med Biol. 1998;25(4):317–22.
117. Kubota R, Yamada S, Kubota K, Ishiwata K, Tamahashi N, Ido T. Intratumoral distribution of fluorine-18-fluorodeoxyglucose in vivo: high accumulation in macrophages and granulation tissues studied by microautoradiography. J Nucl Med. 1992;33(11):1972–80.
118. Yamada S, Kubota K, Kubota R, Ido T, Tamahashi N. High accumulation of fluorine-18-fluorodeoxyglucose in turpentine-induced inflammatory tissue. J Nucl Med. 1995;36(7):1301–6.
119. Kaim AH, Weber B, Kurrer MO, Gottschalk J, Von Schulthess GK, Buck A. Autoradiographic quantification of ^{18}F-FDG uptake in experimental soft-tissue abscesses in rats. Radiology. 2002;223(2):446–51.
120. Ohtori S, Suzuki M, Koshi T, Yamashita M, Yamauchi K, Inoue G, et al. ^{18}F-fluorodeoxyglucose-PET for patients with suspected spondylitis showing Modic change. Spine. 2010;35(26):E1599–603.
121. Kim SJ, Kim IJ, Suh KT, Kim YK, Lee JS. Prediction of residual disease of spine infection using F-18 FDG PET/CT. Spine. 2009;34(22):2424–30.
122. Ito K, Kubota K, Morooka M, Hasuo K, Kuroki H, Mimori A. Clinical impact of ^{18}F-FDG PET/CT on the management and diagnosis of infectious spondylitis. Nucl Med Commun. 2010;31(8):691–8.
123. Nanni C, Boriani L, Salvadori C, Zamparini E, Rorato G, Ambrosini V, et al. FDG PET/CT is useful for the interim evaluation of response to therapy in patients affected by haematogenous spondylodiscitis. Eur J Nucl Med Mol Imaging. 2012;39(10):1538–44.
124. Hungenbach S, Delank KS, Dietlein M, Eysel P, Drzezga A, Schmidt MC. ^{18}F-fluorodeoxyglucose uptake pattern in patients with suspected spondylodiscitis. Nucl Med Commun. 2013;34(11):1068–74.
125. Riccio SA, Chu AK, Rabin HR, Kloiber R. Fluorodeoxyglucose positron emission tomography/computed tomography interpretation criteria for assessment of antibiotic treatment response in pyogenic spine infection. Can Assoc Radiol J. 2015;66(2):145–52.
126. Lee IS, Lee JS, Kim SJ, Jun S, Suh KT. Fluorine-18-fluorodeoxyglucose positron emission tomography/computed tomography imaging in pyogenic and tuberculous spondylitis: preliminary study. J Comput Assist Tomogr. 2009;33(4):587–92.
127. Mazzie JP, Brooks MK, Gnerre J. Imaging and management of postoperative spine infection. Neuroimaging Clin North Am. 2014;24(2):365–74.
128. Fuster D, Tomas X, Granados U, Soriano A. Prospective comparison of whole-body ^{18}F-FDG PET/CT and MRI of the spine in the diagnosis of haematogenous spondylodiscitis: response to comments by Soussan. Eur J Nucl Med Mol Imaging. 2015;42(2):356–7.
129. Skanjeti A, Penna D, Douroukas A, Cistaro A, Arena V, Leo G, et al. PET in the clinical work-up of patients with spondylodiscitis: a new tool for the clinician? Q J Nucl Med Mol Imaging. 2012;56(6):569–76.
130. Rosen RS, Fayad L, Wahl RL. Increased ^{18}F-FDG uptake in degenerative disease of the spine: characterization with ^{18}F-FDG PET/CT. J Nucl Med. 2006;47(8):1274–80.
131. Blom AW, Brown J, Taylor AH, Pattison G, Whitehouse S, Bannister GC. Infection after total knee arthroplasty. J Bone Joint Surg Br. 2004;86(5):688–91.
132. Kurtz S, Mowat F, Ong K, Chan N, Lau E, Halpern M. Prevalence of primary and revision total hip and knee arthroplasty in the United States from 1990 through 2002. J Bone Joint Surg Am. 2005;87(7):1487–97.
133. Parvizi J, Della Valle CJ. AAOS clinical practice guideline: diagnosis and treatment of periprosthetic joint infections of the hip and knee. J Am Acad Orthop Surg. 2010;18(12):771–2.
134. Parvizi J, Zmistowski B, Adeli B. Periprosthetic joint infection: treatment options. Orthopedics. 2010;33(9):659.

135. Zimmerli W, Trampuz A, Ochsner PE. Prosthetic-joint infections. N Engl J Med. 2004;351(16):1645–54.
136. Duus BR, Boeckstyns M, Kjaer L, Stadeager C. Radionuclide scanning after total knee replacement: correlation with pain and radiolucent lines. A prospective study. Investig Radiol. 1987;22(11):891–4.
137. Sousa R, Massada M, Pereira A, Fontes F, Amorim I, Oliveira A. Diagnostic accuracy of combined ^{99m}Tc-sulesomab and ^{99m}Tc-nanocolloid bone marrow imaging in detecting prosthetic joint infection. Nucl Med Commun. 2011;32(9):834–9.
138. van der Bruggen W, Bleeker-Rovers CP, Boerman OC, Gotthardt M, Oyen WJ. PET and SPECT in osteomyelitis and prosthetic bone and joint infections: a systematic review. Semin Nucl Med. 2010;40(1):3–15.
139. Delank KS, Schmidt M, Michael JW, Dietlein M, Schicha H, Eysel P. The implications of ^{18}F-FDG PET for the diagnosis of endoprosthetic loosening and infection in hip and knee arthroplasty: results from a prospective, blinded study. BMC Musculoskelet Disord. 2006;7:20.
140. Estrada WN, Kim CK. Paget's disease in a patient with breast cancer. J Nucl Med. 1993;34(7):1214–6.
141. van Heerden BB, Prins MJ. The value of pinhole collimator imaging in the scintigraphic analysis of vertebral diseases. S Afr Med J. 1989;75(6):280–3.
142. Mirra JM, Brien EW, Tehranzadeh J. Paget's disease of bone: review with emphasis on radiologic features, Part I. Skelet Radiol. 1995;24(3):163–71.
143. Mangham DC, Davie MW, Grimer RJ. Sarcoma arising in Paget's disease of bone: declining incidence and increasing age at presentation. Bone. 2009;44(3):431–6.
144. Bush LA, Toresdahl B, Hoch B, Chew FS. Falsely negative F-18 FDG PET of osteosarcoma arising in Paget disease. Radiol Case Rep. 2009;4(3):295.
145. Hadjipavlou A, Lander P, Srolovitz H, Enker IP. Malignant transformation in Paget disease of bone. Cancer. 1992;70(12):2802–8.
146. Sundaram M, Khanna G, El-Khoury GY. T1-weighted MR imaging for distinguishing large osteolysis of Paget's disease from sarcomatous degeneration. Skelet Radiol. 2001;30(7):378–83.
147. Cook GJ, Maisey MN, Fogelman I. Fluorine-18-FDG PET in Paget's disease of bone. J Nucl Med. 1997;38(9):1495–7.
148. Bourgeois S, Gykiere P, Goethals L, Everaert H, De Geeter FW. Aspecific uptake of ^{68}GA-PSMA in Paget disease of the bone. Clin Nucl Med. 2016;41(11):877–8.
149. Giovacchini G, Samanes Gajate AM, Messa C, Fazio F. Increased C-11 choline uptake in pagetic bone in a patient with coexisting skeletal metastases from prostate cancer. Clin Nucl Med. 2008;33(11):797–8.
150. Cook GJ, Blake GM, Marsden PK, Cronin B, Fogelman I. Quantification of skeletal kinetic indices in Paget's disease using dynamic ^{18}F-fluoride positron emission tomography. J Bone Miner Res. 2002;17(5):854–9.
151. Coleman RE. Metastatic bone disease: clinical features, pathophysiology and treatment strategies. Cancer Treat Rev. 2001;27:165–75.
152. Hage WD, Aboulafia AJ, Aboulafia DM. Incidence, location, and diagnostic evaluation of metastatic bone disease. Orthop Clin North Am. 2000;31:515–28.
153. Macedo F, Ladeira K, Pinho F, Saraiva N, Bonito N, Pinto L, Goncalves F. Bone metastases: an overview. Oncol Rev. 2017;11(1):321. https://doi.org/10.4081/oncol.2017.321.
154. Mantyh PW, Clohisy DR, Koltzenburg M, Hunt SP. Molecular mechanisms of cancer pain. Nat Rev Cancer. 2002;2:201–9.
155. Kougioumtzopoulou A, Zygogianni A, Liakouli Z, Kypraiou E, Kouloulias V. The role of radiotherapy in bone metastases: a critical review of current literature. Eur J Cancer Care (Engl). 2017;26(6) https://doi.org/10.1111/ecc.12724.. Epub 2017 Jun 20
156. Shiloh R, Krishnan M. Radiation for treatment of painful bone metastases. Hematol Oncol Clin North Am. 2018;32:459–68.
157. Krishnamurthy GT, Krishnamurthy S. Radionuclides for metastatic bone pain palliation: a need for rational re-evaluation in the new millennium. J Nucl Med. 2000;41:688–91.
158. Silberstein EB, Buscombe JR, McEwan A, Taylor AT Jr. Society of Nuclear Medicine Procedure Guideline for Palliative Treatment of Painful Bone Metastases. Version 3.0. snmmi.files.cms-plus.com/docs/pg_ch25_0403.pdf. Accessed 25 Jan 2003.
159. Bodei L, Lam M, Chiesa C, Flux G, Brans B, Chiti A, et al. EANM procedure guideline for treatment of refractory metastatic bone pain. Eur J Nucl Med Mol Imaging. 2008;35:1934–40.
160. Handkiewicz-Junak D, Poeppel TD, Bodei L, Aktolun C, Ezziddin S, Giammarile F, et al. EANM guidelines for radionuclide therapy of bone metastases with beta-emitting radionuclides. Eur J Nucl Med Mol Imaging. 2018;45:846–59.
161. Abruzzese E, Iuliano F, Trawinska MM, Di Maio M. ^{153}Sm: its use in multiple myeloma and report of a clinical experience. Expert Opin Investig Drugs. 2008;17:1379–87.
162. Dispenzieri A, Wiseman GA, Lacy MQ, Hayman SR, Kumar SK, Buadi F, et al. A phase II study of ^{153}Sm-EDTMP and high-dose melphalan as a peripheral blood stem cell conditioning regimen in patients with multiple myeloma. Am J Hematol. 2010;85:409–13.
163. Berenson JR, Yellin O, Patel R, Duvivier H, Nassir Y, Mapes R, et al. A phase I study of samarium lexidronam/bortezomib combination therapy for the treatment of relapsed or refractory multiple myeloma. Clin Cancer Res. 2009;15:1069–75.
164. McQuay HJ, Collins SL, Carroll D, Moore RA. Radiotherapy for the palliation of painful bone metastases. Cochrane Database Syst Rev. 2000;(2):CD001793.
165. Bauman G, Charette M, Reid R, Sathya J. Radiopharmaceuticals for the palliation of painful bone metastasis-a systemic review. Radiother Oncol. 2005;75:258–70.
166. Finlay IG, Mason MD, Shelley M. Radioisotopes for the palliation of metastatic bone cancer: a systematic review. Lancet Oncol. 2005;6:392–400.
167. Reisfield GM, Silberstein EB, Wilson GR. Radiopharmaceuticals for the palliation of painful bone metastases. Am J Hosp Palliat Care. 2005;22:41–6.
168. Christensen MH, Petersen LJ. Radionuclide treatment of painful bone metastases in patients with breast cancer: a systematic review. Cancer Treat Rev. 2012;38:164–71.
169. D'Angelo G, Sciuto R, Salvatori M, Sperduti I, Mantini G, Maini CL, et al. Targeted "bone-seeking" radiopharmaceuticals for palliative treatment of bone metastases: a systematic review and meta-analysis. Q J Nucl Med Mol Imaging. 2012;56:538–43.
170. Tomblyn M. The role of bone-seeking radionuclides in the palliative treatment of patients with painful osteoblastic skeletal metastases. Cancer Control. 2012;19:137–44.
171. Tunio M, Al Asiri M, Al Hadab A, Bayoumi Y. Comparative efficacy, tolerability, and survival outcomes of various radiopharmaceuticals in castration-resistant prostate cancer with bone metastasis: a meta-analysis of randomized controlled trials. Drug Des Devel Ther. 2015;9:5291–9.
172. Jong JM, Oprea-Lager DE, Hooft L, de Klerk JM, Bloemendal HJ, Verheul HM, et al. Radiopharmaceuticals for palliation of bone pain in patients with castration-resistant prostate cancer metastatic to bone: a systematic review. Eur Urol. 2016;70:416–26.
173. Zacho HD, Karthigaseu NN, Fonager RF, Petersen LJ. Treatment with bone-seeking radionuclides for painful bone metastases in patients with lung cancer: a systematic review. BMJ Support Palliat Care. 2017;7:230–7.

174. Sartor O, Reid RH, Bushnell DL, Quick DP, Ell PJ. Safety and efficacy of repeat administration of samarium Sm-153 lexidronam to patients with metastatic bone pain. Cancer. 2007;109:637–43.
175. Parker C, Nilsson S, Heinrich D, Helle SI, O'Sullivan JM, Fosså SD, et al. Alpha emitter radium-223 and survival in metastatic prostate cancer. N Engl J Med. 2013;369:213–23.
176. Sartor O, Coleman R, Nilsson S, Heinrich D, Helle SI, O'Sullivan JM, et al. Effect of radium-223 dichloride on symptomatic skeletal events in patients with castration-resistant prostate cancer and bone metastases: results from a phase 3, double-blind, randomised trial. Lancet Oncol. 2014;15:738–46.
177. Parker CC, Coleman RE, Sartor O, Vogelzang NJ, Bottomley D, Heinrich D, et al. Three-year safety of radium-223 dichloride in patients with castration-resistant prostate cancer and symptomatic bone metastases from Phase 3 randomized Alpharadin in symptomatic prostate cancer trial. Eur Urol. 2017; https://doi.org/10.1016/j.eururo.2017.06.021.
178. Poeppel TD, Handkiewicz-Junak D, Andreeff M, Becherer A, Bockisch A, Fricke E, et al. EANM guideline for radionuclide therapy with radium-223 of metastatic castration-resistant prostate cancer. Eur J Nucl Med Mol Imaging. 2018;45:824–45.
179. Oyen WJ, Sundram F, Haug AR, Kalevi K, Lewington V, Mäenpää H, et al. Radium-223 dichloride (Ra-223) for the treatment of metastatic castration-resistant prostate cancer: optimizing clinical practice in nuclear medicine centers. J Oncol Pathol. 2015;3:1–25. https://doi.org/10.13032/tjop.2052-5931.100121.
180. Liepe K, Shinto A. From palliative therapy to prolongation of survival: $^{223}RaCl_2$ in the treatment of bone metastases. Ther Adv Med Oncol. 2016;8:294–304.
181. Du Y, Carrio I, DeVincentis G, Fanti S, Ilhan H, Mommsen C, et al. Practical recommendations for radium-223 treatment of metastatic castration-resistant prostate cancer. Eur J Nucl Med Mol Imaging. 2017;44:1671–8.

Further Reading

Glaudemans AWJM, Jutte PC, Cataldo MA, Cassar-Pullicino V, Gheyesens O, Bores O, et al. Consensus document for the diagnosis of peripheral bone infection in adults: a joint paper by the EANM, EBJS, and ESR (with ESCMID endorsement). Eur J Nucl Med Mol Imaging. 2019;46:957–70.
Signore A, Scofienza LM, Borens O, Glaudemans AWJM, Cassar-Pullicino V, Trampuz A, et al. Consensus document for the diagnosis of prosthetic joint infection: a joint paper by the EANM, EBJS, and ESR (with ESCMID endorsement). Eur J Nucl Med Mol Imaging. 2019;46:971–88.
Signore A, Scofienza LM, Borens O, Glaudemans AWJM, Cassar-Pullicino V, Trampuz A, et al. Correction to: Consensus document for the diagnosis of prosthetic joint infection: a joint paper by the EANM, EBJS, and ESR (with ESCMID endorsement). Eur J Nucl Med Mol Imaging. 2019;46:1203.